
Formation of massive seed black holes by direct collapse in the early Universe

Bhaskar Agarwal



München 2013

Formation of massive seed black holes by direct collapse in the early Universe

Bhaskar Agarwal

Dissertation
an der Fakultät für Physik
der Ludwig–Maximilians–Universität
München

vorgelegt von
Bhaskar Agarwal
aus Udaipur, India

München, den 16 September 2013

Erstgutachter: Dr. Sadegh Khochfar

Zweitgutachter: Prof. Andreas Burkert

Tag der mündlichen Prüfung: 6 December 2013

Dedicated to my fiancée, Sonam.

Contents

Zusammenfassung	xiii
Abstract	xv
1 Explaining the first supermassive black holes	1
2 Cosmic dawn	3
2.1 Cosmological framework	3
2.1.1 Density perturbations	5
2.1.2 Growth of perturbations	8
2.1.3 The first stars and galaxies	9
2.2 Seeds of the quasars at $z > 6$	16
2.2.1 Stellar seeds of quasars	17
2.2.2 Direct collapse seeds of quasars	19
3 Conditions for direct collapse	23
3.1 Introduction	24
3.2 Methodology	27
3.2.1 The N -body simulation	27
3.2.2 Star formation	28
3.2.3 Impact of LW radiation on star formation and direct collapse	31
3.2.4 J_{LW} calculation	33
3.2.5 Escape fraction of LW radiation and reionization feedback	36
3.2.6 Model normalisation	37
3.3 Results	39
3.3.1 The LW intensity	39
3.3.2 Sources responsible for $J > J_{\text{crit}}$	42
3.3.3 Abundance and growth of DCBHs	43
3.3.4 DCBH host haloes	45
3.3.5 Efficiency of DCBH formation	50
3.3.6 Reionisation Feedback	51
3.4 Observability of the stellar seeds of direct collapse black holes	53
3.5 Summary	54

4	Unravelling obese black holes in the first galaxies	59
4.1	Introduction	60
4.2	Methodology	61
4.2.1	DCBH forming haloes	61
4.2.2	Star Formation	64
4.2.3	Growth of a DCBH	66
4.3	Results	68
4.3.1	Observational predictions	70
4.4	Summary	71
5	Direct collapse black hole candidates in FiBY	73
5.1	Introduction	73
5.2	Methodology	74
5.2.1	FiBY Simulation	74
5.3	Results	77
5.3.1	Identifying the DC sites	77
5.3.2	The environment of DCBHs	81
5.3.3	Galaxies producing J_{crit}	86
5.4	Summary and Discussion	87
6	Outlook	89
A	Mass function and distance analysis	91
A.1	Details of Methodology: Chapter 2	91
A.1.1	Mass Function at $z = 6$	91
A.1.2	Selection of LW sources	91
	Acknowledgements	104

List of Figures

2.1	The first galaxies	10
2.2	Cooling function for hydrogen	11
2.3	Gas composition of the early Universe	12
2.4	Density vs. temperature of gas under collapse	13
2.5	Accretion rate for a Pop III proto–stellar core	14
2.6	Accretion onto seed BHs	18
2.7	Reaction speed vs. density for H ₂ dissociation	20
3.1	Critical mass for Pop III star formation	31
3.2	Lyman–Werner emission from Pop II stars	33
3.3	The star formation rate mass function	35
3.4	Star formation rate densities	36
3.5	Mean LW background	38
3.6	LW radiation evolution	40
3.7	The distribution of J_{local}	42
3.8	Formation rate density of DCBH sites	44
3.9	DCBH mass function and cumulative mass density for the fiducial case . .	45
3.10	The correlation function ξ_{total}	48
3.11	Age distribution of the DCBH host haloes	49
3.12	Efficiency of DCBH site formation	50
3.13	DCBH mass function and cumulative mass density for reionisation case . .	52
3.14	Supermassive stellar progenitors of DCBHs	54
4.1	Temperature–spin distribution of DC haloes	62
4.2	$M_{\text{BH}}\text{--}M_{\text{bulge}}$ relation for OBGs	64
4.3	Observability of OBGs	66
4.4	Size versus magnitude relation of OBGs	69
5.1	Evolution of LW radiation in DC3	79
5.2	Evolution of LW radiation in DC5	80
5.3	Merger tree for DC candidate haloes.	82
5.4	LW radiation and metallicity for DC0’s environment	83
5.5	LW radiation and metallicity for DC2’s environment	83

5.6	LW radiation and metallicity for DC3's environment	84
5.7	Galaxies in the neighbourhood of the DC candidates	85
A.1	The mass function of haloes at $z = 6$	92
A.2	Lightcone diagram for the selection of LW sources	93
A.3	Infinite Universe	93

List of Tables

2.1	Time evolution of the Universe	6
3.1	Pop III functional fits for age and emission	34
3.2	Case Summary: DC sites in SAM	38
3.3	Fits to DCBH number density evolution	46
3.4	Fit parameters for DCBH site efficiency	51
4.1	Case Summary: OBGs	68
5.1	Properties of the DC candidate haloes	78

Zusammenfassung

Das Ziel der in dieser Dissertation vorgestellten Arbeit ist es, zu verstehen wie sich die ersten Schwarzen Löcher im frühen Universum bilden, die die Saat von superschweren Schwarzen Löcher mit einer Masse größer als $10^8 M_{\odot}$ ca. 800 Millionen Jahre nach dem Big Bang sind. Mit welcher Masse sich die "Saatkörner" superschwerer Schwarzen Löcher gebildet haben und ihre Akkretionsgeschichte ist Gegenstand der Diskussion. Wir untersuchen das Szenario zur Entstehung schweren "Saatguts" Schwarzer Löcher (BH), das es zulässt, Gas mit $10^6 M_{\odot}$, *direkt* in ein BH (DCBH) mit vergleichbarer Masse zu kollabieren. Das Szenario erfordert ein Reservoir aus metallfreiem Gas in einem dunkle Materie Halo, das überwiegend aus atomarem Wasserstoff zusammengesetzt ist, wobei die Häufigkeit des molekularen Wasserstoffs durch eine hohe Lyman-Werner (LW) Strahlung subkritisch gehalten wird. Die hier präsentierte Arbeit beabsichtigt die Häufigkeit solcher Regionen des frühen Universum zu untersuchen, die im Anschluss des Gaskollapses zur Entstehung eines DCBHs folgen könnten.

Wir haben verschiedene semi-analytischer Modelle (SAM) entwickelt, die an eine kosmologischen N-Körper Simulation gekoppelt sind, um die lokale Abweichung des LW Strahlungsflusses zu modellieren, die aus Population III und Population II Sternen hervorgeht. Das SAM berücksichtigt selbstkonsistent die Entstehung von Sternen und die Entwicklung der Metallizität, basierend auf der Halo Vorgeschichte. Die Resultate zeigen, dass es bis zu eine DCBH Region pro Mpc^3 bei $z = 6$ gibt, welches extrem viel ist, verglichen mit den SMBHs, bei denen nur wenige pro Gpc^3 bei $z = 6$ vorhanden sind. Unter Verwendung eines Modells, das den Gaskollaps im Detail beschreibt, verfeinern wir unsere Auswahl der Halos weiter in denen das Gas sich zu einer marginal stabilen Scheibe absetzt und den Transport des Drehimpulses zulässt. Dies ermöglicht uns Halo's zu wählen, die am wahrscheinlichsten DCBHs formen. Auf der Grundlage dieser Auswahl sagen wir die Existenz einer vollkommen neuen Klasse von Galaxien vorher, in welchen sich das zentrale Schwarze Loch durch direkten Kollaps zuerst bildet und die Sterne später erzeugt werden. Wir bezeichnen diese Objekte als "übergewichtige" Schwarze Loch Galaxien, oder OBGs, und prognostizieren, dass ihre Häufigkeit bis zu 0.03 Mpc^{-3} bei $z = 6$ sein könnte. OBGs haben ausgeprägte beobachtbare Merkmale, und könnten uns helfen, die Wege zur lokalen BH- Sphäroid Massen-Korrelation zu verstehen. Wir präsentieren des Weiteren eine selbstkonsistenten kosmologische hydrodynamische Simulation, die Teil des *First Billion Years* Projekts (FiBY) ist, um die Plausibilität des DCBH Szenarios besser zu verstehen. Die Simulation berücksichtigt Anreicherung schwere Elemente in Halos über Stellare Winde

und Supernovae, und modelliert selbstkonsistent das Ansteigen der globalen und lokalen Abweichungen des LW Strahlungsflusses. Wir finden die Existenz einer Handvoll von DCBH Regionen im Simulationsvolumen von $\sim 64 \text{ Mpc}^3$, ein Ergebnis, das konsistent ist mit denen des SAM, die wir anfangs entwickelt haben.

Sowohl durch die Verwendung des SAMs, als auch kosmologischen hydrodynamischen Simulationen haben wir gezeigt, dass es einige DCBH Regionen pro Mpc^3 bei $z = 6$ geben könnte. Ob diese Orte direkten Kollaps durchlaufen, in dem sie Sternentstehung standhalten, oder nicht, ist noch eine offene Frage und Gegenstand einer unserer geplanten zukünftigen Studien.

Abstract

The aim of the work presented in this thesis is to understand the formation of the seeds of the first supermassive black holes, with masses larger than $10^8 M_{\odot}$, that existed when the Universe was only 800 Myr old. The mass at which the seeds of these supermassive black holes formed, and their accretion history is a matter of debate. We study the scenario of massive seed black hole formation which allows $10^6 M_{\odot}$ of gas to *directly* collapse into a black hole (DCBH) of similar mass. This scenario requires a reservoir of metal-free gas in a halo that is predominantly composed of atomic hydrogen, where the molecular hydrogen's abundance can be made sub-critical by a high level of external Lyman-Werner (LW) radiation flux. The work presented here is aimed at investigating the occurrence of such sites in the early Universe where subsequent gas collapse could lead to the formation of a DCBH.

We developed a suite of semi-analytical models (SAM) that operate on the output of a cosmological N-body simulation, to model the local variation of the LW radiation flux emanating from both Population III and Population II stars. The SAM self-consistently accounts for star formation and metallicity evolution on the basis of halo histories. We find that there could be as many as 1 DCBH site per Mpc^3 at $z = 6$, which is extremely high as compared to that of SMBHs which is few per Gpc^3 at $z = 6$. Using a model for the detailed collapse of gas, we further refine our selection to the haloes in which the gas can settle in a marginally stable disc and allow for the transport of angular momentum. This enables us to select haloes that are most likely to form DCBHs. On the basis of this selection, we propose the existence of an entirely new class of galaxies where the central black hole forms first via direct collapse and the stars are acquired later. We call them obese black hole galaxies, or OBGs, and predict that their abundance could be up to 0.03 Mpc^{-3} at $z = 6$. OBGs have distinct observational features and could help us in understanding the pathways to the local black hole-bulge mass correlations. We then employ a fully cosmological hydrodynamic simulation, that is a part of the *First Billion Years* Project (FiBY), to better understand the plausibility of the DCBH scenario. The simulation accounts for metal enrichment of haloes via stellar winds and supernovae, and self consistently models the build up of the the global and local variation of the LW radiation flux. We find the existence of a handful of DCBH sites in the simulation volume of $\sim 64 \text{ Mpc}^3$, a result that is consistent with the SAM we developed earlier.

Using both SAMs and cosmological hydrodynamical simulations, we have shown that there could be a few DCBH sites per Mpc^3 at $z = 6$. Whether or not these sites undergo

direct collapse by withstanding star formation is still an open question and the topic of one of our planned future studies.

Chapter 1

Introduction

Explaining the first supermassive black holes in the universe

The discovery of the black hole, Sagittarius A* (see for e.g. Becklin & Neugebauer, 1968; Genzel et al., 1994) at the centre of our galaxy confirmed the existence of supermassive black holes¹ (SMBH) in the local Universe. On studying the stellar velocity dispersions of galaxies in the local Universe, we now understand that a SMBH is an essential component of the present day galaxy system (for e.g. Gebhardt et al., 2003; Gültekin et al., 2009b). It is now also believed that galaxies in the Universe form hierarchically, where gas clouds of a few $10^{4-5} M_{\odot}$ collapse and form stars in dark matter (DM) overdensities, and evolve via gas accretion and mergers with other galaxies. These two ideas pose an interesting conundrum:

“At what point in its lifetime does a galaxy acquire its central black hole and how do they co-evolve?”

The observations of Quasi-stellar Objects (QSOs or Quasars) out to $z \sim 7$ (Mortlock et al., 2011) suggest that there were at least a few SMBHs with masses larger than $10^8 M_{\odot}$ when the Universe was less than a billion years old. Given that the current age of the Universe is $\approx 13.7 \times 10^9$ years, it is one of the greatest puzzles of modern day astrophysics to explain the existence of these beasts at a time when the Universe was less than 10% of its current age. What makes this puzzle even more interesting is that stellar astrophysics can explain the formation of BHs of a few solar masses as the remnants of giant stars (see for e.g. Janka et al., 2007), but there is no consensus on their growth to supermassive scales (see for e.g. Johnson et al., 2012b). Explaining how such a stellar BH seed could grow by 6 – 7 orders of magnitude in mass, in few hundred million years, is another daunting task given the limits on accretion that we will explain later in the following chapter.

The idea, that a set of very specific physical conditions, found only in the early Universe,

¹In this study, we refer to a black hole with mass $> 10^6 M_{\odot}$ as *supermassive*.

could have allowed for the formation of *massive seed black holes* with masses in the range of $10^{4-5} M_{\odot}$, could be a potential solution to this problem (Rees, 1978) as the seed would now need to grow by only 3–4 orders of magnitude in mass to attain supermassive scales. This is referred to as the *direct collapse* (DC) channel of forming massive seed black holes. The aim of the thesis is to understand the plausibility of the set of physical conditions required for direct collapse and its impact on the evolution of the first galaxies. The emphasis is on understanding how frequently do the conditions required for DC occur at $z > 6$ and not on the actual formation process itself (see however Chapter 6). In order to investigate how feasible these conditions are, a semi-analytical-model (SAM) was developed which operates on the output of a high-resolution DM-only N-body simulation. The SAM and all its details are discussed in Chapter 3 where we report that DC sites can be as abundant as 0.1 per co-moving Mpc^3 at $z = 6$, which is mainly due to the self-consistent treatment of the evolution of the local and global levels of Lyman–Werner radiation in the SAM. As a result of which, we speculate the possible existence of a new class of obese black hole galaxies (OBGs) at $z > 6$ in Chapter 4. Finally the existence of DC sites in a state of the art fully cosmological hydrodynamical simulation project, the *First Billion Years Simulation*, FiBY, is discussed in Chapter 5, which tackles issues like metal pollution of the intergalactic medium via stellar winds and supernovae, and employs a more physical treatment of star formation as compared to the SAM. Chapter 6 includes a critical overview of the work presented in this thesis and the future prospects. We will now discuss the theoretical background of the work in the following chapter.

Chapter 2

Cosmic dawn

2.1 Cosmological framework¹

According to the current model of structure formation and evolution, the Universe is expanding and originated from a singularity ~ 13.7 billion years ago. The big bang theory, which has gained widespread acceptance over the past few decades, describes the initial stages of the Universe as a *hot-sea* of particles and radiation, which were coupled with one another in the first 10^{13} seconds. It was after this epoch that the first atoms formed and eventually led to the formation of the first galaxies.

The time evolution of the first 0.3 Myr of the Universe is summarised in Table 2.1. The Universe cooled as it expanded, and after ≈ 0.3 Myr (or 10^{13} s), the coupling between matter and radiation broke down. The radiation that decoupled at this epoch with a temperature of ≈ 3000 K, can still be observed today as the *Cosmic Microwave Background* (CMB) (Penzias & Wilson, 1965; Mather et al., 1994; Planck-Collaboration, 2013), but with a much lower temperature owing to the expansion of the Universe. The latest *Planck* results (Planck-Collaboration, 2013), preceded by the Wilkinson Microwave Anisotropy Probe, *WMAP*, (see for e.g. Spergel et al., 2003; Hinshaw et al., 2012) and the Cosmic Background Explorer, *COBE*, (see for e.g. Mather et al., 1994), have led to a very insightful understanding of the CMB. The CMB is observed as a blackbody with a mean temperature of ≈ 3 K and shows fluctuations in the temperature maps at the order of 10^{-5} K. This was one of the major predictions of the big bang theory (Dicke et al., 1965), and the observations of the same by COBE (Mather et al., 1994; Wright et al., 1994; Fixsen et al., 1996) was what led to the widespread acceptance of the theory today.

It is now understood that the Universe is composed mostly of dark matter (DM), baryonic matter and the dark energy parameter, Λ . When one refers to matter in the Universe, it could imply either the baryonic matter that constitutes the stars, galaxies, planets and the elements in the periodic table, or DM. Dark matter is composed of particles

¹The following text books were used for this section: Andrew Liddle: ‘*An Introduction to Modern Cosmology*’ (Liddle, 2003); Houjun Mo, Frank van den Bosch, Simon White: ‘*Galaxy Formation and Evolution*’ (Mo et al., 2010).

that are envisioned to be pressureless, non-relativistic and collisionless in nature, thereby interacting only gravitationally. It is crucial in explaining properties like the rotation curves of disk galaxies (Rubin et al., 1985) and imperative for the hierarchical model of structure formation (Searle & Zinn, 1978). The dark energy is able to explain the ever-expanding state of our Universe, as seen by supernovae observations (Perlmutter et al., 1999), however the nature and composition of dark energy is unknown.

To parameterise the expanding nature of the Universe, one can construct a *comoving* set of coordinates that account for the expansion of the Universe at each redshift. One can relate the physical coordinate, \mathbf{r} , to the comoving one, \mathbf{x} , by writing

$$\mathbf{r} = a\mathbf{x} , \quad (2.1)$$

where a is the expansion factor which is a function of redshift as $a = 1/(1+z)$.

The evolution of the Universe can be understood with the help of the Friedmann equation which naturally folds in the Λ parameter when derived from Einstein's general relativistic framework

$$H^2(a) \equiv \left(\frac{\dot{a}}{a}\right)^2 = \frac{8\pi G\rho}{3} - \frac{kc^2}{a^2} + \frac{\Lambda c^2}{3} , \quad (2.2)$$

where H is the Hubble parameter measured at any given redshift, ρ is the density which can be expressed as a sum of various components, k denotes the curvature (which is 0 for a flat Universe²) and Λ denotes the dark energy component.

Writing $\rho = \rho_m + \rho_r$, and $\rho_\Lambda = \frac{\Lambda c^2}{8\pi G}$, where ρ_m , ρ_r and ρ_Λ represent the mass density of non-relativistic matter (i.e. both DM and baryonic), radiation and dark energy component respectively, we can write

$$H^2 \equiv \left(\frac{\dot{a}}{a}\right)^2 = \frac{8\pi G}{3} (\rho_m + \rho_r + \rho_\Lambda) - \frac{kc^2}{a^2} . \quad (2.3)$$

Upon using the result that the Universe is flat (for e.g. de Bernardis et al., 2000; Hinshaw et al., 2012; Planck-Collaboration, 2013), i.e. $k = 0$, one can define a critical density for the Universe. The critical density, ρ_c , is defined as the density at which the Universe assumes a flat geometry. At any given time during the Universe's evolution

$$\rho_c = \frac{3H^2}{8\pi G} , \quad (2.4)$$

which at $z = 0$, can be written as

$$\rho_{c,0} = \frac{3H_0^2}{8\pi G} . \quad (2.5)$$

Note that an additional superscript/subscript of 0 with any of the density parameters explicitly implies its value at $z = 0$.

²The curvature of the Universe would be spherical, or *closed*, for $k > 0$ and hyperbolic, or *open*, for $k < 0$.

The composition of the Universe can now be parameterised by expressing the different density components as a ratio between the density of the component and the critical density of the Universe. Therefore at any given redshift, the density parameters written as, Ω with the appropriate subscript, take the form

$$\Omega_m = \frac{\rho_m}{\rho_c}, \quad \Omega_\Lambda = \frac{\rho_\Lambda}{\rho_c}, \quad \Omega_b = \frac{\rho_b}{\rho_c}, \quad \Omega_r = \frac{\rho_r}{\rho_c}. \quad (2.6)$$

An interesting outcome of the current cosmological observations is that the density parameters sum up to ≈ 1 (Planck-Collaboration, 2013)

$$\Omega_\Lambda + \Omega_m + \Omega_r = 1.001_{-0.0062}^{+0.0065}, \quad (2.7)$$

which, is also indicative of a flat Universe as $\Omega_k = \frac{\rho_k}{\rho_c} = 0$ since $k = 0$ for a flat universe. Note that in the above equation, Ω_m is a combination of the DM and baryonic matter, i.e. the non-relativistic components. The evolution of each of the density components with redshift can be obtained by solving their corresponding equation of state, leading to

$$\rho_m \propto \frac{1}{a^3}, \quad \rho_r \propto \frac{1}{a^4}, \quad \rho_\Lambda \equiv \text{constant}, \quad (2.8)$$

with which we can rewrite Eq. 2.3 for a flat Universe as

$$H^2 \equiv \left(\frac{\dot{a}}{a}\right)^2 = \frac{8\pi G}{3} \left(\rho_{m,0} \left(\frac{a_0}{a}\right)^3 + \rho_{r,0} \left(\frac{a_0}{a}\right)^4 + \rho_{\Lambda,0} \right), \quad (2.9)$$

where $a_0 = 1/(1+z_0) = 1$ since $z_0 = 0$.

The evolution of these densities, and the corresponding perturbations (see next Section), led to the formation of the first stars and galaxies.

2.1.1 Density perturbations

Recall that the matter and radiation were strongly coupled prior to the origin of the CMB, which means that the fluctuations that we see in the CMB on small scales today are an imprint of the baryonic density perturbations that were present in the Universe prior to recombination (see for e.g. Planck-Collaboration et al., 2013).

To understand the collapse and growth of the density perturbations, we can start by treating the Universe just after recombination, as a non-relativistic fluid with an average matter density, $\bar{\rho}$, under the effect of a gravitational potential Φ . This treatment is representative of baryonic gas where the collisions among the particles can establish local thermal equilibrium, or for pressureless DM where the velocity dispersion of the particles is small enough to not cause diffusion at the scales of interest. We will now concern ourselves with the evolution of perturbations for baryonic gas only, however, later we will briefly explore the implications of including the DM component as well.

The perturbations in the density field can be characterised by expressing them in the form of a fractional over density

Table 2.1: Time evolution of the Universe (adapted from Liddle (2003)).

Time	Temperature	Specifics	Dominant
$10^{-10} < t < 10^{-14}$ s	$10^{12} < T < 10^{15}$ K	Strongly coupled state: e^-, q, γ, ν	Radiation
$10^{-4} < t < 1$ s	$10^{10} < T < 10^{12}$ K	Strongly coupled state: e^-, p, n, γ, ν . The quarks have now resulted in the existence of p and n	Radiation
$1 < t < 10^{12}$ s	$10^4 < T < 10^{10}$ K	The first atomic nuclei have formed but co-exist with e^-, γ, ν . Except for the neutrinos, the matter and radiation is in a strongly interactive state	Radiation
$10^{12} < t < 10^{13}$ s	$3000 < T < 10^4$ K	The first atomic nuclei have formed but co-exist with e^-, γ, ν . Except for the neutrinos, the matter and radiation is in a strongly interactive state	Matter
$10^{13} < t < t_0$ s	$3 < T < 3000$ K	The first atoms have now formed and the radiation and matter is no longer coupled	Matter

$$\delta(\mathbf{x}) = \frac{\rho(\mathbf{r})}{\bar{\rho}} - 1 . \quad (2.10)$$

At any given point in the Universe, the proper velocity, $\mathbf{u} = \dot{\mathbf{r}}$, can be expressed as a sum of the peculiar velocity, \mathbf{v}_{pec} , and the velocity arising due to expansion of the Universe, \mathbf{v}_H

$$\dot{\mathbf{r}} = a\dot{\mathbf{x}} + \mathbf{x}\dot{a} , \quad (2.11)$$

or

$$\mathbf{u} = \mathbf{v}_{pec} + \mathbf{v}_H , \quad (2.12)$$

where $\mathbf{v}_{pec} = a\dot{\mathbf{x}}$ and $\mathbf{v}_H = \mathbf{x}\dot{a}$.

For a Newtonian–ideal–fluid, the interactions between the baryonic particles can establish local thermal equilibrium at the collapsible scales. In the framework of comoving co–ordinates, substituting the density (Eq. 2.10) and velocity flow (Eq. 2.12) in the continuity, Euler, and Poisson equations, one can derive the following relations:

$$\frac{\partial\delta}{\partial t} + \frac{1}{a}\nabla \cdot [(1 + \delta)\mathbf{v}_{pec}] = 0 , \quad (2.13)$$

which represents the continuity equation,

$$\frac{\partial\mathbf{v}_{pec}}{\partial t} + \frac{\dot{a}}{a}\mathbf{v}_{pec} + \frac{1}{a}(\mathbf{v}_{pec} \cdot \nabla)\mathbf{v}_{pec} = -\frac{\nabla\Phi}{a} - \frac{\nabla P}{a\bar{\rho}(1 + \delta)} , \quad (2.14)$$

which represents the Euler equation, where P represents the pressure, and

$$\nabla^2\Phi = 4\pi G\bar{\rho}a^2\delta , \quad (2.15)$$

which represents the Poisson equation where $\Phi \equiv \phi + a\ddot{a}x^2/2$. The above set of equations can be solved, given that immediately after recombination, the Universe can be assumed to be predominantly composed of hydrogen atoms. Thereby, using the standard thermodynamical relations, for an adiabatic evolution, one can write

$$\frac{\partial^2\delta}{\partial t^2} + 2\frac{\dot{a}\partial\delta}{a\partial t} = 4\pi G\bar{\rho}\delta + \frac{c_s^2}{a^2}\nabla^2\delta + \frac{2\bar{T}}{3a^2}\nabla^2 S , \quad (2.16)$$

where c_s is the sound speed, \bar{T} is mean background temperature of the fluid and S is the entropy. The second term on the left is responsible for suppressing the growth of perturbations as it expresses the Hubble drag, and the last two on the right account for the pressure terms. The first term on the right is the gravity term that leads to the growth of the perturbations due to gravitational instabilities.

2.1.2 Growth of perturbations

If we consider that $|\delta| \ll 1$, then in Eq. 2.16, one can ignore the pressure terms that deal with the growth of the density perturbations, leading to

$$\frac{\partial^2 \delta}{\partial t^2} + 2 \frac{\dot{a} \partial \delta}{a \partial t} = 4\pi G \bar{\rho} \delta . \quad (2.17)$$

Furthermore, for a flat universe the perturbations can be expressed by their Fourier transforms

$$\delta(\mathbf{x}, t) = \sum_{\mathbf{k}} \delta_{\mathbf{k}}(t) \exp(i\mathbf{k} \cdot \mathbf{x}) , \quad (2.18)$$

$$\delta_{\mathbf{k}}(t) = \frac{1}{V_u} \int \delta(\mathbf{x}, t) \exp(-i\mathbf{k} \cdot \mathbf{x}) d^3x , \quad (2.19)$$

where V_u is the volume of the region in which the perturbations are assumed to be periodic. Note that the operator $\nabla^2 \equiv (i\mathbf{k})^2 = -\mathbf{k}^2$. Substituting these relations into Eq. 2.16 for a complete solution, we get

$$\frac{\partial^2 \delta_{\mathbf{k}}}{\partial t^2} + 2 \frac{\dot{a} \partial \delta_{\mathbf{k}}}{a \partial t} = 4\pi G \bar{\rho} \delta_{\mathbf{k}} - k^2 \frac{c_s^2}{a^2} \delta_{\mathbf{k}} - \frac{2\bar{T}}{3a^2} k^2 S_k , \quad (2.20)$$

with the Poisson equation taking the form

$$-k^2 \Phi_{\mathbf{k}} = 4\pi G \bar{\rho} a^2 \delta_{\mathbf{k}} . \quad (2.21)$$

Note that, ignoring the entropy term in Eq. 2.20, i.e. assuming that the perturbations evolve adiabatically, we can write

$$\frac{d^2 \delta_{\mathbf{k}}}{dt^2} = -\omega^2 \delta_{\mathbf{k}} , \quad (2.22)$$

$$\omega^2 = \frac{k^2 c_s^2}{a^2} - 4\pi G \bar{\rho} , \quad (2.23)$$

where the above description of ω is representative of a wave-solution which results in a stationary wave that either decays or grows with time for $\omega^2 < 0$, whereas for $\omega^2 > 0$, it results in a propagating sound wave, travelling with the sound speed c_s .

In case of a fluid composed of both DM and baryonic component, assuming that the DM component dominates the mean density, and ignoring the entropy term, Eq. 2.20 can be written as

$$\frac{\partial^2 \delta_{\text{tot}}}{\partial t^2} + 2 \frac{\dot{a} \partial \delta_{\text{tot}}}{a \partial t} = 4\pi G \bar{\rho}_0 \frac{a_0^3}{a^3} \delta_{\text{tot}} - k^2 c_s^2 \frac{a}{a^3} \delta_{\text{tot}} , \quad (2.24)$$

where $\bar{\rho}_0 \sim \bar{\rho}_{dm,0}$ is the mean DM density at the present time. Furthermore, for a case where $P \propto \rho^\gamma$, where γ is the adiabatic index, and $a(t) \propto t^{-2/3}$, as in the case of a matter dominated universe, $c_s^2 a$ can be assumed to be constant, leading to the solution

$$\delta_{\text{tot}}(\mathbf{k}, t) = \frac{\delta_{\text{dm}}(\mathbf{k}, t)}{1 + k^2/k_J^2}, \text{ with } k_J^2 = \frac{3a^2 H^2}{2c_s^2}. \quad (2.25)$$

On large scales, $k \ll k_J$, the baryonic perturbations are coupled to the DM perturbations where the pressure of the baryonic fluid can be neglected. However on small scales, $k \gg k_J$, the baryonic pressure can give rise to acoustic oscillations which will slowly damp as the Universe expands. We will now go back to the baryonic treatment of the perturbations to understand the physics behind the collapse of the first gas clouds.

2.1.3 The first stars and galaxies

In order to understand the collapse of the first gravitationally bound gas clouds, one can derive a characteristic scale length, the *Jeans length*, by equating the left side of Eq. 2.23 to zero, which essentially implies that the gravity term is able to balance the pressure term

$$\lambda_J \equiv \frac{2\pi a}{k_J} = c_s \sqrt{\frac{\pi}{G\bar{\rho}}}. \quad (2.26)$$

Using Eq. 2.23 and 2.26, one can deduce the following. If $\lambda > \lambda_J$ (or $k < k_J$), the above expression expresses a sound wave that is not able to withstand gravity and would lead to the collapse of the overdensity. However, if $\lambda < \lambda_J$ (or $k > k_J$), the pressure is greater than the gravity and collapse can not ensue. Post recombination, the sound speed for the non-relativistic mono-atomic gas can be written as

$$c_s = \sqrt{\gamma \frac{P}{\rho}} = \sqrt{\frac{5k_B T}{3m_p}}, \quad (2.27)$$

where we have used the adiabatic index, $\gamma = 5/3$, for mono-atomic gas and m_p is the mass of a proton. Using this in Eq. 2.26, we can derive a jeans length at any given redshift as

$$\lambda_J = \sqrt{\frac{5k_B T}{3m_p} \frac{\pi}{G\bar{\rho}}} = \sqrt{\frac{5\pi k_B T_{\text{CMB},0}(1+z)}{3m_p G \Omega_{b,0} \rho_{c,0}(1+z)^3}} \approx \frac{0.07}{1+z} \text{Mpc}, \quad (2.28)$$

where $\bar{\rho} = \Omega_{b,0} \rho_{c,0} (1+z)^3$, $\Omega_{b,0}$ and $\rho_{c,0}$ represent the baryonic matter density and critical density of the Universe at $z = 0$, and $T_{\text{CMB},0} = 2.72548 \pm 0.00057$ K is the CMB temperature at $z = 0$ (Fixsen, 2009). The temperature of the gas can be assumed to be that of the CMB at an epoch just after recombination, $z \sim 1100$, as the matter has recently de-coupled from the radiation.

A corresponding Jeans Mass can now be defined by using the above scale length as a proxy for the diameter of a sphere that undergoes gravitational collapse, at any given redshift

$$M_J = \frac{4}{3}\pi \left(\frac{\lambda_J}{2}\right)^3 \bar{\rho} = \frac{\pi}{6} \left(\frac{0.07 \text{ Mpc}}{1+z}\right)^3 \Omega_{b,0} \rho_{c,0} (1+z)^3, \quad (2.29)$$

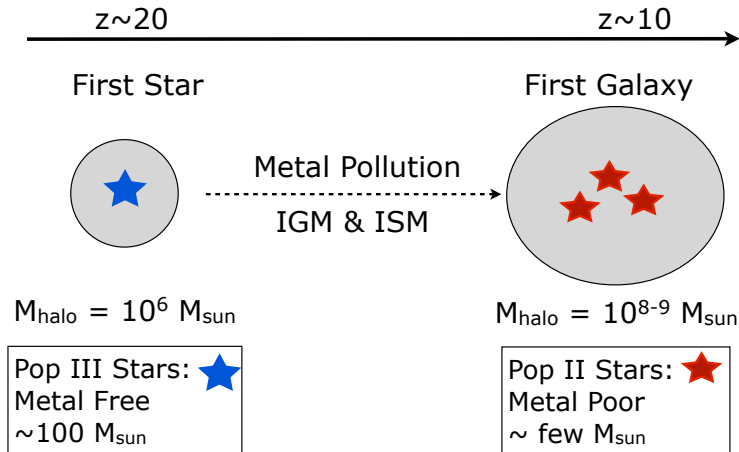


Figure 2.1: A schematic for the formation of the first stars and galaxies as per our current understanding of galaxy formation. The first stars pollute the inter galactic (IGM) and inter stellar medium (ISM) with metals, thereby leading to the formation of Pop II stars.

which gives a characteristic mass

$$M_J \approx 8 \times 10^5 M_\odot . \quad (2.30)$$

This mass is comparable to the gas mass contained in the smallest DM haloes, where the first stars could form, which are referred to as *mini-haloes* with a typical mass of $\sim 10^6 M_\odot$ (Tegmark et al., 1997). The first generation of stars that form in the mini-haloes, are called Population III or Pop III stars and the succeeding generation is referred to as Population II or Pop II stars. Pop III stars form from primordial gas and are essentially *metal-free*. These first stars are able to *pollute* the intergalactic medium (IGM) and the interstellar medium (ISM) with metals that were ejected via winds or supernovae (SNe) explosions, as a result of which the primordial gas is no longer metal-free. Pop II stars are the ones that form from this metal-enriched gas with $Z > 10^{-4} Z_\odot$ which is still metal-poor as compared to the solar metallicity (for e.g. Schneider et al., 2002; Maio et al., 2011).³ A schematic for the formation of the first stars and galaxies is shown in Fig. 2.1.

The characteristic mass of these stellar populations depends on the gas from which they form. The cooling and collapse of the gas in the first mini-haloes is subject to the composition of the gas. The cooling function of primordial-type gas is shown in Fig. 2.2. Molecular hydrogen is efficient at cooling if the gas temperature is $T_{gas} \lesssim 10,000$ K and can cool the gas down to $O(100)$ K. Atomic hydrogen on the other hand can cool the gas

³Metallicity is defined as $Z = \sum \frac{m^s}{M}$, where M is the total mass of the star and m^s is the mass of the species heavier than He, with the solar metallicity, $Z_\odot = 0.02$.

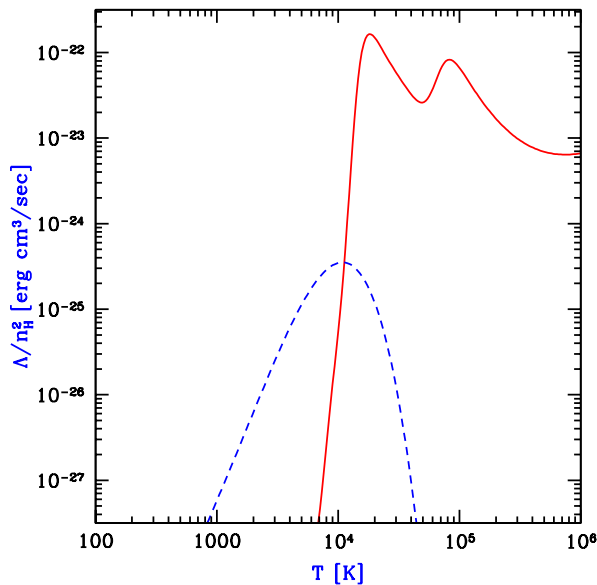


Figure 2.2: Cooling curves for atomic (red) and molecular hydrogen (blue) computed for a gas density of $n_H = 0.045 \text{ cm}^{-3}$ and $n_{H_2} = 0.1\%n_H$ (taken from Barkana & Loeb, 2001).

down to only 10,000 K. This is critical to the formation of the first stars in both: mini-haloes with a *virial temperature*⁴ of $2000 < T_{vir} < 10,000 \text{ K}$ and atomic cooling haloes with $T_{vir} > 10,000 \text{ K}$. Virial temperature is often used as a proxy for the potential of the halo at a given redshift and refers to the mean temperature of the gas at the virial radius of the the haloes.

$$T_{vir} \propto V_c^2 = \frac{GM}{r_{vir}}, \quad (2.31)$$

where V_c represents circular velocity at the virial radius, r_{vir} , and the mass of the halo is denoted by M .

How the gas collapses once it is confined in the gravitational bounds of a halo is subject to the composition of the gas and the cooling mechanisms that govern the collapse. The composition of the baryonic matter after recombination provides an excellent understanding of initial conditions that led to the formation of the first stars.

Primordial chemistry and H_2

After recombination, the Universe was composed of the elements that were produced during the big bang nucleosynthesis (primary species), and the ones that formed subsequently (secondary species). Primary species mainly consist of H, D, He, Li (and the associated ions) and together give rise to the secondary species. One of the most important secondary

⁴See Chapter 3 for formulae relating to virial quantities

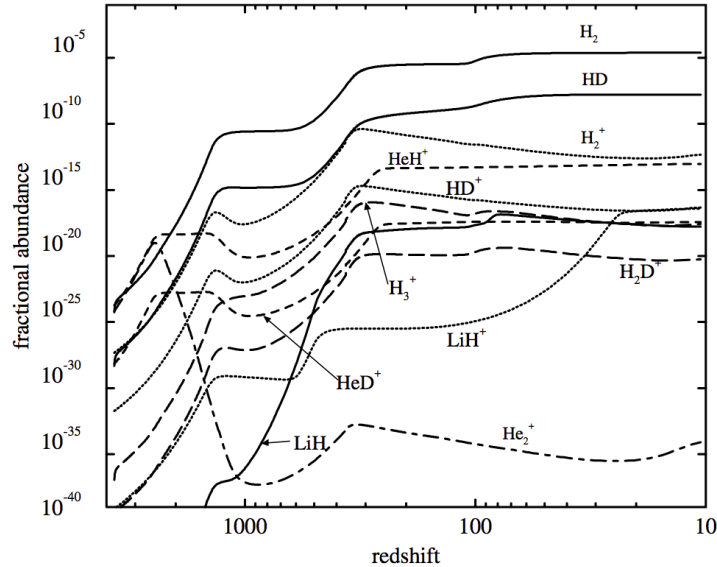
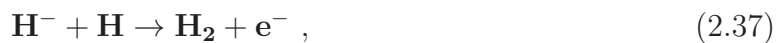


Figure 2.3: Fractional abundance of various species in the primordial gas (taken from Lepp et al., 2002). The highest fractional abundance is noted for molecular hydrogen but that said, it is capped at 10^{-5} at $z \sim 100$.

species that governs the collapse of gas into the first stars (or black holes as we will see in the later sections) is molecular hydrogen, which can form in the early Universe via the following reactions (Glover, 2011)



From the above reactions and Fig. 2.3, it can be deduced that H_2 is produced by two main channels, the H^- and H_2^+ channels, both operating at different epochs. The H^- channel for H_2 formation is the most efficient, given that it can operate efficiently at lower densities and is dominant when the Universe has cooled down sufficiently ($z < 100$) whereas the H_2^+ channel is relatively inefficient given the low cross sections of the reactants (Lepp et al., 2002) as the Universe expands. The fact that H^- is efficient at $z < 100$ is also due to the fact that it can be photo-detached by 0.76 eV photons⁵, thereby the channel can only operate once the CMB photons have cooled down sufficiently. That said, note

⁵ H^- plays a critical role in the gas collapse, as we will see in later chapters.

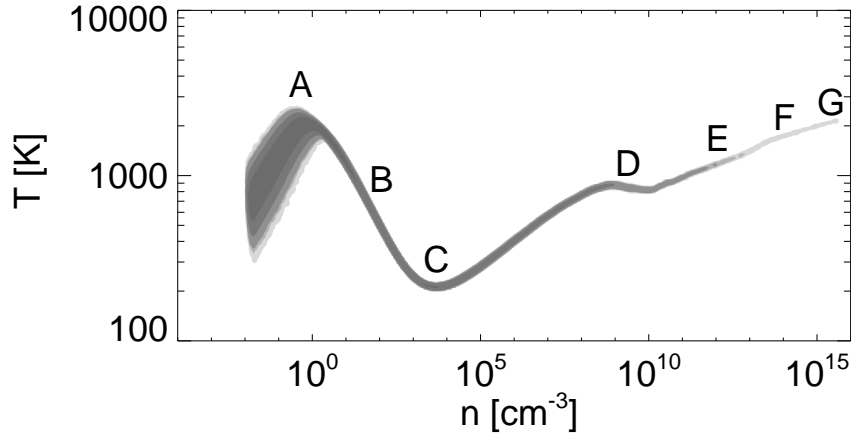


Figure 2.4: The density vs. temperature of pristine gas undergoing spherical collapse (taken from Yoshida et al., 2006). (A) gas is shock heated to the virial temperature and H_2 forms by two-body processes; (B) gas cools down to 200 K due to H_2 cooling; (C) H_2 cooling rate saturates and reaches the LTE value; (D) onset of three-body reactions, leading to the gas becoming fully molecular; (E) the line cooling becomes inefficient because of the high optical depth as the density of the gas increases; (F) collision-induced emission dominates cooling process; and (G) onset of H_2 dissociation at $T \sim 2000$ K.

that the fractional abundance of H_2 in the IGM is still only $\sim 10^{-5}$ at $z = 100$, however, a large fraction of H_2 is in fact formed within the collapsing gas clouds that shape the first galaxies.

Collapsing gas clouds and the first stars

Having understood what constitutes the primordial gas in the early Universe, we can now understand what governs the fate of gas collapse in the regions of overdensities we parameterised in Sec. 2.1.2 and 2.1.3. The cooling functions of the constituents of the gas will govern the fate of collapse in the halo and to better understand the same, the cooling curves for atomic (red) and molecular hydrogen (blue) are shown in Fig. 2.2. We also plot the density–temperature phase diagram for a collapsing gas cloud in Fig. 2.4 which will now be explained in detail.

As the gas falls into a halo it is shock heated to the virial temperature. This results in the production of free electrons and H ions from neutral H atoms which in turn leads to the formation of H_2 via reaction 2.37 and leads to efficient cooling of the gas, down to \sim few 100 K (see Fig. 2.2). The gas accumulates at the centre of the collapsing halo with a mean temperature of ~ 100 K and the accumulation of this *cold gas* continues till $n_{\text{H}_2} = 10^4 \text{ cm}^{-3}$, a density at which the rotational and vibrational levels for the H_2 molecule attain local thermodynamical equilibrium (LTE).

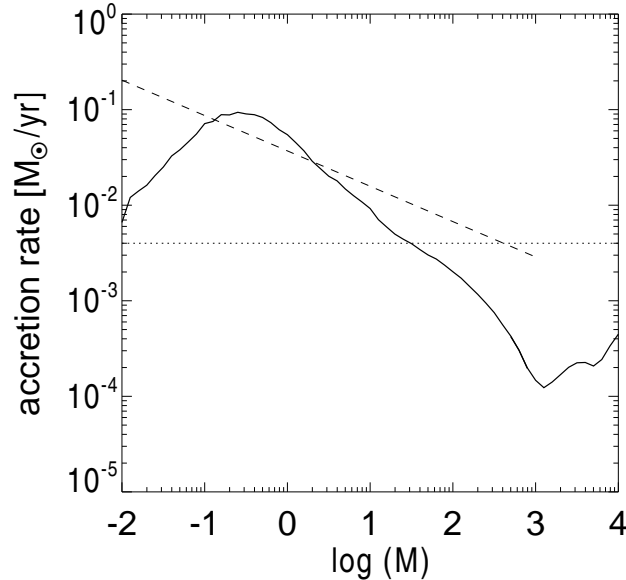


Figure 2.5: The accretion rate for the Pop III proto-stellar core (taken from Yoshida et al., 2006). The dashed line represents the theoretical estimate of Omukai & Nishi (1998). The dotted line is the critical accretion rate derived from the limit that the total luminosity of the accreting proto-stellar core can not exceed the Eddington limit (see next Section).

Recalling the relation for Jeans collapsible masses, we can write from Eq. 2.26 and 2.27

$$M_J = \frac{4}{3} \pi \lambda_J^3 \rho = \frac{\pi^{\frac{5}{2}} c_s^3}{6 G^{\frac{3}{2}} \sqrt{\rho}}, \quad (2.39)$$

where ρ is the mean gas density in the collapsing region. If one is to assume that the very initial state of collapse is isothermal and is in pressure equilibrium with its surrounding, the Jeans mass is often referred to as the *Bonnor-Ebert Mass*.

$$\frac{M_{BE}}{M_\odot} = 40 T^{\frac{3}{2}} n^{-\frac{1}{2}}, \quad (2.40)$$

where n is the number density of gas in cm^{-3} . For the gas at the centre of the halo, inputting the values $T = 200$ K, $n_{\text{H}_2} = 10^4 \text{ cm}^{-3}$ returns $M_{BE} = 1000 M_\odot$. Therefore, if the gas mass in the central region is larger than this value, the cloud can undergo collapse. Once the collapse ensues, HD cooling could become important and cool the gas to temperatures as low as that of the CMB. However, HD cooling is highly dependent on the ionisation state of the gas (as compared to the IGM), i.e. higher the ionisation state, more HD can be produced, thereby more cooling can occur. This is true even for low ionisation state of the gas, but either way, the gas can cool to CMB like temperatures and condense up to $n_{\text{HD}} \sim 10^6 \text{ cm}^{-3}$. Inputting this in the above formula leads to $M_{BE} = 40 M_\odot$, and once the gas mass goes beyond this limit, collapse ensues again with the gas being re-heated to ~ 1000 K (Glover, 2011).

As the gas collapses beyond the HD regime to a higher number density for H_2 , $n_{\text{H}_2} > 10^8 \text{ cm}^{-3}$, the three body processes govern the collapse, the most noteworthy reaction of which is (Palla et al., 1983)



As the remaining H in the gas is converted into H_2 , one would expect cooling to become increasingly efficient, which is not the case. The reaction releases the binding energy of 4.5 eV every time a H_2 molecule is formed, which results in heating the gas since molecular hydrogen can not cool below ~ 100 K. What happens beyond this density with respect to cooling and the rate coefficient for the above reaction is unclear (Turk et al., 2011). However, simulations suggest that beyond $n_{\text{H}_2} \sim 10^{10} \text{ cm}^{-3}$, the H_2 cooling could get suppressed since the rotational and vibrational lines of H_2 start becoming optically thick, but the inefficient cooling still allows the gas to collapse to even higher densities without significantly increasing the temperature (e.g. Omukai & Nishi, 1998; Clark et al., 2011). At very high densities of $n_{\text{H}_2} \sim 10^{14} \text{ cm}^{-3}$, the collision induced cooling from hydrogen molecules is able to cool the gas, despite the high optical depth of the gas (e.g. Ripamonti & Abel, 2004). As the gas quickly becomes optically thick, the collision induced cooling becomes inefficient at densities of 10^{16} cm^{-3} (for e.g. Omukai & Nishi, 1998). As a result, the gas temperature rises leading to H_2 dissociation and resulting in a final gas temperature of ~ 3000 K. The temperature does not rise any further as the energy released from the collapse is spent on dissociating the H_2 molecules. Once all the H_2 is dissociated, the temperature rises again leading to an increase in the thermal pressure that halts the collapse. This results in a *proto-stellar* core of $\sim 0.01 M_\odot$ and a mean density $O(10^{20}) \text{ cm}^{-3}$ within a region of 0.1 AU (Yoshida et al., 2008).

Several hydrodynamical simulations run from cosmological initial conditions have attempted to understand the evolution of the proto-stellar mass that forms at such densities (e.g. Stacy et al., 2012; Greif et al., 2012; Dopcke et al., 2013), which finally results in a Pop III star. The characteristic mass of a Pop III star forming from such metal free gas would depend on the accretion rate that the proto-stellar core can sustain over a given period of time (see Fig. 2.5) which is subject to radiative feedback effects (amongst others) (Hosokawa et al., 2011), setting the current limits on the Pop III stellar masses to $\sim 30 - 100 M_\odot$. These *first* stars produced the *first* metals that polluted the gas in the IGM and ISM and which later led to the formation of the second generation, Pop II stars. The effects of metals ejected as SNe or winds from the first stars highly depends on the mass of the halo or the potential well in which these stars form (Muratov et al., 2012). It is also widely accepted that the first Pop III stars form either as single stars or as clusters of a few stars, but either way, at the end of their brief lifetime they are able to blow out most of the gas from the halo in which they formed, thereby making it highly implausible that the *first galaxies* could be entirely made up of Pop III stars alone (for e.g. Bromm & Yoshida, 2011).

The critical metallicity at which the Pop III stars transition to Pop II stars is still debated, but a value of $Z \sim 10^{-4}$ is often adopted as the transitioning threshold (e.g. see

the review Bromm & Yoshida, 2011). This limit is applicable in the absence of dust grains⁶ where metal cooling can dominate over H₂ cooling owing to the high fractional abundance of metals in the collapsing gas and can lower the characteristic stellar mass to $\sim 10 M_{\odot}$. A ratio of dust mass to gas mass higher than $\sim 10^{-9}$ is critical to the formation of stars with sub-solar masses (Schneider et al., 2011), due to the highly efficient cooling that the dust grains can induce. The formation of Pop II stars can be envisioned as a combination of what happens in case of Pop III and the stars we see today in our local neighbourhood (Pop I). Since the gas that Pop II stars form from is of a metallicity that lies between that of the Pop III and Pop I, their characteristic masses are also higher than those of Pop I but lower than those of Pop III.

Having discussed how the first stars formed in the Universe, we will now overview the pathways to the first SMBHs.

2.2 Seeds of the quasars at $z > 6$

With Becker et al. (2001) reporting the presence of Quasars, believed to be SMBHs, at $z > 5$, the idea of SMBHs only existing in our local neighbourhood suffered a huge paradigm shift. Given that the age of the Universe, t_{age} , at $z = 6$ is ~ 1 Gyr, and that the epoch of first stars is believed to be $z \sim 30$ or $t_{age} \sim 100$ Myr (Tegmark et al., 1997), that leaves only 900 Myr for a SMBH to form and have grown from a stellar seed BH. In order to understand the difficulty in reaching such high masses, it is important to understand the accretion mechanism via which they accumulate matter.

Consider a black hole of mass M , accreting at a radius r . Assuming the matter being accreted is composed of H atoms in a neutral or ionised state, the luminosity, L , resulting from the matter being accreted can now be converted into a *radiation-force*, F_{rad}

$$F_{rad} = \frac{L}{c} \frac{\sigma_T}{4\pi r^2}, \quad (2.42)$$

where σ_T is the Thompson scattering cross section.

The gravitational force exerted on a single H atom being accreted, of mass $\sim m_p$, can be written as

$$F_{grav} = \frac{GMm_p}{r^2}. \quad (2.43)$$

One can define an Eddington limit, the luminosity at which gravitational force exactly equals the force exerted by the radiation, resulting in

$$L_{edd} = \frac{4\pi GMm_p c}{\sigma_T}. \quad (2.44)$$

The above equation can be re-written in order to express the luminosity in terms of the Eddington fraction, f_{edd}

⁶Dust refers to irregularly shaped grains of carbon or silicates.

$$f_{edd} = \frac{L}{L_{edd}}, \quad (2.45)$$

where at $f_{edd} = 1$, the Eddington luminosity limit is reached.

The Eddington limit is often used as the upper-limit⁷ for the efficiency at which a BH can accrete matter.

In order to understand the limiting luminosity better, we can assume that a fraction, ϵ , of the gravitational potential energy of the matter being accreted can be radiated away. The luminosity can then be expressed in terms of ϵ times the rest mass energy of the matter being accreted

$$L = \epsilon \dot{M} c^2. \quad (2.46)$$

Equating the above equation to Eq. 2.45, we get

$$\frac{\dot{M}}{M} = f_{edd} \frac{4\pi G m_p}{\epsilon \sigma_T c}, \quad (2.47)$$

and solving the above differential equation results in

$$M(t) = M_{ini} \exp\left(\frac{f_{edd}}{\epsilon} \frac{t}{450 \text{ Myr}}\right), \quad (2.48)$$

where the Salpeter time, equal to 450 Myr, appears in the denominator of the exponential often also referred to as the *e-folding time*.

Any BH seeding model that attempts to explain the presence of Quasars at $z = 6$ is subject to the accretion equation we derived above and is bound by the time available for growth into a SMBH. The type of BH seeds that can lead to the *first quasars* at $z = 6$ is still unclear, and the next Sections discuss the various ways that have been proposed in order to explain the first Quasars. The aim of the thesis is to decrease the uncertainty that surrounds the seeding models, especially the one of *direct collapse*.

2.2.1 Stellar seeds of quasars

The most intuitive way to explain the first quasars is by considering the BHs that are remnants of Pop III stars as the seeds, and allowing them to grow via gas accretion. Pop III stars with masses in the range $M_* \sim 30 - 100 M_\odot$ and $M_* > 250 M_\odot$ could end up as BHs with similar masses as their stellar progenitors (e.g. Heger & Woosley, 2002). Assuming a stellar BH seed with mass $M_{*,seed} = 100 M_\odot$, let us now look at the possible growth scenarios.

Assume that a Pop III BH forms at $z = 20, 15, 10$, i.e. $t_{age} \sim 200, 300, 500$ Myr respectively. The growth of the BH seeds with $f_{edd} = 1$ and $\epsilon = 0.1$ is plotted in Fig. 2.6. It is clear from the plot that if a Pop III BH forms at $z > 15$ and constantly accretes at

⁷This limit, when exceeded, (usually for short periods) is often referred to as *super-Eddington*.

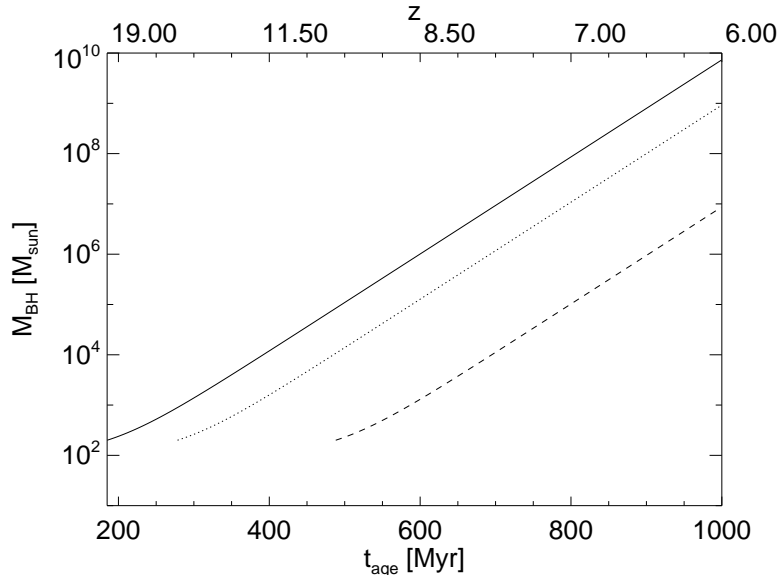


Figure 2.6: Accretion onto Pop III seed BHs formed at $z = 20, 15, 10$ (solid, dotted, dashed lines respectively) via the Eddington formula using $f_{edd} = 1$ and $\epsilon = 0.1$.

$f_{edd} = 1$, it may attain supermassive scales by $z = 6$. However, there are some challenges that this scenario faces, namely

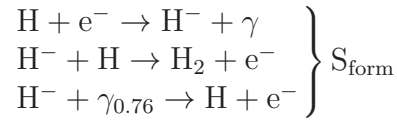
1. Availability of gas: as we saw earlier, the first Pop III stars likely formed in haloes with masses $\sim 10^{5-6} M_{\odot}$ and gas masses in the range $\sim 10^{4-5} M_{\odot}$. After the BH forms and has accreted the gas in the halo, it is unclear as to where the gas required for subsequent accretion comes from. Mergers seem to be a likely solution, however, note that depending on the masses of the merging systems, the merging time scale could be $O(t_{age})$.
2. Sustained accretion for extended periods of time: accretion onto the BH would produce feedback which could heat up the infalling gas, thereby making accretion inefficient. Also, the radiation–feedback from the Pop III star that is the precursor for the BH seed could also induce negative feedback by heating the gas in the surrounding medium.

The main challenge for the stellar seed BH mechanism is the ~ 7 orders of magnitude growth in mass that is required in 700 – 800 Myr. However, if one is to assume a larger seed mass, say $M_{seed} \sim 10^{4-5} M_{\odot}$, then the growth in mass required is only $\sim 4 - 5$ orders of magnitude. The idea of a cluster of young Pop III stars *merging* in order to give rise to a larger seed mass has also been proposed (see the review Volonteri, 2010, and references therein). However, one of the main conditions required by this scenario is that the stars merge before the end of their lifetimes. The typical lifetime for a $100 M_{\odot}$ Pop III star is 3 Myr, therefore, the cluster of Pop III stars must merge within this time and withstand the radiative feedback that the stars might induce in the surrounding region.

2.2.2 Direct collapse seeds of quasars

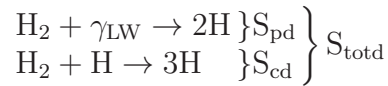
Another idea has been proposed in order to create massive seed BHs out of pristine gas with either no star formation in the previous stages, or a very short lived super-massive (or quasi-star) star phase (Oh & Haiman, 2002). Recall that molecular hydrogen plays a critical role in the cooling of the pristine gas and formation of the first stars (Fig. 2.2) in minihaloes and atomic cooling haloes.

For the sake of the discussion relating to H_2 dissociation, let us collectively label the speed of reactions that compete for H_2 formation that we saw earlier as S_{form}



where $\gamma_{0.76}$ represents a 0.76 eV photon that can photodissociate a H^- molecule.

However, in atomic cooling haloes (i.e. haloes with $T_{\text{vir}} > 10^4$ K), if all⁸ of molecular hydrogen was destroyed, due to for e.g. photodissociation, the only coolant available would be atomic H. In fact, Lyman-Werner (LW) photons with an energy range of 11.2 – 13.6 eV are capable of photo-dissociating H_2 (Haiman et al., 1997) (S_{pd}), besides the collisional dissociation that operates at $n > 10^3 \text{ cm}^{-3}$ (S_{cd})



where γ_{LW} represents a LW photon. These photons are typically produced by young stellar populations, with Pop III stars giving rise to a higher number of LW photons per unit stellar mass than Pop II stars, owing to their higher surface temperatures, i.e. $T_{*,\text{III}} \sim 10^5$ K (Pop III), $T_{*,\text{II}} \sim 10^4$ K (Pop II). The LW radiation is often expressed as a specific intensity, J_{21} , in units of $10^{-21} \text{ erg/s/cm}^2/\text{sr/Hz}$ and the expected global mean in the Universe at $z \sim 10$ is $J_{21} \sim 1$ (Greif & Bromm, 2006; Trenti & Stiavelli, 2009). Since LW radiation is able to dissociate H_2 molecules, it can delay Pop III star formation in pristine minihaloes (Machacek et al., 2001; O’Shea & Norman, 2008). A high level of LW flux, J_{crit} , is required to dissociate a critical fraction of H_2 , in order to make molecular cooling inefficient. The value of J_{crit} depends on the type of stellar population with $J_{\text{crit,III}} \sim 1000 - 10,000$ (from Pop III stars) and $J_{\text{crit,II}} \sim 30 - 100$ (from Pop II stars), owing to the nature of the black-body curves and the amount of 0.76 eV photons produced relative to the LW photons by these stellar populations (Shang et al., 2010; Wolcott-Green et al., 2011). The 0.76 eV photons play a critical role in determining the H_2 fraction where the reaction rate can be expressed as $k_{\text{H}^-,\text{pd}} = \alpha J_{21}$ with $\alpha = 0.1$ for Pop III stars and $\alpha = 2000$ for Pop II stars (see also Sec. 3.2.3 and Omukai et al., 2008). For a fixed number of LW photons, if a large number of 0.76 eV are available in the early stages of gas collapse, where at low number densities the H^- formation is critical to H_2 formation (via the reaction 2.37),

⁸In principle, the molecular hydrogen fraction in the gas needs to be at a subcritical level required to suppress H_2 cooling (Shang et al., 2010).

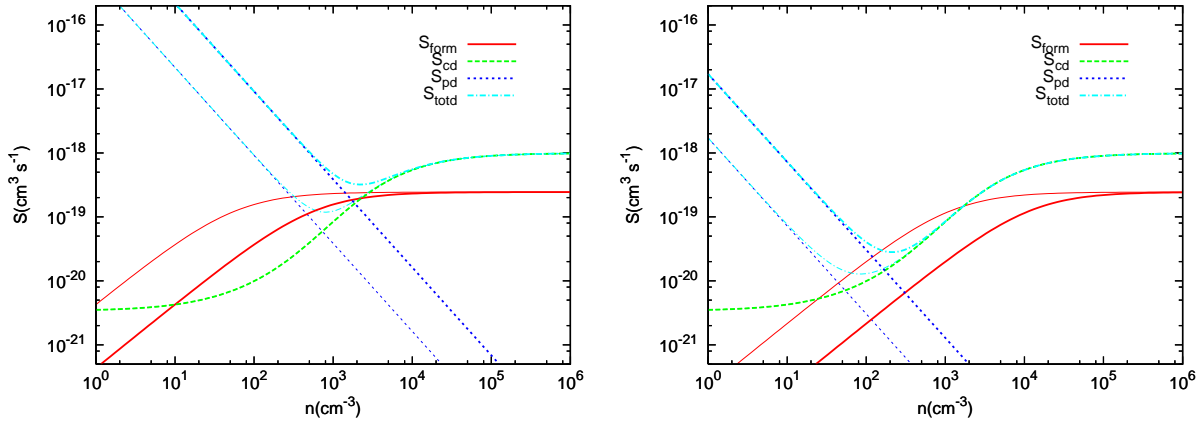


Figure 2.7: The reaction speeds for the net H_2 photodissociation rate, S_{totd} for a Pop III type (left) and Pop II type (right) radiation flux incident on a pristine atomic cooling halo (taken from Shang et al., 2010).

then H_2 formation at later times could be suppressed as a result of H^- dissociation and LW photons dissociating H_2 . This is the reason why from Pop II stars, the J_{crit} required for DC is about 2 orders of magnitude lower than that required from Pop III stars. To illustrate this point further, we show the reaction speeds of H_2 formation and dissociation as computed by Shang et al. (2010) in Fig. 2.7. In the left panel, the S_{totd} is dominated by photodissociation i.e. S_{form} is suppressed by the LW photons (S_{pd}), when finally the S_{cd} effectively kicks in at densities of $> 10^3 \text{ cm}^{-3}$. In the right panel however, the S_{form} is suppressed early on due to the 0.76 eV photons, even though S_{pd} is at a lower level than in the left panel. This effectively results in collisional dissociation kicking in at roughly the same density, and a lower J_{crit} from Pop II type stars.

If a pristine halo is exposed to J_{crit} , it would result in the gas being able to cool to only $\sim 8000 \text{ K}$, as the molecular hydrogen has now been dissociated into atomic hydrogen, thereby resulting in a higher Bonnor–Ebert mass (recall Eq. 2.40), $M_{BE} \sim 10^5 M_\odot$ (for $n = 10^4 \text{ cm}^{-3}$, $T=8000 \text{ K}$). The collapse would proceed isothermally, in the absence of any other coolant and the *entire* gas cloud may collapse provided the the mass is larger than M_{BE} . One can compute the typical accretion rate using the free fall time of the gas cloud, t_{ff} , which can be derived by solving the differential equation

$$m \frac{d^2 r}{dt^2} = - \frac{GMm}{r^2}, \quad (2.49)$$

where m is a test particle experiencing the gravitational force of the cloud with mass M , falling in from the outermost radius of the cloud, r_0 , to the centre. Solving the above equation and writing $M = 4/3\rho_0 r_0^3$, where ρ_0 is the mean density of the cloud, we get

$$t_{ff} = \sqrt{\frac{3\pi}{32Gm_p n}}, \quad (2.50)$$

where n is the number density of H atoms and initially, assuming it to be $\sim 10^4 \text{ cm}^{-3}$ we get $t_{ff} \sim 0.5 \text{ Myr}$. Assuming the gas mass in a typical atomic cooling halo to be $\sim 10^6 M_\odot$, and dividing it by the t_{ff} , one can estimate the accretion rate during collapse, $\dot{M} \sim 1 \frac{M_\odot}{\text{yr}}$, which is 4–5 orders of magnitude higher than what is seen during the formation of Pop III stars. The fate of the gas cloud after the initial state of collapse could take one of the following pathways

1. *Supermassive star* (for e.g. Bromm & Loeb, 2003; Wise et al., 2008; Regan & Haehnelt, 2009; Dotan & Shaviv, 2012; Schleicher et al., 2013)

Early simulations showed that when H_2 cooling is suppressed by a high level of LW radiation, the atomic cooling haloes could accumulate $O(10^4) M_{\text{sun}}$ of gas in the central $\sim 0.1 \text{ pc}$ region with $n > 10^9 \text{ cm}^{-3}$. The subsequent collapse process would lead to even more mass being accumulated in the centre at even higher densities, which hints towards the formation of a supermassive star (SMS). This star would be short lived and could undergo a collapse into a BH with a mass that could be up to 90% of that of the SMS. Recent simulations that are able to probe the gas to densities of $n \sim 10^{18} \text{ cm}^{-3}$ have shown that even in the presence of a turbulent medium, a central compact object of $O(10^6) M_\odot$ could form in the central region, with a diameter of a few A.U., with high accretion rates, thus providing further support for the SMS theory. The SMS, if non-rotating, would gradually release its binding energy and collapse into a DCBH, or withstand collapse, if rotating, and lose a considerable fraction of its mass due to nuclear burning of H and could assume stellar properties at later times.

2. *Quasi star* (see for e.g. Begelman et al., 2006, 2008)

At the very initial stages of collapse in the absence of H_2 , a small amount of atomic cooling gas could accumulate at the centre of the halo which could also be pressure supported against collapse if radiative losses from the accumulating gas are inefficient. This initial state is that of a ‘quasi-star’ (QS). The QS configuration would result in the formation of a small BH with $\sim O(10) M_\odot$, still embedded in the dense gas cloud which is radiation–pressure supported. If a mechanism like ‘bars–within–bars’, where the gas can effectively shed angular momentum, can feed this central BH with high accretion rates, one could imagine that the central BH is fed by super-Eddington accretion and can grow to $\sim 10^{4-6} M_\odot$ depending on the efficiency of the radiative feedback due to accretion and mergers with other galaxies.

3. *The marginally stable disc leading to a DCBH* (see for e.g. Eisenstein & Loeb, 1995; Koushiappas et al., 2004; Lodato & Natarajan, 2006)

In low spin environments, where H_2 cooling has been suppressed, the gas could settle in a disc, lose angular momentum and accumulate to the centre of the disc provided the disc is not too massive and is marginally Toomre–stable. A high spin environment would imply a rotationally supported disc and if the disc is too massive, the centrally–migrating gas clumps could fragment due to their own gravitational torques. This approach relies on a critical accretion rate, for the thin disc approximation, in order

to fuel the central region and get rid of the angular momentum. This approach will be discussed in detail in Chapter 4.

Chapter 3

Are the conditions ever right for direct collapse? ¹

Abstract

We study for the first time the environment of massive black hole (BH) seeds ($\sim 10^{4-5} M_{\odot}$) formed via the direct collapse of pristine gas clouds in massive haloes ($\geq 10^7 M_{\odot}$) at $z > 6$. Our model is based on the evolution of dark matter haloes within a cosmological N -body simulation, combined with prescriptions for the formation of BH along with both Population III (Pop III) and Population II (Pop II) stars. We calculate the spatially-varying intensity of Lyman Werner (LW) radiation from stars and identify the massive pristine haloes in which it is high enough to shut down molecular hydrogen cooling. In contrast to previous BH seeding models with a spatially constant LW background, we find that the intensity of LW radiation due to local sources, J_{local} , can be up to $\sim 10^6$ times the spatially averaged background in the simulated volume and exceeds the critical value, J_{crit} , for the complete suppression of molecular cooling, in some cases by 4 orders of magnitude. Even after accounting for possible metal pollution in a halo from previous episodes of star formation, we find a steady rise in the formation rate of direct collapse (DC) BHs with decreasing redshift from $10^{-3} \text{ Mpc}^{-3} z^{-1}$ at $z = 12$ to $10^{-2} \text{ Mpc}^{-3} z^{-1}$ at $z = 6$. The onset of Pop II star formation at $z \approx 16$ simultaneously marks the onset of the epoch of DCBH formation, as the increased level of LW radiation from Pop II stars is able to elevate the local levels of the LW intensity to $J_{\text{local}} > J_{\text{crit}}$ while Pop III stars fail to do so at any time. The number density of DCBHs is sensitive to the number of LW photons and can vary by over an order of magnitude at $z = 7$ after accounting for reionisation feedback. Haloes hosting DCBHs are more clustered than similar massive counterparts that do not host DCBHs, especially at redshifts $z \gtrsim 10$. Also, the DCBHs that form at $z > 10$ are found to reside in highly clustered regions whereas the DCBHs formed around $z \sim 6$ are more common. We also show that planned surveys with *James Webb Space Telescope* should be able to detect the supermassive stellar precursors of DCBHs.

¹This chapter is a modified and updated version of the study Agarwal et al. (2012)

3.1 Introduction

It is now an established fact that galaxies host black holes (BH) at their centres Gebhardt et al. (2000); Ferrarese & Merritt (2000); Gültekin et al. (2009a) with BH masses ranging from $10^{6-9.5} M_{\odot}$. The most massive BHs or supermassive black holes (SMBH) are believed to fuel quasars observed as early as $z > 6$ (see e.g. Fan et al., 2003, 2006; Willott et al., 2003; Mortlock et al., 2011). This implies that the seeds of these SMBHs must have formed and grown to supermassive scales in the short time before the Universe was even one billion years old. It has also been suggested recently (Treister et al., 2011, T11 here after) that there might be a population of obscured intermediate mass black holes (IMBHs) at $z > 6$ (however also see e.g. Willott, 2011; Fiore et al., 2012, who challenge the claim). However, the origin of these SMBHs or IMBHs in the early Universe is still an open question.

The most obvious way to make the SMBH seeds is from the stellar BHs in the early Universe. Detailed studies have shown that the first generation of stars (Pop III) form from metal-free gas, comprising mainly of atomic and molecular hydrogen at early times (see reviews by Bromm & Larson, 2004; Ciardi et al., 2001, and references therein). Pop III stars with masses in the range $40 M_{\odot} < M_* < 140 M_{\odot}$ and $M_* > 260 M_{\odot}$ collapse into a black hole with $M_{\bullet} = 0.5 - 1 M_*$ (Heger et al., 2003) and accretion of gas onto these stellar BHs offers a natural way to grow SMBHs, given their abundance and early formation times.

This scenario however, has been challenged given that Pop III remnant BHs may not constantly accrete at or near the Eddington limit, which is likely required for $100 M_{\odot}$ seed black holes to reach a mass of $10^9 M_{\odot}$ by $z \sim 6$. Both the radiation from the Pop III progenitor star (e.g. Yoshida, 2006; Johnson & Bromm, 2007; Alvarez et al., 2009) and the radiation emitted in the accretion process itself (e.g. Milosavljević et al., 2009; Park & Ricotti, 2011; Li, 2011), result in feedback which might slow down gas accretion. The constant availability of gas in the halo during the accretion period would also require the haloes to grow rapidly via mergers since episodes of star formation and feedback from supernovae can deplete the gas in such primordial haloes (e.g. Mori et al., 2002). On the other hand, a scenario where the accretion must be super-Eddington for a short period of time has been proposed in order to allow fast BH growth (e.g. Volonteri & Rees, 2005), which could be a result of the inefficient radiative losses due to the trapping of photons in the accretion disc (see e.g. Begelman, 1978; Wyithe & Loeb, 2011).

Another possibility of growing stellar black holes is via mergers of haloes hosting either stars or BHs. A dense cluster or group of stars provides conditions under which frequent mergers can occur, leading to a runaway collapse (Zwart et al., 1999) that result in BHs with masses of around $10^5 M_{\odot}$. Mergers of Pop III seed BHs at high redshifts can also, in principle, build up supermassive BHs (Tanaka & Haiman, 2009), although slingshot effects and merger time scales pose problems for this scenario (see e.g. the reviews by Natarajan, 2011; Volonteri, 2010, and references therein).

An alternative scenario is to make seed BHs with an initial $M_{\bullet} = 10^{4-5} M_{\odot}$ via the direct collapse of pristine gas in haloes with $T_{\text{vir}} \geq 10^4$ K (see e.g. Eisenstein & Loeb, 1995; Oh & Haiman, 2002; Bromm & Loeb, 2003; Koushiappas et al., 2004; Lodato & Natarajan,

2006). The key idea is to keep the haloes free of molecular hydrogen so that the gas collapses isothermally only via atomic hydrogen. For the gas collapse to proceed without fragmenting into stars, it also has to redistribute its angular momentum and various processes have been suggested in order to allow this, as explained below.

In low spin haloes the gas settles down into a disc where the angular momentum can then be redistributed via gravitational instabilities, hence keeping the Toomre parameter close to unity and preventing the disc from further fragmentation (Lodato & Natarajan, 2006, LN06 hereafter). The central core of $M = 10^{4-5} M_{\odot}$, fed by the streams resulting from the non-axisymmetric disc instabilities, ultimately collapses into a BH with a similar mass. An important feature of LN06 is that they explicitly link the dark matter halo properties, like spin and virial temperature, to the properties of the BH seed. Their model predicts the required ratio of the gas temperature to the virial temperature and the maximum halo spin which determines the final mass of the BH seed.

The redistribution of angular momentum can occur via the ‘bars-within-bars’ scenario as explored by Begelman et al. (2006) where the gas collapses into a dense self-gravitating core surrounded by an envelope supported by radiation pressure. The gas finally cools and collapses catastrophically via neutrino emission into a central BH with an intermediate stage of a quasi-star (Begelman et al., 2008).

Spaans & Silk (2006) showed that if the collapse of gas (comprised of atomic H) in such haloes proceeds via an equation of state with a polytropic index larger than unity, Lyman-alpha photons can get trapped in highly dense regions owing to the large optical depth of the medium. The time required for the Lyman-alpha photons to escape the medium becomes larger than the free fall time of the gas which prevents the gas from cooling and forming Pop III stars. Hence, the collapse can result in a massive BH which is of the order of 3 – 20% of the total baryonic mass of such haloes.

Also, Regan & Haehnelt (2009) explored the gas collapse in rare atomic cooling haloes which could in principle host a DCBH in cosmological hydrodynamic simulation. They find cases where the inflow rates are high enough ($> 1 M_{\odot}\text{yr}^{-1}$) to allow for the formation of massive BH seeds.

All these scenarios end in a *direct collapse* black hole (DCBH) with $M_{\bullet} \sim 10^{4-6} M_{\odot}$. Another alternative scenario includes the formation of a supermassive star (SMS) in an intermediate step on the way to the formation of a DCBH (Begelman, 2010). For this to occur the gas does not only need to be free of H_2 and metals but the accretion rate onto the SMS needs to be high enough to allow the rapid growth to $10^{4-6} M_{\odot}$ (Begelman, 2010; Johnson et al., 2012a).

Although these scenarios take place in haloes with $T_{\text{vir}} > 10^4$ K, which are mostly composed of atomic hydrogen, molecular hydrogen can form in these haloes when the densities are high enough to allow three-body hydrogen interactions. Such high particle densities are found at the halo centre and during the end stages of gas collapse. Hence these scenarios require a critical level of H_2 photo-dissociating Lyman Werner (LW) radiation ($h\nu = 11.2 - 13.6$ eV) in order to keep the abundance of H_2 molecules very low, as otherwise H_2 cooling will lower temperatures to $T \approx 200$ K, thereby reducing the Jeans mass and leading to fragmentation of the gas cloud, which would ultimately result in star

formation instead of a central BH seed.

The main challenge in all the above DCBH formation scenarios is to reach the critical level of Lyman Werner radiation required to dissociate H_2 molecules in the halo. Typical levels of a smooth uniform LW background, J_{bg} , range from 0.001–0.1 (where J is expressed in units of $10^{-21} \text{ erg s}^{-1} \text{ cm}^{-2} \text{ Hz}^{-1} \text{ sr}^{-1}$) and depends on the stellar density at a given redshift (Greif & Bromm, 2006), whereas the critical value, J_{crit} , required for direct collapse is ~ 30 (from Pop II) and ~ 1000 (from Pop III) (Shang et al., 2010; Wolcott-Green et al., 2011, CS10 and WG11 hereafter). It has been argued that a halo can be exposed to a radiation level higher than J_{crit} if it lives close to a star forming region (Dijkstra et al., 2008, D08 hereafter). They use an analytical approach employing Poisson statistics and extended Press-Schechter mass functions to model their halo distribution which accounts for clustering of the DM haloes and the spatial distribution of LW sources.

Previous studies of DCBH formation have either assumed a spatially constant LW background (Regan & Haehnelt, 2009; Petri et al., 2012) or a spatially varying LW background using analytical prescriptions for clustering of sources D08. The latter study showed that the clustering of sources plays a crucial role in elevating the levels of LW radiation above the critical value required for DCBH formation. While it is important to model the clustering of sources properly, it is also crucial to know whether a halo, which is exposed to the critical level of LW radiation, had previous episodes of star formation which enriched the gas in the halo with metals. In contrast to D08, Petri et al. (2012) attempted to model the merging histories of haloes using Monte-Carlo merger trees however, they did not account for the self consistent build up of the spatially varying LW radiation field.

Due to the importance of LW feedback at high redshifts, some recent studies have explored the effects of LW radiation on early structure formation (e.g. Kuhlen et al., 2011), Pop III star formation (Safranek-Shrader et al., 2012; Whalen et al., 2008; Ricotti, 2008), the evolution of pair instability supernovae (Wise, 2012; Hummel et al., 2011) and also on the formation of SMBH seeds by Pop III stars (Devecchi et al., 2012).

In this paper we simultaneously follow the build up of the spatially varying LW radiation field as well as track the enrichment histories of dark matter (DM) haloes in a cosmological DM only, N -body simulation using a semi-analytical model (SAM). We investigate the conditions under which the LW intensity seen by an individual halo will reach a value $\gtrsim J_{\text{crit}}$ and we describe the resulting consequences for the formation of seed BHs via direct collapse. The aim of our work is to determine the plausibility of the existence of DCBH sites and probe the clustering features of such haloes.

This paper is organised as follows. We describe the simulation and our model in the next section (Sec. 4.2) followed by which the results of our work are presented in Sec. 4.3. The observability of the supermassive stellar seeds of DCBHs by the *James Webb Space Telescope* (JWST) is discussed in Sec. 3.4. Finally we present the summary and discussion of our work in Sec. 3.5.

3.2 Methodology

In the following section(s) we describe our SAM that models the build up of the LW radiation field on top of our N -body simulation. We model both Pop III and Pop II star formation and include a prescription for the evolution of the star forming and non-star-forming gas within an individual halo. This allows us to track the star formation histories of the haloes and account for the LW photon travel times which is needed in order to self consistently model the global and spatial level of the LW radiation at each point in our box.

3.2.1 The N -body simulation

We use a DM only N -body simulation with 768^3 particles in a $3.4 \text{ Mpc} h^{-1}$ co-moving periodic box using the GADGET code (Springel et al., 2001; Springel, 2005). We assume a Λ CDM cosmology with $\Omega_0 = 0.265$, $\Omega_b = 0.044$, $\Omega_\Lambda = 0.735$, $h = 0.71$ and $\sigma_8 = 0.801$ consistent with the WMAP 7 results (Komatsu et al., 2011). The resulting individual DM particle mass is $6500 M_\odot h^{-1}$. Merger trees are constructed on the SUBFIND output (Springel et al., 2001) using the same method as in Springel et al. (2005). Information on each subhalo includes its mass as assigned by SUBFIND, along with its host friends-of-friends (FoF) mass. The smallest resolved DM halo contains at least 20 particles, which corresponds to $1.3 \times 10^5 M_\odot h^{-1}$. We run the simulation down to $z = 6$ and the snapshots are taken a few tens of Myr apart. As in Springel et al. (2005) and Croton et al. (2006), our merger trees are based on subhaloes. Note that we shall use the term *halo* instead of *subhalo* in the remainder of this work for the sake of simplicity.

At a given snapshot, we label the haloes as *minihaloes* and *massive haloes* if their virial temperature is $2000 \text{ K} \leq T_{\text{vir}} < 10^4 \text{ K}$ and $T_{\text{vir}} \geq 10^4 \text{ K}$, respectively. Also, J or the combination of the variable with any superscript/subscript explicitly implies J_{LW} in units of $10^{-21} \text{ erg}^{-1} \text{ s}^{-1} \text{ cm}^{-2} \text{ Hz}^{-1} \text{ sr}^{-1}$ unless specified otherwise.

We define the infall mass, M_{infall} , of the halo as its mass at the last snapshot where it was the most massive subhalo within its FoF halo. We did this by tracking the halo's main progenitor branch back in time. The infall redshift is defined as the redshift when the infall mass was found.

We use the relations from Barkana & Loeb (2001) for the virial temperature, virial radius, R_{vir} , and circular velocity, V_c , of a halo

$$T_{\text{vir}} = 1.98 \times 10^4 \left(\frac{\mu}{0.6} \right) \left(\frac{M_{\text{infall}}}{10^8 h^{-1} M_\odot} \right)^{\frac{2}{3}} \left(\frac{\Omega_0}{\Omega_m(z)} \frac{\Delta_c}{18\pi^2} \right)^{\frac{1}{3}} \left(\frac{1+z}{10} \right) \text{ K} , \quad (3.1)$$

$$R_{\text{vir}} = 0.784 \left(\frac{M_{\text{infall}}}{10^8 h^{-1} M_\odot} \right)^{\frac{1}{3}} \left(\frac{\Omega_0}{\Omega_m(z)} \frac{\Delta_c}{18\pi^2} \right)^{-\frac{1}{3}} \left(\frac{1+z}{10} \right)^{-1} \text{ kpc} , \quad (3.2)$$

$$V_c = \left(\frac{GM_{\text{infall}}}{R_{\text{vir}}} \right)^{1/2} , \quad (3.3)$$

where μ is the mean molecular weight (1.22 for neutral primordial gas), Ω_0 is the matter density of the Universe at $z = 0$, $\Omega_m(z)$ is the matter density of the Universe as a function of redshift and Δ_c is the collapse over-density and z denotes the infall redshift as computed from our trees.

3.2.2 Star formation

In order for the first star to form out of the gas in a virialised pristine halo, the cooling time, t_{cool} , for the gas must be less than the Hubble time, t_{Hubble} . The primordial gas mostly comprises of either atomic or molecular hydrogen and the cooling time depends on their respective cooling functions. Atomic hydrogen cooling is effective at $T > 10^4$ K whereas molecular cooling can operate at lower temperatures. In our model, since we probe the universe at $z \leq 30$, we use the results from the study by Tegmark et al. (1997) which showed that the critical fraction of H_2 molecules required in order to satisfy the condition $t_{\text{cool}} < t_{\text{Hubble}}$ is found in haloes with $T_{\text{vir}} \sim 2000$ K at $z = 25$. Hence, the first star to form from a pristine gas cloud would be a Pop III star forming in a minihalo. The metals ejected from the first Pop III star would be enough to pollute the gas and Pop II stars could form subsequently in the same halo (e.g. Maio et al., 2010). We discuss the Pop III and Pop II star formation in more detail in the following sections.

As explained above, since it is critical to resolve minihaloes of mass $\sim 10^{5-7} M_\odot$, this requirement limits the volume that we can probe with sufficient resolution in our study. We plot the mass functions of the FoF and subhaloes in our work at $z = 6$ in the Appendix.

Pop III stars

In our model, we allow a single episode of instantaneous Pop III star formation in pristine haloes with $T_{\text{vir}} \geq 2000$ K (Tegmark et al., 1997; Maio et al., 2010). Here, we consider a halo to be pristine if none of its progenitors have hosted a star in the past. In addition, our implementation of LW feedback, as explained in Sec. 3.2.3, regulates which pristine haloes form Pop III stars. Hence the non-Pop III-forming minihaloes can later to grow into pristine massive haloes.

We assume a Salpeter IMF (Salpeter, 1955) with a mass range between 100 and 500 M_\odot and assume that one Pop III star forms per minihalo (see e.g. Bromm & Larson, 2004). However, in massive pristine haloes ($T_{\text{vir}} \gtrsim 10^4$ K) we form 10 stars following a Salpeter IMF, with mass cut offs at 10 and 100 M_\odot (e.g. Greif et al., 2008; Johnson et al., 2008; Wise & Abel, 2008). Our choice of IMFs and mass cut-offs in both minihaloes and massive haloes is primarily to maximise the LW output from the stars. Forming multiple lower mass stars as opposed to a single very massive star gives an upper limit to the amount of LW radiation that can be emitted from a massive pristine halo as, for instance, the number of LW photons produced by five 100 M_\odot stars is larger than for one 500 M_\odot star (see Sec. 3.2.4).

Since the formation time for a Pop III star is few Myr (e.g. Bromm et al., 2009) and our snapshots are ≈ 10 Myr apart, Pop III stars are assigned a time of birth and distributed

uniformly in the time interval between two subsequent snapshots (see Appendix). The masses of individual stars within a pristine halo are generated randomly following the respective IMFs assumed.

Pop II stars

The second generation of stars, Pop II, is also expected to exist at high redshifts within metal-enriched regions (e.g. Wise & Abel, 2008; Greif et al., 2010). These stars are metal rich as compared to Pop III but have metallicities much smaller than the solar metallicity, Z_{\odot} . The metals ejected from Pop III stars pollute the host and neighbouring haloes via stellar and SN winds (Mori et al., 2002; Maio et al., 2011). Any further collapse of the polluted gas in the haloes would result in cooling to lower temperatures, thereby reducing the Jeans mass and forming metal-enriched stars with lower masses than the Pop III stars (e.g. Clark et al., 2008; Smith et al., 2009). The critical metallicity at which the transition occurs from Pop III to Pop II ranges from 10^{-4} to $10^{-6} Z_{\odot}$ (e.g. Frebel et al., 2007). For simplicity, we consider a halo that has hosted a Pop III star (or merged with a halo hosting or having hosted a Pop III or Pop II star) polluted with metals and a possible site for Pop II star formation (see e.g. Johnson, 2010).

Since metals are the coolants required for making Pop II stars, we assume that a large enough potential well would be required to constrain the metals ejected from Pop III SNe and additionally add a constrain by setting the threshold halo mass² for Pop II star formation to $10^8 M_{\odot}$ (e.g. Kitayama et al., 2004; Whalen et al., 2008). Within these candidate haloes, we assume that the baryons can exist in either of the three phases i.e. non-star-forming gas, star-forming gas or stars. Below we describe the transition between these phases which ultimately regulates the Pop II star formation in a halo.

- *Non-star-forming gas phase:* We assume in our model that once a DM halo crosses our resolution limit of 20 particles, it is initially comprised of non-star-forming gas, $M_{\text{hot}} = f_{\text{b}} M_{\text{DM}}$, where $f_{\text{b}} = 0.16$ is the universal baryon fraction and M_{DM} is the halo's current DM mass.

While the DM halo grows between two snapshots, we add non-star-forming gas to the halo by calculating the accretion rate, \dot{M}_{acc} , defined as

$$\dot{M}_{\text{acc}} \equiv \frac{f_{\text{b}} \Delta M_{\text{DM}} - M_{*,\text{p}} - M_{\text{out,p}}}{\Delta t}, \quad (3.4)$$

where ΔM_{DM} is amount by which the DM halo grows between two snapshots which are Δt apart, $M_{*,\text{p}}$ and $M_{\text{out,p}}$ represent the total stellar mass and net mass lost in previous SN outflows summed over the incoming merging haloes respectively.

²See Section 3.5 for a critical view on how the choice of the Pop II threshold mass sets the clock for DCBH formation.

- *Star forming gas phase:* In order for the gas to form stars, it must cool and collapse within the halo. We model the transition from the non-star-forming gas phase to the star-forming gas phase, M_{cold} , by allowing M_{hot} to collapse over the dynamical time of the halo, $t_{\text{dyn}} = \frac{R_{\text{vir}}}{V_c}$. This estimate is justified by the fact that at such high redshifts, the radiative-cooling time is shorter than the dynamical time of the halo.
- *Star formation law:* We then model the Pop II star formation via a Kennicutt-type relation (Kennicutt, 1998)

$$\dot{M}_{*,\text{II}} = \frac{\alpha}{0.1 t_{\text{dyn}}} M_{\text{cold}} , \quad (3.5)$$

where α is the star formation efficiency (SFE). The factor $0.1 t_{\text{dyn}}$, which is the star formation time scale, is motivated by Kauffmann et al. (1999); Mo et al. (1998) .

Local observations indicate an $\alpha \sim 0.2$, however, at this stage it is not clear if this also holds at high redshifts ($z > 6$), (Khochfar & Silk, 2011). We therefore treat α as a free parameter and normalise our model to the observations of the cosmic SFRD at $z \gtrsim 6$.

- *Outflows:* In addition to star formation, we also consider the SN feedback processes in a star forming halo. We model the outflow rate of gas from a Pop II star forming halo via the relation

$$\dot{M}_{\text{out}} = \gamma \dot{M}_{*,\text{II}} , \quad (3.6)$$

where

$$\gamma = \left(\frac{V_c}{V_{\text{out}}} \right)^{-\beta} . \quad (3.7)$$

The functional form of γ is taken from Cole et al. (2000). We normalise the parameters in Eq. 3.7 to the results of the high resolution hydrodynamical simulations of the high redshift Universe (Dalla Vecchia and Khochfar 2012, in prep) and for the halo mass range considered in this work. This yields an outflow velocity $V_{\text{out}} = 110 \text{ km s}^{-1}$ and $\beta = -1.74$ resulting in typical values of $\gamma \approx 20$. We assume that the outflows are generated in the star-forming gas phase and hence M_{out} is subtracted from M_{cold} .

- *Implementation:* Each time interval between two consecutive snapshots, Δt , is divided into 100 smaller intervals and the following set of coupled differential equations (along with Eqs. 3.4, 3.5 and 3.6) for the individual baryonic components are numerically solved over the small time steps:

$$\dot{M}_{\text{cold}} = \frac{M_{\text{hot}}}{t_{\text{dyn}}} - \dot{M}_{*,\text{II}} - \dot{M}_{\text{out}} , \quad (3.8)$$

$$\dot{M}_{\text{hot}} = -\frac{M_{\text{hot}}}{t_{\text{dyn}}} + \dot{M}_{\text{acc}} . \quad (3.9)$$

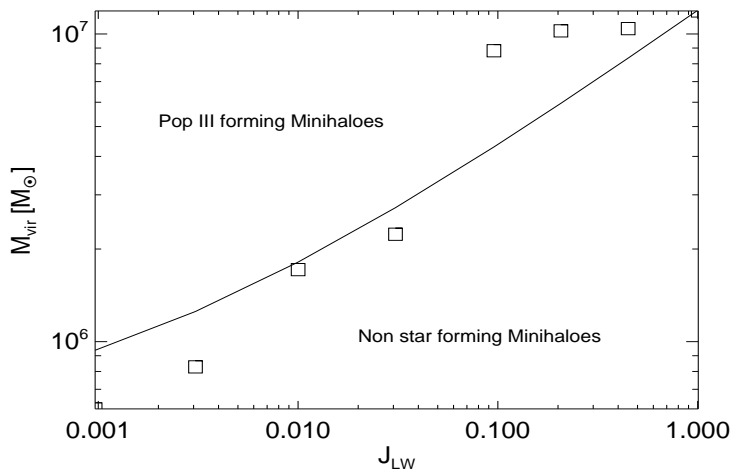


Figure 3.1: The fit used in our model based on the O’Shea & Norman (2008), Fig. 3(c) (square-symbols) which determines the minimum mass of a pristine minihalo that can host a Pop III star for a given level of external LW radiation it is exposed to. For a metal-free minihalo exposed to a given J_{LW} , if its mass lies above the line it is considered Pop III star forming. The solid line represents Eq. 3.10.

3.2.3 Impact of LW radiation on star formation and direct collapse

Once the first generation of stars form in the Universe, the effects of LW radiation become important for subsequent star formation (e.g. Haiman et al., 2000; Omukai, 2001). Even a small, uniform $J_{LW} \approx 0.01$ from these stars can affect Pop III star forming minihaloes by dissociating a fraction of the H_2 molecules and preventing the gas from cooling and collapsing (Machacek et al., 2001; Yoshida et al., 2003; Wise & Abel, 2007; O’Shea & Norman, 2008). The amount of H_2 molecules that can be dissociated depends directly on the LW background it is exposed to.

The minimum mass, M_{crit} , of a pristine halo in which the gas is able to cool, collapse and form Pop III stars in the presence of a given external LW radiation intensity can be approximated by

$$M_{crit} = \psi \left(1.25 \times 10^5 + 8.7 \times 10^5 (4\pi J_{LW})^{0.47} \right), \quad (3.10)$$

where the expression within the brackets is the functional fit to the numerical simulations carried out by Machacek et al. (2001). The correction factor ψ has been set to 4 following the higher resolution simulations of O’Shea & Norman (2008), as shown in Figure 3.1.

One might argue from Fig. 3.1 that $J_{LW} = 1$ is sufficient to set the threshold mass to $10^7 M_{\odot}$, which is the mass beyond which pristine haloes can cool via atomic hydrogen and hence, direct collapse should ensue. However, detailed simulations by CS10 and WG11 show that only the H_2 molecules in the outer regions of such haloes are dissociated and a

considerable fraction of molecular hydrogen ($\sim 10^{-3}$) still exists in the central region of the halos in the presence of such low levels of J_{LW} . In order to prevent star formation in the central parsec region of the halo, it is essential to bring down the H_2 fraction in the gas to 10^{-8} which can be achieved by a $J_{\text{crit}}^{\text{III}} = 1000$ from Pop III stars (WG11) or $J_{\text{crit}}^{\text{II}} = 30 - 300$ from Pop II stars (CS10). The difference in the values of J_{crit} for Pop III and Pop II stars is due to the difference in the spectral shapes of the two stellar populations. As shown by CS10, the lower value of $J_{\text{crit}}^{\text{II}}$ can be partly attributed to the fact that the H^- dissociation rate from Pop II stars is $\approx 10,000$ times larger than that from Pop III stars, due to the softer shape of the Pop II spectrum at 0.76 eV. Since, H^- is a precursor to H_2 formation, destruction of H^- is critical as it results in a lower rate of H_2 production.³

Thus, if a metal free halo with $T_{\text{vir}} > 10^4$ K is exposed to a critical level of LW radiation, a direct collapse can ensue. In this scenario, the cooling is suppressed and the gas stays at $\approx 8000\text{K}$. Due to the large Jeans mass and high accretion rates that these high temperatures imply, a SMS forms and subsequently collapses into a BH (e.g. Bromm & Loeb, 2003; Johnson et al., 2012a). The central BH then continues to accrete, embedded in an envelope of gas, at super-Eddington efficiencies reaching a quasi-star state and collapsing into a $M_{\bullet} = 10^{4-5} M_{\odot}$ black hole (Begelman et al., 2008).

To summarize, only metal-free minihaloes with masses larger than M_{crit} (see Eq. 3.10) are considered to be Pop III star-forming. Also, if these minihaloes are exposed to a $J_{\text{LW}} \geq 1$ then they are considered to be non Pop III star-forming. The metal-free massive haloes still make Pop III stars irrespective of J_{LW} , given that $J_{\text{LW}} < J_{\text{crit}}$ otherwise they can be considered to be DC candidates. Also, the Pop II haloes are unaffected by any value of J_{LW} since they are polluted by previous generations of stars, have $M_{\text{infall}} > 10^8 M_{\odot}$ and the coolants are metals. Therefore, the Pop II star-forming criteria for these haloes is that $M_{\text{infall}} > 10^8 M_{\odot}$ and that the halo has hosted stars previously or has undergone a merger with a previously star-forming halo.

Hence, for pristine minihaloes, i.e. haloes with masses in the range corresponding to $2000 \leq T_{\text{vir}} < 10^4$ K,

$$\left. \begin{array}{l} M \geq M_{\text{crit}} \\ J_{\text{LW}} < 1 \end{array} \right\} \text{Pop III}$$

The other pristine minihaloes that do not satisfy the above conditions can not form Pop III stars.

For pristine massive haloes i.e. haloes with masses corresponding to $T_{\text{vir}} \geq 10^4$ K,

$$J_{\text{LW}} < J_{\text{crit}} \left. \right\} \text{Pop III}$$

$$J_{\text{LW}} \geq J_{\text{crit}} \left. \right\} \text{DCBH}$$

³ H^- is dissociated by the following photoreaction:



The dissociation rate can be written as $k_{28} = 10^{-10} \text{ s}^{-1} \alpha J_{\text{LW}}$. Here, $\alpha_{\text{III}} = 0.1$ for Pop III stars and $\alpha_{\text{II}} = 2000$ for Pop II stars. Since H^- can lead to H_2 formation, this reaction is of prime importance in order to keep the gas at a low H_2 fraction.

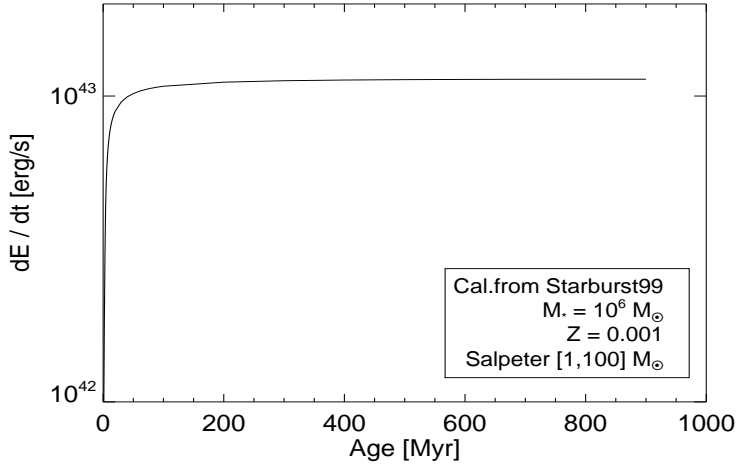


Figure 3.2: Emission in the LW band from a Pop II population as a function of its age computed using the data from STARBURST99 catalogue (Leitherer et al., 1999, Fig. 8e).

3.2.4 J_{LW} calculation

We describe our calculation of the mean and local LW intensities from both the Pop III and Pop II stellar populations in this section.

Mean J_{LW} calculation

The first stellar populations in the Universe mark the onset of the ultra-violet (UV) background which has a negative effect on star formation as described in the previous sections. The LW photon horizon is larger than our box size (~ 10 Mpc, Haiman et al., 2000). Therefore the contribution to the background must come also from outside our simulated volume. In order to account for this, we assume that the SFRD in our volume is representative of a larger cosmological volume. The mean LW background in our volume, is then assumed to exist everywhere in the Universe and is assumed to be the minimum level of LW radiation that a halo is exposed to at any given redshift. It can be computed following the formulae in Greif & Bromm (2006):

$$J_{\text{bg}}^{\text{III}} \simeq f_{\text{esc}} \frac{hc}{4\pi m_{\text{H}}} \eta_{\text{LW}}^{\text{III}} \rho_{*}^{\text{III}} (1+z)^3, \quad (3.12)$$

$$J_{\text{bg}}^{\text{II}} \simeq f_{\text{esc}} \frac{hc}{4\pi m_{\text{H}}} \eta_{\text{LW}}^{\text{II}} \rho_{*}^{\text{II}} (1+z)^3, \quad (3.13)$$

where f_{esc} is the escape fraction of LW photons from the halo, $\rho_{*}^{\text{III}}, \rho_{*}^{\text{II}}$ denote the comoving density of Pop III and Pop II stars respectively at the given redshift z , η_{LW} is the number

Table 3.1: Functional fits used to compute the radiation output and age of Pop III stars. Values are taken from Schaerer (2002) for a zero metallicity, no mass loss case.

X	a₀	a₁	a₂	a₃
age (Myr)	9.785	-3.759	1.413	-0.186
Q_{H₂}	44.03	4.59	-0.77	-
Q_H	43.61	4.90	-0.89	-

of LW photons per stellar baryon ($\eta_{\text{LW}}^{\text{III}} = 10^4$ and $\eta_{\text{LW}}^{\text{II}} = 4 \times 10^3$ for the assumed IMFs in our study and as in Greif & Bromm, 2006) and h , c , m_{H} are the Planck's constant, speed of light and mass of a hydrogen atom respectively. In our model, the parameters ρ_{*}^{III} , ρ_{*}^{II} are computed by checking if a star or stellar population is active at the current snapshot. Each stellar source in our model is given a time of birth, which is the epoch at which the star is formed and a lifetime depending upon the mass (see Appendix for more details).

Spatial variation of J_{LW}

It is important to note that Eqs. 3.12 and 3.13 are valid for a mean, uniform LW background. However, it is possible that a halo would have some stellar sources in neighbouring haloes which would produce levels of J_{LW} higher than the global mean value, which would depend on the clustering scale of haloes (Ahn et al., 2009, KA09 hereafter).

In order to calculate the effects of a spatially varying Lyman Werner specific intensity from individual Pop III stars, we write

$$J_{\text{local}}^{\text{III}} = \frac{f_{\text{esc}}}{\pi} \frac{h\nu_{\text{avg}}}{\Delta\nu_{\text{LW}}} \frac{Q_{\text{LW}}}{4\pi d^2}, \quad (3.14)$$

were $h\nu_{\text{avg}}$ is the average energy of a photon emitted from a Pop III star in the LW band, $\Delta\nu_{\text{LW}}$ is the difference in the maximum and minimum value of the LW frequency range, d is the luminosity distance, and Q_{LW} (expressed as; $Q_{\text{LW}} = Q_{\text{H}_2} - Q_{\text{H}}$) is the number of photons produced per second in the LW energy range. The factor of π in Eq. 3.14 ($\frac{f_{\text{esc}}}{\pi}$) arises from the conversion of the flux into specific intensity, assuming that each Pop III star is a uniform bright sphere (Rybicki & Lightman, 1986). The specific values that we use for these parameters in the case of Pop III stars have been computed using the functional fits from Schaerer (2002) where they track the evolution of stars with different masses and metallicities in their models. They express a given parameter X (see Table 3.1) as a function of the stellar mass M_* , as follows:

$$\log(X) = a_0 + a_1 m + a_2 m^2 + a_3 m^3, \quad (3.15)$$

where $m = \log(\frac{M_*}{M_{\odot}})$.

For the contribution of LW photons from Pop II stellar sources, since we only form a total mass in Pop II stars ($M_{*,\text{II}}$, see section 3.2.2), we calculate Pop II properties using

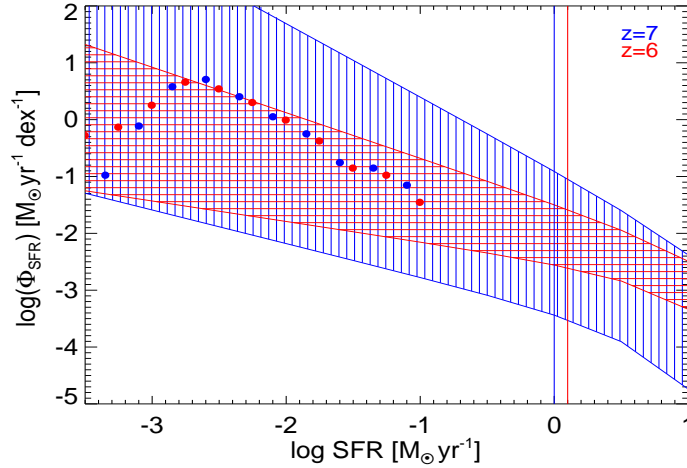


Figure 3.3: Comparison between the SFR-function as computed from S12 and our work. The Φ_{SFR} bounds at $z = 6$ and 7 as computed from S12 are represented by the red and blue regions whereas the data from our simulation is marked as the red ($z = 6$) and blue ($z = 7$) filled circles. The current observational surveys are able to probe the SFRs rightwards of the vertical lines denoting $\text{SFR} \sim 1 M_{\odot} \text{ yr}^{-1}$ (e.g. Smit et al., 2012).

the data⁴ obtained from the STARBURST99 catalogue. We integrated the curve(s), in the LW range to obtain a function \dot{E} which is the energy per unit time (in units of erg sec^{-1}) emitted by a $10^6 M_{\odot}$ Pop II stellar population as a function of the age, as shown in Fig. 3.2. We then calculate

$$J_{\text{local}}^{\text{II}} = \frac{f_{\text{esc}}}{\pi} \frac{\dot{E}}{\Delta\nu_{\text{LW}}} \frac{M_{6,*,\text{II}}}{4\pi d^2}, \quad (3.16)$$

where $M_{6,*,\text{II}}$ is the mass of the stellar population normalised to $10^6 M_{\odot}$. Similar to Eq. 3.14, the factor of π in Eq. 3.16 ($\frac{f_{\text{esc}}}{\pi}$) arises from the conversion of the flux into specific intensity, assuming that the Pop II stellar population is a uniform bright sphere (Rybicki & Lightman, 1986). We form Pop II stars following the prescriptions described in Sec. 3.2.2. As discussed in Section 3.2.4, we assume each halo is exposed to a minimum level of $J = J_{\text{bg}}$ calculated in each of our runs at each snapshot. We then add up the LW contribution from each star on top of the background to get the total value of the LW radiation that a halo is exposed to. This slightly overestimates the LW contribution by a factor of less than a few percent. However as we will show later this will not impact our results. To summarise, we have

$$J^{\text{III}} = J_{\text{bg}}^{\text{III}} + J_{\text{local}}^{\text{III}}, \quad (3.17)$$

⁴ The data from STARBURST99, Fig. 7e assumes a Salpeter IMF with a mass cut off at $1,100 M_{\odot}$, instantaneous star formation, total stellar mass = $10^6 M_{\odot}$, metallicity of $Z = 0.001$ and no nebular emission. These parameters are the closest to a Pop II stellar population.

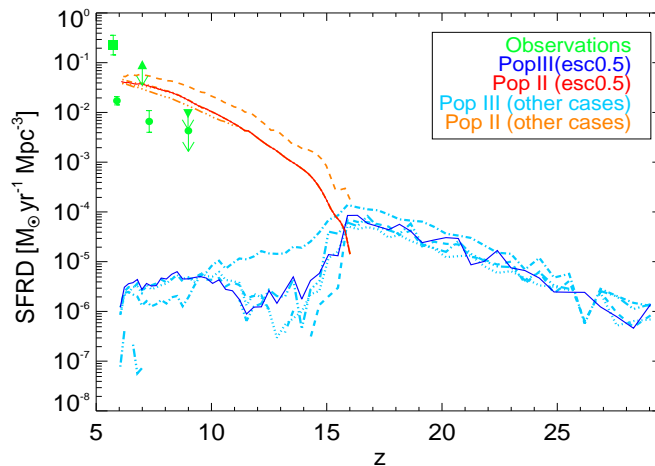


Figure 3.4: SFRD computed using the methods described in Sec. 4.2 for all the cases in our work (see Table. 4.1). Solid, dotted, dashed, dash-dot-dash and dash-double-dot-dash represent the cases *esc0.5*, *esc1.0*, *esc0.5HSFE*, *esc0.1* and *esc0.5reion* respectively. The green square, upright triangle, inverted triangle and circles represent observational data from Hopkins (2004), Mannucci (2007), Bouwens et al. (2008) and Laporte et al. (2012) respectively.

$$J^{\text{II}} = J_{\text{bg}}^{\text{II}} + J_{\text{local}}^{\text{II}} , \quad (3.18)$$

$$J_{\text{total}} = J^{\text{III}} + J^{\text{II}} . \quad (3.19)$$

The quantity J_{total} is only used for determining if the pristine minihaloes can host Pop III stars (see Fig. 3.1). In their work, O’Shea & Norman (2008) analysed the gas collapse within haloes in the presence of a J_{LW} flux. The photons could be coming from Pop II, Pop III or both as long as the photons are in the correct energy band, hence Eq. 3.19 is valid for analysing pristine minihaloes for Pop III star formation.

On the other hand, due the importance of the spectrum at lower energies for the dissociation of H^- , the quantities J^{III} and J^{II} are used to determine if the gas in the halo can undergo DC by comparing the values to $J_{\text{crit}}^{\text{III}}$ and $J_{\text{crit}}^{\text{II}}$ respectively.

3.2.5 Escape fraction of LW radiation and reionization feedback

Recent studies (Wise & Cen, 2009; Yajima et al., 2011; Paardekooper et al., 2011) have shown that the escape fraction for UV photons could vary with the parent halo mass, however, the precise values of LW escape fractions from haloes is still unclear. One might argue that once a pristine halo has hosted a Pop III star (or even a Pop II stellar cluster), most of the H_2 is depleted in the halo and the LW photons should, in principle, escape the halo unobstructed, implying $f_{\text{esc,halo}} \simeq 1.0$ (KA09). However, the stars (which form in dense environments within the halo) are expected to be surrounded by molecular hydrogen,

hence implying a $f_{\text{esc,halo}} < 1.0$. Previous studies, (Ricotti et al., 2001; Kitayama et al., 2004) have found that the minimum escape fraction for LW photons can be 0.1 but can also reach values of $\gtrsim 0.8$ in minihaloes.

In addition to the $f_{\text{esc,halo}}$, the optical depth, τ_{LW} , of the inter-galactic medium (IGM) would also impact the number of LW photons reaching a neighbouring halo. Ciardi et al. (2000) find that, typically, $\tau_{\text{LW}} \lesssim 3$, and including this in our calculations would imply an additional factor of $e^{-\tau_{\text{LW}}}$ in Eqs. 3.12, 3.13, 3.14 and 3.16. Note that effectively, the f_{esc} used in our work can be viewed as a degenerate combination of an escape fraction of LW photons from the halo, $f_{\text{esc,halo}}$, and the optical depth of the IGM i.e. $f_{\text{esc}} = f_{\text{esc,halo}} \times e^{-\tau_{\text{LW}}}$.

Given the uncertainty in $f_{\text{esc,halo}}$ and τ_{LW} , we chose three cases to bracket the range of possibilities: $f_{\text{esc}} = 0.1, 0.5, 1.0$. We also ran a case for our model in which we implemented an additional reionisation feedback from hydrogen-ionising photons by setting a circular velocity threshold of 20 km s^{-1} for all the haloes with $T_{\text{vir}} > 10^4 \text{ K}$ at $6 < z < 10$. This choice is motivated by the work of Dijkstra et al. (2004) where they study the gas collapse in haloes under a photo-ionising flux and find that a halo must be above a certain mass threshold (characterised by circular velocity in their work) to allow for at least half of the gas to undergo collapse. Other studies (e.g. Okamoto et al., 2008; Mesinger & Dijkstra, 2008) have also looked into the feedback process and have found similar mass thresholds.

3.2.6 Model normalisation

For our fiducial case, esc0.5, we set $f_{\text{esc}}=0.5$ for the LW radiation, $\alpha=0.005$ and implement LW feedback in the model. The choice of α is made in order to match the observations of the cosmic SFRD at $z \gtrsim 6$. We normalise our free model parameter for the star formation efficiency against recent observations of the SFRD (Hopkins, 2004; Mannucci, 2007; Bouwens et al., 2008; Laporte et al., 2012). Due to the sensitivity limits of present surveys, the range in star formation rates probed in our simulations is not observed. Thus we chose the fiducial value of α in our model to lie within the error limits of the extrapolated faint-end slope of the SFR-function, Φ_{SFR} , of star forming galaxies at $z = 6$ and 7 as shown in Smit et al. (2012) (S12 hereafter). In Fig. 3.3, the red and blue regions enclose the limits on Φ_{SFR} at $z = 6$ and 7 respectively, constructed using the fit parameters provided in S12. The blue and red filled circles denote the data from our work which is in fair agreement with the expected values of Φ_{SFR} .

We vary f_{esc} to 0.1, 1.0, keeping α constant at 0.005 and name the cases esc0.1 and esc0.5 respectively. The model labelled esc0.5Reion is where we also account for reionisation feedback effects on top of the fiducial case. We also implemented a high star formation efficiency for Pop II stars by setting $\alpha=0.1$ and label the model as esc0.5HSFE. All our cases are summarised in Table 4.1.

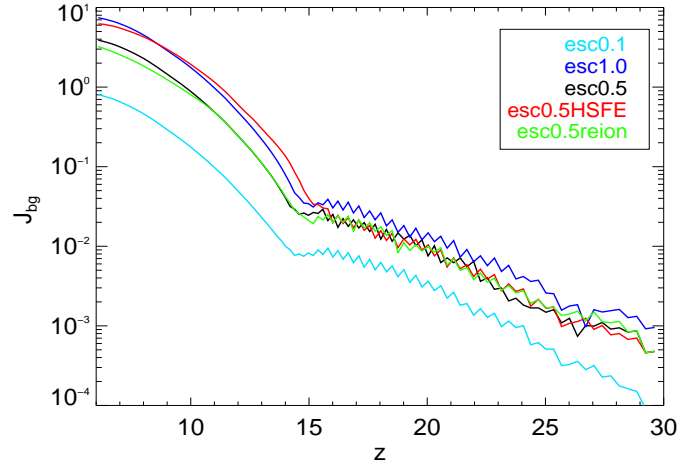


Figure 3.5: The self consistent build up of J_{bg} , defined as the addition of the LW background radiation from both the stellar populations, plotted against redshift. In all the cases except `esc0.5reion`, higher J_{bg} leads to a higher number of total DCBHs due to the efficient LW feedback and the resulting higher J_{total} .

Table 3.2: Summary of cases considered in our work. The fiducial case is marked in bold.

Case	f_{esc}	Feedback	α
esc0.1	0.1	LW	0.005
esc1.0	1.0	LW	0.005
esc0.5	0.5	LW	0.005
esc0.5HSFE	0.5	LW	0.1
esc0.5Reion	0.5	LW + reionisation	0.005

3.3 Results

The evolution of the SFR density (SFRD) with redshift for all cases is plotted in Fig. 3.4. The green symbols represent the cosmic SFRD as inferred from observations. The SFRD we compute is within the observational constraints at $z \sim 6$. Pop II stars first appear in our box at $z \sim 16$. The red and blue solid lines in the plot represent our fiducial case of `esc0.5` and the light blue and orange lines represent the other cases in our work. The Pop II SFR is roughly the same in all the cases except for `esc0.5HSFE` and `esc0.5Reion`. However, due to the different escape fractions assumed for the cases, the Pop III star formation varies over all redshifts. This is due to the fact that in our model, although the Pop III star formation is critically affected by the self consistent build up of the LW radiation, Pop II star formation is not. In general, the Pop III SFRD is inversely proportional to the number of LW photons produced, which is directly proportional to the escape fraction. This is illustrated by the higher level of the Pop III SFRD in the `esc0.1` case (light blue, dash-dot-dash line) than all the others.

After $z \sim 16$, the increase in the LW radiation due to the Pop II stars (see the following sections) is able to further suppress the Pop III star formation. Also, maximal suppression of Pop III star formation is observed in the `esc0.5Reion` case where the additional mass constraint of $V_c = 20 \text{ km s}^{-1}$ between $6 < z < 11$ prohibits the pristine minihaloes and massive haloes from making Pop III stars. The additional circular velocity threshold in the `esc0.5Reion` case also causes a drop in the Pop II SFRD at $z < 11$ which is again due to the fact that the halo mass corresponding to $V_c \geq 20 \text{ km s}^{-1}$, the assumed mass threshold for structure formation in `esc0.5Reion`, is slightly higher than $10^8 M_\odot$ which is the mass threshold for Pop II star formation in all the other cases.

3.3.1 The LW intensity

We start by expressing the total mean LW intensity at a snapshot as the sum of the contribution from the Pop III and Pop II stellar sources.

$$J_{\text{bg}} = J_{\text{bg}}^{\text{III}} + J_{\text{bg}}^{\text{II}} . \quad (3.20)$$

The evolution of J_{bg} for all our cases is plotted in Fig. 3.5. Note that in each case, J_{bg} scales as the product of the escape fraction and SFRD at a given redshift. This is illustrated by the fact that although the level of the Pop II SFRD for `esc0.5` and `esc0.1` is similar, as seen in Fig. 3.4, the level of J_{bg} is lower for `esc0.1` than `esc0.5` in Fig. 3.5. The higher level of J_{bg} for `esc0.5HSFE` than `esc1.0` for $11 < z < 16$ can be explained by the SFRD in the respective cases. The SFRD is considerably higher between $11 < z < 16$ for `esc0.5HSFE`, however once the SFRD approaches that of `esc1.0` (not visible in Fig. 3.4 as it is hidden by the red line), the `esc1.0` case produces more LW photons and hence a higher value of J_{bg} is seen for `esc1.0` at $z < 11$ as compared to `esc0.5HSFE`. The build up of J_{bg} is in sync with the the SFRD in each of the cases and hence, consistent with our implementation. In Fig. 3.6, we plot the individual backgrounds from both stellar populations and the maximum level of the LW flux seen in a pristine halo at each redshift, for our fiducial case. The

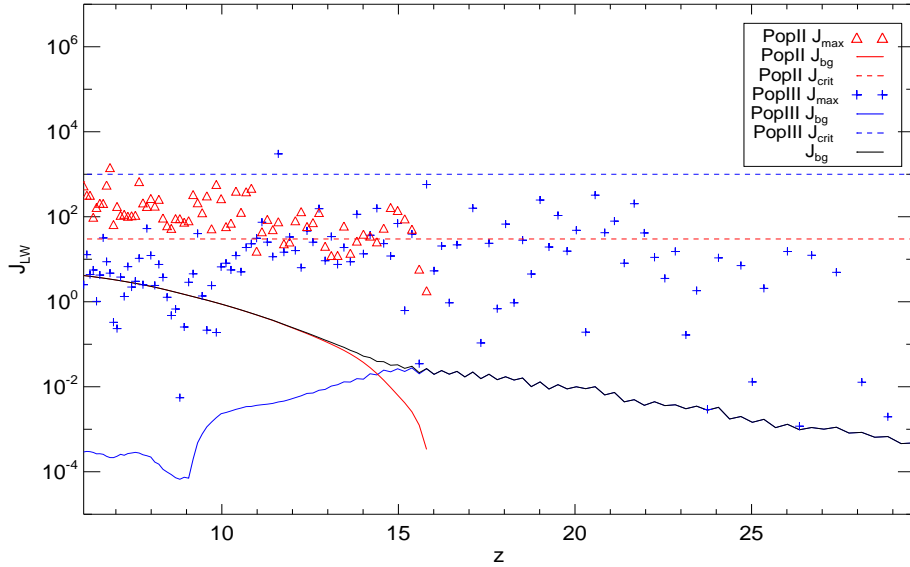


Figure 3.6: The mean and maximum level of LW radiation plotted for each redshift in our fiducial case. The red triangles (J^{II}) and blue crosses (J^{III}) indicate the maximum value of LW radiation to which a pristine halo is exposed at each redshift in the simulated volume. The red and blue dashed lines represent $J_{\text{crit}}^{\text{II}}$ and $J_{\text{crit}}^{\text{III}}$ respectively. It is interesting to see that the maximum value of J^{III} (blue crosses) falls short of $J_{\text{crit}}^{\text{III}}$ (blue dashed line). However, in the case of Pop II sources, the maximum value of J^{II} (red triangles) is several orders of magnitude higher than the $J_{\text{crit}}^{\text{II}}$ (red dashed line). Hence we deduce that in our simulation, Pop II sources are most likely the ones to produce the J_{crit} required for direct collapse. Note that the spatial LW radiation is computed only in the pristine haloes with $T_{\text{vir}} > 2000$ K.

solid blue and red lines represent $J_{\text{bg}}^{\text{III}}$ and $J_{\text{bg}}^{\text{II}}$ respectively which add up to the solid black line, J_{bg} . The J_{bg} computed at each timestep is assumed to be the minimum level of LW radiation to which a halo is exposed at that timestep. As expected, the maximum local level of the LW flux for a stellar population is always higher than the background (and in some rare cases equal to the background level). At all redshifts (except two cases at $z \approx 12, 30$ where the $J_{\text{crit}}^{\text{III}}$ is seen by minihaloes), Pop III stars produce a $J_{\text{III}} < J_{\text{crit}}^{\text{III}}$. On the other hand, Pop II stars are able to produce a $J_{\text{II}} > J_{\text{crit}}^{\text{II}}$ in at least one of the pristine haloes at all redshifts, which is shown by the the red triangles being above the red dashed line. The epoch of DCBH formation in each of our cases is only observed after the Pop II star formation kicks in.

We plot the distribution of the local J_{LW} as seen by pristine haloes in Fig. 3.7 before and after the Pop II star formation begins at $z \sim 16$. We define f_{pris} as the fraction of pristine haloes with $T_{\text{vir}} > 2000$ K exposed to a given J_{LW} . The red and blue solid histograms represent J^{II} (Eq.3.18) and J^{III} (Eq.3.17) respectively. In Fig. 3.7, we see that less than one percent of pristine haloes (which roughly translates into a fraction of 5×10^{-4} of the total number of haloes) see a $J^{\text{II}} > J_{\text{crit}}^{\text{II}}$ whereas the Pop III LW flux is always subcritical even before the Pop II star formation begins. The low fraction of pristine haloes that are exposed to $J_{\text{crit}}^{\text{II}}$ can be attributed to the rarity of the event where a pristine halo is clustered (hence close enough) to the neighbouring haloes hosting Pop II stars. The trend of the distribution function is similar to D08, where they plot the PDF of all the haloes exposed to varying levels of J_{LW} . The Fig. 3.7 further supports our result from Fig. 3.6 i.e. Pop III stars are always subcritical to DCBH formation and that the LW radiation required for DCBH formation is always produced by Pop II stars.

The value of J_{bg} that we compute in our work for esc0.5 and esc0.5Reion is within 5% of the previous estimates of Greif & Bromm (2006) at $z = 10$, where they self-consistently study the impact of two types of stellar populations and their feedback on star formation at $z \gtrsim 5$. The value of $J_{\text{bg}}^{\text{III}}$ that we find for all our cases, denoted by the solid lines at $z \gtrsim 16$ in Fig. 3.5, is also consistent with Johnson et al. (2008), i.e. it does not exceed their value of the maximum level of the LW background expected from Pop III stars (~ 0.13 at $z \sim 16$). We also find a good agreement with Trenti & Stiavelli (2009) as our SFRD and J outputs resemble their estimates, but it is difficult to draw exact comparisons as they used an analytical Press-Schechter modelling and the parameter choices of the studies differ considerably. In cases esc0.5 and esc0.5Reion, we find $J_{\text{bg}} \approx 1$ at $z \approx 10$ (also see Fig. 3.5) which is very close to the expected value during the reionization era⁵ (Omukai, 2001; Bromm & Loeb, 2003).

In accordance with KA09, we find that the local LW intensity, which can be orders of magnitude higher than the mean LW intensity, is observed in highly clustered regions. This becomes even more evident in Sec. 3.3.4 where we present the cross-correlation functions of DCBH haloes. Note that although KA09 carried out full radiative transfer cosmological

⁵ In a recent attempt to model the DCBH formation, Petri et al. (2012) find a very high global LW flux of $J_{\text{LW}} \simeq 1000$ at the epoch of reionisation and they argue for even higher levels in spatially clustered regions. Our self-consistent methods to calculate the background and spatial variation of the LW flux show that such a high background is difficult to achieve.

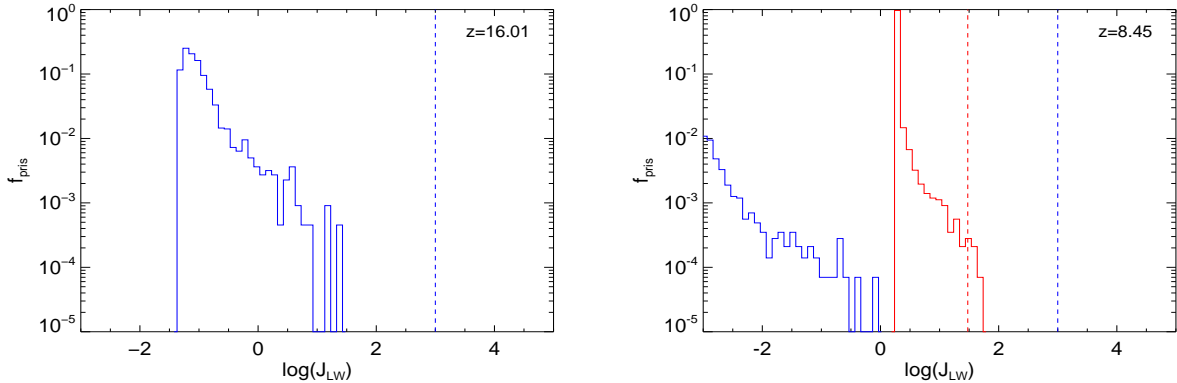


Figure 3.7: The distribution of J_{local} for all the pristine haloes at a given redshift for our fiducial case. The red and blue solid histograms (dashed lines) indicate J_{II} ($J_{\text{II}}^{\text{crit}}$) and J_{III} ($J_{\text{III}}^{\text{crit}}$) respectively. The absence of the red histogram in the top panel is because Pop II star formation begins at $z = 16$ in our box.

simulations to model the spatial variation of the LW intensity, they lacked the resolution required to study the impact of LW radiation feedback on structure formation (namely star formation in minihaloes) at such high redshifts.

3.3.2 Sources responsible for $J > J_{\text{crit}}$

With the change in the relative fraction of Pop III to Pop II star formation, the relative contribution to the LW background undergoes a change as well. As seen in Fig. 3.5, 3.6 and 3.7, the main contribution within our model comes from Pop II stars. At almost all times the contribution from Pop III stars is subcritical for DCBH formation. The critical level of radiation required for direct collapse is always produced by Pop II stars. This can be attributed to the way in which Pop III and Pop II stars form. We checked the effect of allowing Pop III stars to form as single stars, in binary systems or in a group of 10 stars (which maximises the LW flux from a halo) with varying IMFs, and in all the cases the total number of stars was insufficient in producing the critical LW flux in a neighbouring halo.

Also, the short lifetime of a Pop III star poses a problem as they reach the end of their lifetime in a few 10^6 yr as compared to a Pop II stellar population which can actively contribute towards critical levels of LW radiation for up to a few 10^7 yr (see Fig. 3.2). Hence even if it could produce J_{crit} , a Pop III star is less likely to be near a massive pristine halo (and hence contribute towards J_{crit}) than a Pop II stellar population. The result is in good agreement with Inayoshi & Omukai (2011), where they also argue that for a stellar source to produce the J_{crit} , it must be a Pop II/I star cluster or very top heavy Pop III galaxies. As per our current understanding, Pop III stars form in (at most) groups of a few with masses \sim few tens of solar masses (e.g. Greif et al., 2011). The occurrence of Pop III galaxies at such high redshift is expected to be extremely rare as metal pollution in Pop

III hosting haloes is quite fast (Maio et al., 2011) and it is highly unlikely that a cluster of these short lived Pop III stars could end up in a galaxy (Johnson et al., 2008; Johnson, 2010). If a massive, pristine halo is to undergo direct collapse, we would expect it to have an external close by neighbour hosting a Pop II stellar population giving rise to J_{crit} .

The variation in the spatial LW intensity we find is also consistent with KA09. Using a full radiative transfer prescription in a cosmological box, they found that LW radiation varies on the clustering scale of sources at high redshifts, but they did not resolve the Pop III star forming minihaloes important for such studies.

3.3.3 Abundance and growth of DCBHs

The rate at which DCBHs are found to be forming in our simulation volume is shown in Fig. 3.8. We find a steady rise in the DCBH formation rate density with decreasing redshift (in units of Mpc^{-3}) which can be expressed as

$$\frac{dN}{dz} = b_1 (1 + z)^{b_2} , \quad (3.21)$$

where b_1 , b_2 are the fit parameters for the DCBH formation rate in each of our cases as shown in Table 3.3. As we are neglecting possible metal pollution from neighbouring halos (Maio et al., 2011) the formation rates are strict upper limits in each of the cases. The fact that we find a few DCBH candidates in our $3.4 \text{ Mpc} h^{-1}$ simulation volume implies that the conditions for a DCBH are achievable in the early Universe and many such intermediate mass BH (if not SMBH) should exist at high redshifts.

The DCBH formation rate increases as a function of the number of LW photons that are emitted from a star forming halo. In esc0.1 we find 13 times fewer DCBHs than in esc0.5, which is due to the lower escape fraction assumed for LW photons in the former case. As the escape fraction increases from 0.5 to 1.0, the DCBH formation rate increases considerably. In all the above cases, this can be explained by the effect arising from the change in J_{total} (Eq. 3.19) which is two fold

- a higher J_{total} implies that more minihaloes are prevented from Pop III SF due to efficient LW feedback which makes them available for DCBH formation at later times since they are not metal-enriched.
- a higher J_{total} directly affects the efficiency of DCBH formation as it easier to exceed J_{crit} .

The lower formation rate of DCBHs in esc0.5HSFE than esc1.0 can be attributed to the lower level of J_{bg} in the former case at $z < 11$. Also, since the majority of DCBHs form at $z < 11$, the fits are dominated by the DCBH formation rate at later times and hence a lower slope for esc0.5HSFE than esc1.0 is seen.

The esc0.5reion case produces an interesting outcome where we find only 4 DCBHs which is roughly 10 percent of the DCBHs produced in our fiducial case. Note that before the reionisation feedback kicks in at $z = 11$, both esc0.5 and esc0.5Reion have the

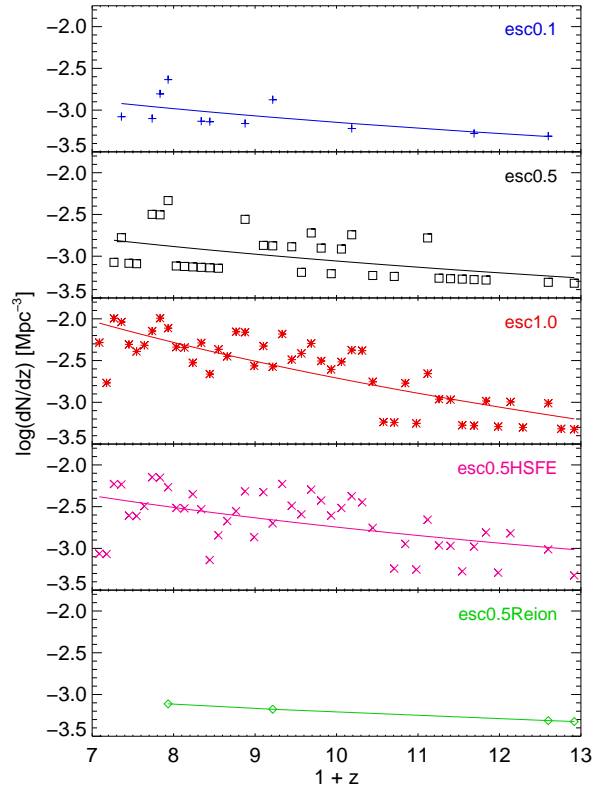


Figure 3.8: Formation rate density of black holes in all the models plotted against redshift. The line represents a fit (Eq.3.21) to the formation rate density in each case.

same DCBH formation rate. One would expect photo-ionisation effects and the photo-evaporation of pristine minihaloes in the early Universe, which is accounted for by our reionisation feedback model, to greatly reduce the number of haloes into which primordial gas can collapse at later times. We discuss this case in more detail in Sec. 3.3.6.

To explore the impact of BH growth via accretion after their formation, we allow the BHs to grow via Eddington accretion using the relation

$$M_{\bullet}(t) = M_{\bullet,0} \exp\left(f_{\text{edd}} \frac{1 - \epsilon}{\epsilon} \frac{t}{450 \text{ Myr}}\right), \quad (3.22)$$

where M_{\bullet} is the final mass of the black hole, $M_{\bullet,0}$ is the initial mass of the black hole set to $10^4 M_{\odot}$ for a DCBH (e.g. Johnson et al., 2012a, CS10), t is the accretion time, ϵ is the radiative efficiency and f_{edd} is the Eddington fraction. We explore the $(f_{\text{edd}}, \epsilon)$ parameter space by choosing $\epsilon = 0.07, 0.1, 0.2$ to account for a range in radiative efficiencies for Eddington ($f_{\text{edd}} = 1$), sub-Eddington ($f_{\text{edd}} < 1$) and super-Eddington ($f_{\text{edd}} > 1$) accretion (Johnson et al., 2011; Shapiro, 2005). Since there is a lot of ambiguity regarding the early

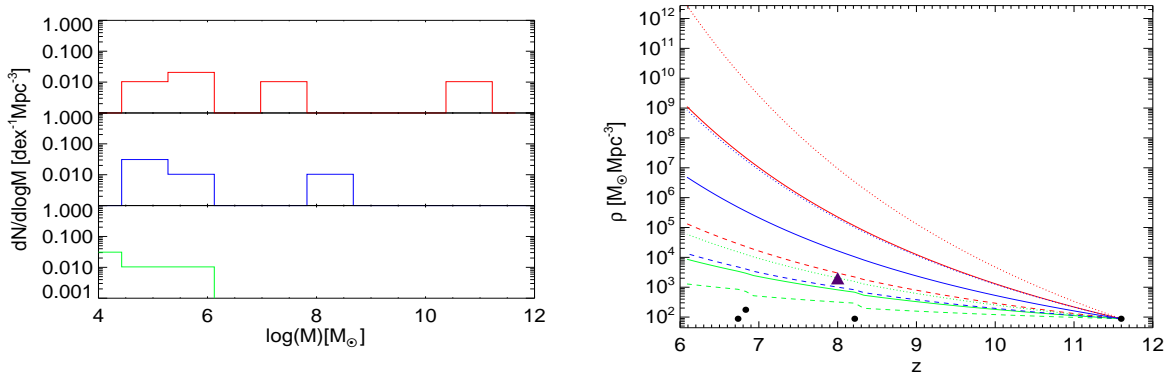


Figure 3.9: DCBH mass function and cumulative mass density for the fiducial case (esc0.5). Red ($f_{\text{edd}} = 1.5$), blue ($f_{\text{edd}} = 1$) and green ($f_{\text{edd}} = 0.4$) represent the super-Eddington, Eddington and sub-Eddington scenarios respectively. *Top Panel*: mass function of accreting DCBHs at $z = 6$ for radiative efficiency $\epsilon = 0.1$. *Bottom Panel*: cumulative mass density of the accreting DCBHs vs. redshift for $\epsilon = 0.07, 0.1, 0.2$ represented by dotted, solid and dashed lines respectively and following the same colour coding as the top plot for f_{edd} . The black circles represent the total mass density of the newly formed DCBHs at each redshift. The solid purple triangle marks the claim of T11 at $z \approx 8$.

regimes of BH accretion, we varied our Eddington accretion parameters ($f_{\text{edd}} = 0.4, 1.0, 1.5$) to account for a range of possibilities in the overall accretion mode of the BH.

For our fiducial case (esc0.5), Fig. 3.9 shows the DCBH mass function constructed for $f_{\text{edd}} = 0.4, 1, 1.5$ and $\epsilon = 0.1$ (top panel) and the cumulative mass density of these DCBHs at $z = 6$ (bottom panel) plotted for different choices of f_{edd} and ϵ . It is clear from the top panel that the DCBHs can almost reach SMBH scales with Eddington accretion and quite easily attain a mass larger than $10^9 M_{\text{sun}}$ if we assume super Eddington accretion. A wide range of evolved BH mass densities is seen in the bottom panel. Each filled black circle in the bottom panel represents the mass density of newly formed DCBH at that redshift, assuming an initial DCBH mass of $10^4 M_{\odot}$. The solid purple triangle in the bottom panel is the observational claim made by T11 for the mass density of the IMBH at $z \sim 8$. Although we do not match T11’s claim for esc0.5, we do so for esc0.5Reion as explained in section 3.3.6.

3.3.4 DCBH host haloes

In the following sections, we explore the regions where we find the conditions for direct collapse and the histories of the DCBH host haloes.

Table 3.3: Fit parameters lines in Fig. 3.8 which follow Eq.3.21 and total DCBH number density at $z = 6$ in each of our cases

Case	b_1	b_2	Total DCBH (Mpc^{-3})
esc0.1	0.035	-1.69	0.13
esc0.5	0.054	-1.79	0.518
esc1.0	49	-4.4	2.09
esc0.5HSFE	0.48	-2.43	1.58
esc0.5Reion	0.0061	-1.0	0.035

Environment

In order to understand the environmental differences between the haloes that host DCBHs and the ones that do not, we construct cross-correlation functions for the distribution of sources around them. In our case, the cross-correlation function is the excess probability of encountering a source in a given distribution of sources around a halo as compared to a uniform distribution. Consequently, we define the cross correlation function as

$$\xi(d) = \frac{DD(d)}{RR(d)} - 1, \quad (3.23)$$

where $DD(d)$ represents the *data-data* pair counts at a given distance d , constructed from our model. The data-data pairs in our work refer to the halo-source pairs. We fix the halo and loop over all the qualifying⁶ sources thereby computing the physical distances. This is done for all the halo-sources pairs in a given redshift range.

$RR(d)$ represents the *random-random* pair counts constructed from a uniform distribution of sources around a random halo. Similar to Li et al. (2012), we use the formulation of $\xi(d)$ to qualitatively compare the small scale clustering properties of DCBH-hosting and non-DCBH hosting haloes with their respective sources. Note that in our case, $RR(d)$ is the same as $DR(d)$, as used by Li et al. (2012), since the position of the halo is arbitrary.

Following the prescription described above, we first construct a cross-correlation function $\xi_{\text{Halo(DC)}}$ which is computed over all the newly formed DCBHs, in a given redshift range, and their respective sources. We then define a similar cross-correlation function $\xi_{\text{Halo(NoDC)}}$ for haloes that do not host a DCBH with all their respective sources.⁷ Both $\xi_{\text{Halo(DC)}}$ and $\xi_{\text{Halo(NoDC)}}$, are constructed using the same bins at a given snapshot with the first bin placed at a distance larger than the typical virial radius (~ 1 kpc) of a massive

⁶The qualifying sources for a given halo refer to the ones that satisfy the conditions described in section A.1.2 of the Appendix.

⁷ The non DCBH hosting haloes are chosen in the same mass range as the haloes hosting a DCBH. This is done for consistency in the construction of the cross-correlation function in the two cases.

halo. This is done in order to exclude sources that formed within a non DCBH hosting halo at earlier times. This choice does not affect the nature or trend of $\xi_{\text{Halo(NoDC)}}$.

Finally, to check for a variation in the clustering of sources around DCBH hosting haloes versus non-DCBH hosting haloes, we define

$$\xi_{\text{total}} = \frac{\xi_{\text{Halo(DC)}}}{\xi_{\text{Halo(NoDC)}}} . \quad (3.24)$$

If $\xi_{\text{Halo(DC)}} = \xi_{\text{Halo(NoDC)}}$ in each distance bin, it implies that the DCBH host haloes are as clustered as the non-DCBH host haloes at all scales. Therefore, a value of unity for ξ_{total} at a given distance scale would imply the lack of clustering for the DCBH host haloes. Additionally, a variation in ξ_{total} with distance would imply the difference in clustering of the DCBH host haloes vs. non-DCBH host haloes with the neighbouring sources. A negative slope would imply over-clustering for DCBH host haloes at smaller distances whereas a positive slope would imply an over-dense environment at smaller distances for the non-DCBH hosting haloes. The results of our calculations for the cases *esc0.5* and *esc1.0* are plotted in Fig. 3.10.⁸

It can be inferred from the value of ξ_{total} and the slope of the fits that the haloes that host a DCBH are more clustered than the non-DCBH hosting haloes especially at a scale of few tens of kpc. This trend can be attributed to the fact that in order to reach J_{crit} near a pristine halo, a source (or a population of sources) must exist very close by.

The different escape fractions make this trend even more prominent since in both the cases, the line gets flatter as we move to lower redshifts but the relative change in the slope of the lines is inversely dependent on the escape fraction. This can be understood by noting that to produce the same level of LW radiation in a neighbouring halo, the sources would need to be closer to the halo (hence more clustered) if the escape fraction was set to 0.5 instead of 1.0. This also implies that the haloes that host DCBH in *esc0.5* form from regions of higher over-densities than in *esc1.0*. Hence, the flattening trend is most pronounced in the *esc1.0* (red line) as compared to the *esc0.5* (black line).

By using our detailed prescription for the spatial variation of the LW flux, we find that the haloes which are exposed to J_{crit} always have a source within a few kpc. We note that our results are in accordance with previous work done by D08 which shows that the distance scale within which a halo should have a close by LW source in order to undergo direct collapse is ~ 10 kpc.

The function ξ_{total} follows a linear fit in log space which can be parameterised as

$$\log(\xi_{\text{total}}) = c_1 + c_2 \log(d_{\text{phy}}) , \quad (3.25)$$

where d_{phy} is the physical distance between a halo and LW source in parsec and the parameters c_1 and c_2 are indicated on the bottom left of each plot in Fig. 3.10.

⁸ The chosen cases have at least a few DCBHs in the specified redshift bins. The case *esc0.5Reion* and *esc0.1* have very few DCBHs and the case *0.5HSFE* has not been plotted just to avoid repetition as it lies between the two plotted cases.

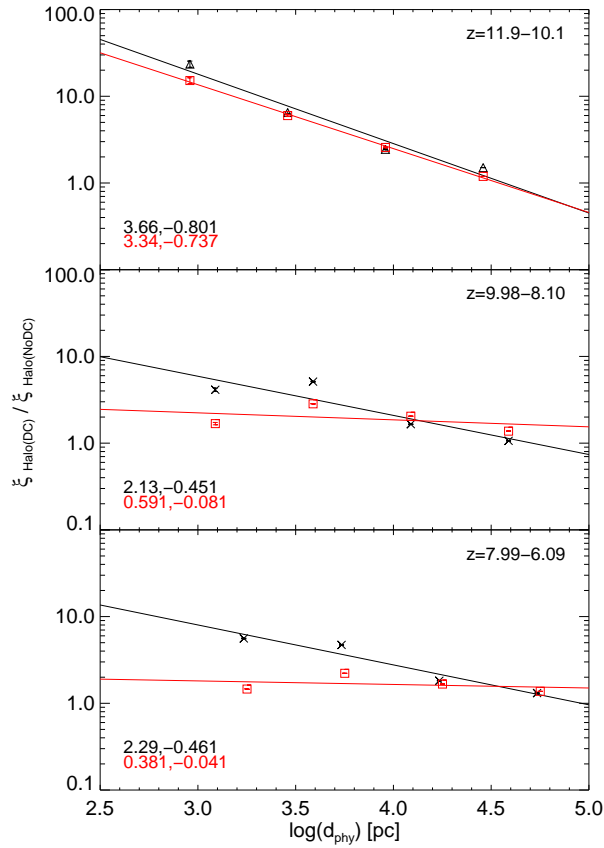


Figure 3.10: The correlation function ξ_{total} plotted for a range of redshifts (top right of each plot). Black crosses (line) and red squares (line) indicate the correlation data points (fit to the points) computed from the function ξ_{total} for the cases $\text{esc}0.5$ and $\text{esc}1.0$ respectively. The numbers on the bottom left indicate the fit parameters c_1 and c_2 in Eq.3.25

The flattening of the slope can be attributed to the fact that it is more common for a halo to be in an environment with close by sources at later redshifts due to the higher overall SFRD in the box. Also, the haloes that host DCBHs at $z > 10$ originate from regions of larger overdensities than the ones at lower redshifts. This is evident from the larger negative slope of ξ_{total} at $z > 10$. At lower redshifts, a lower- σ fluctuation is required to produce a halo of $\sim 10^7 M_{\odot}$, which roughly corresponds to a $T_{\text{vir}} = 10^4$ K halo, supporting that DCBHs must arise from regions of high over densities in the early Universe.

An important inference can be drawn from the points above. If the DCBHs which form early on (at $z > 10$) in the Universe arise from highly clustered regions, their environment can only get more clustered as the halo progresses to later times. This is an important result as it supports the idea that the most massive SMBH that we observe at the centres of ellipticals or as highly clustered AGNs, might have originated from regions of high over-densities quite early on in the Universe, possibly as DCBHs.

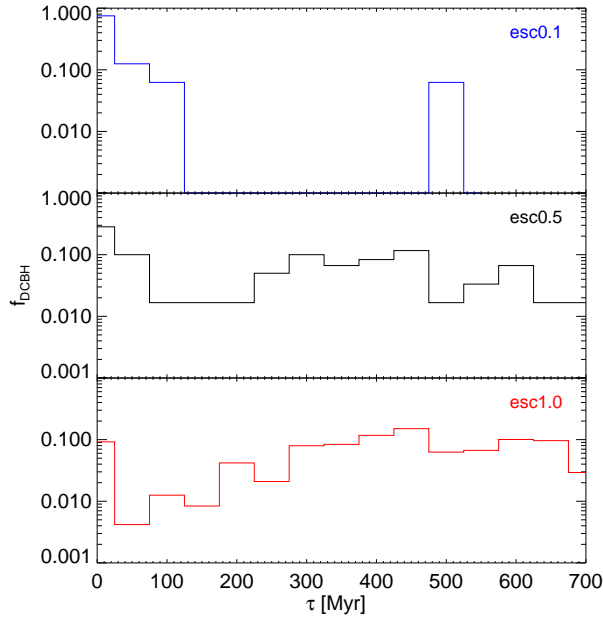


Figure 3.11: Age distribution of the DCBH host haloes in our three main cases.

History

It is interesting to check when the haloes that host DCBHs first originated during their cosmic evolution. We checked the most massive progenitor of each of the DCBHs and tracked it back in time until the halo was found to have a mass equal to the mass resolution in our work (20 DM particles or $1.8 \times 10^5 M_\odot$). We label this time as the time of the halo’s birth, t_{birth}^h . We define the age of the halo when it was first found to host a DCBH as

$$\tau = t_{\text{DC}}^h - t_{\text{birth}}^h, \quad (3.26)$$

where t_{DC}^h is the time when a halo is found to host a newly formed DCBH.

The histograms of τ for our 3 main cases are plotted in in Fig. 3.11. In the case of esc0.1 (blue), 90% of the haloes hosting a DCBH were born within 150 Myr, with the remaining haloes being 500 Myr old. However, for esc0.5 (black) and esc1.0 (red), all the DCBH host haloes are distributed over the age parameter. Part of the reason for this changing trend is that a larger f_{esc} implies a faster build-up of the LW flux to larger values which leads to a higher suppression of Pop III star formation over a longer time. The aforementioned suppression of Pop III star formation would also be in minihalos formed at earlier times which could later grow into massive haloes and form a DCBH if they have a close by Pop II source. Thus while in the case of esc0.5, 41% of the haloes are less than 150 Myr old, only 11% of similarly aged haloes are seen in esc1.0.

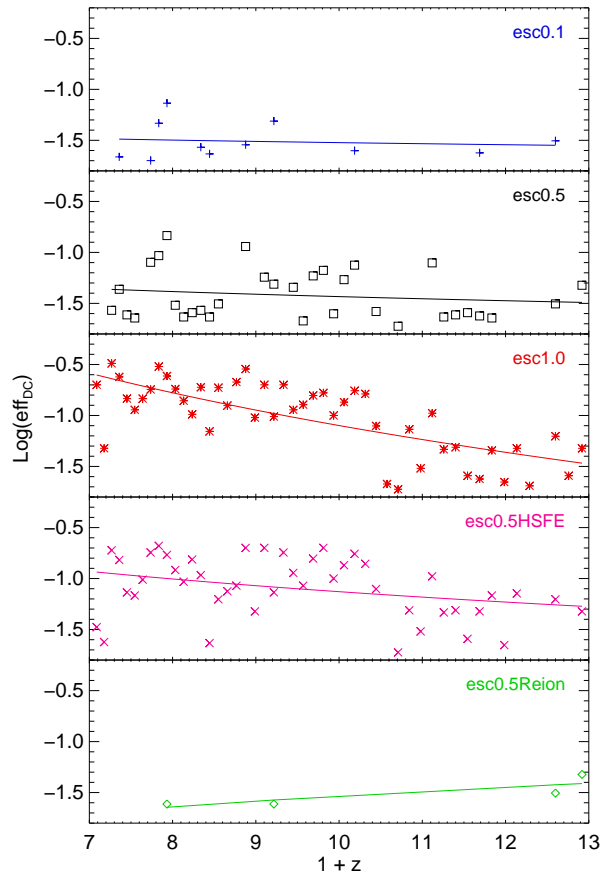


Figure 3.12: The efficiency of DCBH , measured as the ratio of the number of DCBHs and the total number of newly formed massive halos, as a function of redshift. The fit parameters to the lines are listed in Table 3.4.

3.3.5 Efficiency of DCBH formation

We plot the redshift evolution of the efficiency of DCBH formation, eff_{DC} in Fig. 3.12. The efficiency at a redshift is defined as the number of newly formed DCBHs (which by definition form in pristine massive haloes) divided by number of newly formed massive haloes at that redshift. Note that in our model a newly formed pristine halo with $T_{vir} \geq 10^4$ K at a given redshift will immediately form either a DCBH (if $J_{LW} \geq J_{crit}$) or a Pop III star (if $J_{LW} < J_{crit}$). The eff_{DC} can be expressed as a function of redshift

$$eff_{DC} = e_1 (1+z)^{e_2}, \quad (3.27)$$

where the fit parameters e_1 and e_2 are listed in Table 3.4 for all our five cases. Since the efficiency of DCBH formation is a combination of DCBH formation rate and the formation rate of newly formed massive haloes (which is the same in all the cases), the trends in Fig. 3.12 are similar to the ones in Fig. 3.8. Again, the same reasoning that applies to

Table 3.4: Fit parameters to Eq.3.27 for each case.

Case	e_1	e_2
esc0.1	0.055	-0.26
esc0.5	0.12	-0.51
esc1.0	170	-3.32
esc0.5HSFE	1.4	-1.29
esc0.5Reion	0.0023	1.1

the DCBH formation rate, applies to the trends in the efficiency. A higher number of LW photons leads to a higher efficiency of DCBH formation. The case1.0 has the highest efficiency of DCBH formation followed by esc0.5HSFE which is due to the fact that a higher output of LW photons is seen in the former case than the latter at $z < 11$ (see Fig. 3.5). However, the efficiency in esc0.5Reion decreases at later times which is in accordance with the low overall DCBH formation rate for this case and due to the flattening in the formation rate of pristine haloes we find at later times. Note that the similar values of the fit parameters for esc0.1 and esc0.5 is due to two reasons: the formation rate densities of DCBHs in these two cases are similar and the formation rate of massive pristine haloes in all the cases is exactly the same since it is drawn from the same N -body simulation.

For the first time, we are able to constrain the seeding mechanism of BHs at high redshifts by self consistently accounting for the physical processes that give rise to the conditions for massive BH seed formation. Equation 3.27 encapsulates information about the number of massive metal free haloes appearing at a given epoch, their clustering with the sources (or haloes) and the rate at which these DCBHs form.

3.3.6 Reionisation Feedback

We ran our fiducial case with the addition of a simple reionisation feedback prescription motivated by Dijkstra et al. (2004). During reionisation, the atomic H ionising photons ionise the gas in massive haloes (predominantly comprised of atomic hydrogen) which results in the delayed collapse of gas. As a consequence a larger potential well is required for gas collapse due to the added gas pressure from photoheating. In accordance with Dijkstra et al. (2004), a circular velocity threshold of $V_c = 20 \text{ km s}^{-1}$ was added on top of the fiducial model to account for the reionisation feedback in haloes with $T_{\text{vir}} > 10^4 \text{ K}$ between $6 < z < 11$. In essence, this models the impact of instantaneous reionization at $z \approx 11$.

The results reflect an immediate quenching of Pop III SF at $z < 11$ in massive haloes in Fig. 3.4. The mini-haloes are also unable to make Pop III stars due to the high J_{bg} already in place but the Pop II SFR remains almost unaffected. This is because our Pop II SF threshold already requires a halo to have $M_{\text{infall}} > 10^8 M_{\odot}$ which roughly translates

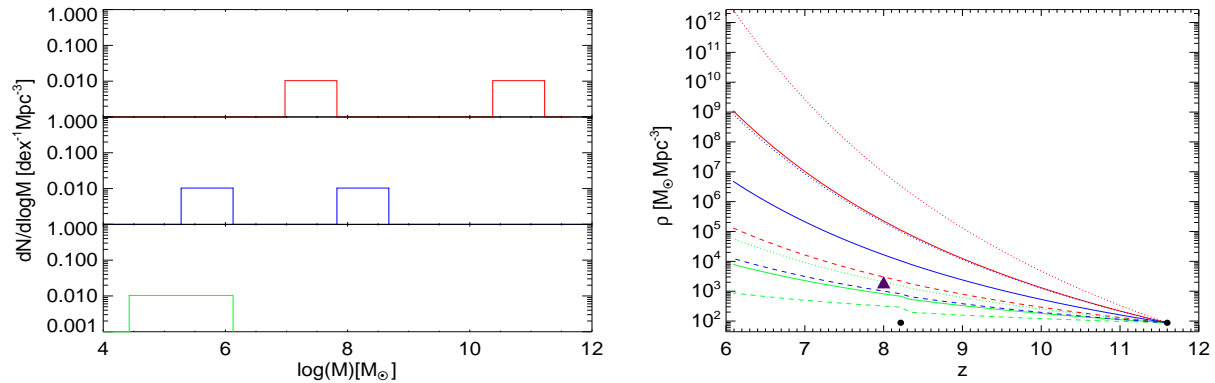


Figure 3.13: Same as Fig. 3.9 but for the esc0.5Reion case. The presence of only 4 DCBHs has severe consequences on the BH mass function. We are able to match the claim of T11, marked as the solid purple triangle, with both Eddington and sub-Eddington accretion modes. The zero points in the mass function arise due to the lower (factor of 10) number of DCBHs in the esc0.5reion case as compared to esc0.5.

to a $V_c \approx 20 \text{ km s}^{-1}$.

The most interesting outcome is the appearance of only 4 DCBHs in our box, as compared to the 59 in our fiducial case of esc0.5, with no DCBHs seen between $8 < z < 11$. This accounts for the effect where even though a pristine massive halo in this redshift range might be exposed to J_{crit} , most of the gas would be in a hot ionised state which would prevent it from collapsing and forming a DCBH. Only once the halo has a circular velocity greater than 20 km s^{-1} , the gas inside it can collapse and form a DCBH, which happens in our box at $z < 8$. The DCBHs that form before the onset of reionisation at $z > 11$ are the ones found in pristine massive haloes with no constraints on their circular velocity. This is one reason why even though the green and black lines trace each other in Fig. 3.5, only 4 DCBHs are seen in the esc0.5reion case as compared to the 59 in the esc0.5 case.

We allowed the DCBHs in the esc0.5Reion run to grow in the same way as the in esc0.5 run (described in Sec. 3.3.3). The early appearance of the 3 DCBHs at $z > 11$ in this case allows them to grow into SMBHs (see Fig. 3.13) by $z \sim 6$ with $f_{\text{edd}} = 1$.

We match the recent claim made by T11 for a population of obscured IMBHs, at $z \approx 8$, by setting the $f_{\text{edd}} = 0.1$ and $\epsilon = 0.2$ or $f_{\text{edd}} = 0.4$ and $\epsilon = 0.1$. It is interesting to that we are able to match T11’s claim with a sub-Eddington efficiency in the case where we find the least number of DCBHs.

The fact that DCBH-hosting halos are clustered, also suggests that they form in regions of the Universe that are reionised at relatively early times, as well, due to the concentration of ionising sources around them. This suggests that the feedback from reionisation could be even stronger than what we have found assuming instantaneous reionisation at $z = 11$.

3.4 Observability of the stellar seeds of direct collapse black holes

We have found that a significant number of direct collapse black holes are likely to have formed in the early Universe. Now we turn to the question of whether these objects are plentiful enough for future surveys to detect them. As discussed by e.g. Bromm & Loeb (2003) and Begelman (2010), the hot protogalactic gas is expected to first collapse to a supermassive primordial star which subsequently accretes gas until it attains a mass of $\gtrsim 10^4 M_\odot$ and collapses to a black hole (see also Dotan & Shaviv, 2012; Hosokawa et al., 2012; Johnson et al., 2012a). Here we focus on the prospects for uncovering these supermassive stellar progenitors of direct collapse black holes, as these objects are expected to be very bright and possibly detectable by JWST (e.g. Gardner et al., 2006). We shall address the question of the detectability of accreting direct collapse black holes in future work.

In order to estimate the likelihood that a given deep survey could find SMSs, the precursors of DCBHs, we use the fits provided in Table 3 to the rate $|dN/dz|$ of SMS formation (equal to the rate of black hole formation) shown in Fig. 7. With this, we find that the expected number n_{SMS} of SMS that lie within a region of the sky, as a function of redshift z , is given by

$$\begin{aligned} \frac{dn_{\text{SMS}}}{dz} &= \frac{dV}{dz} \left| \frac{dz}{dt} \right| \left| \frac{dN}{dz} \right| t_{\text{life}} \\ &\simeq 100 \text{ deg}^{-2} \left(\frac{1+z}{10} \right) \\ &\times \left(\frac{|dN/dz|}{10^{-3} \text{ Mpc}^{-3}} \right) \left(\frac{t_{\text{life}}}{10^6 \text{ yr}} \right), \end{aligned} \quad (3.28)$$

where dV/dz is the comoving volume element per unit redshift, $|dt/dz|$ is the rate of change of the Hubble time with redshift, and t_{life} is the lifetime of a SMS. To obtain the second equation above we have neglected the effect of dark energy on the rate of Hubble expansion, which is a reasonable assumption at the high redshifts ($z \gtrsim 6$) we are considering here; otherwise, we have adopted the same cosmological parameters as described in Section 2.1. Finally, note that the longer the stellar lifetime t_{life} , the more objects will be visible within a given redshift interval.

Fig. 3.14 shows the number of SMS per square degree per redshift interval that we find for each of the five cases shown in Fig. 7, normalized to $t_{\text{life}} = 10^6$ yr, a typical value expected for a rapidly accreting SMS (see Begelman, 2010; Johnson et al., 2012a). Also shown is the minimum number of SMS that would yield an average of one SMS per redshift interval ($\Delta z = 1$) within the area of sky covered by the Deep-Wide Survey (DWS) planned for the JWST (e.g. Gardner et al., 2006). Clearly, the prospects of detection are good, as in each of the cases we find that at least a few SMS should lie within the survey area $\sim 100 \text{ arcmin} \times \text{arcmin}$.

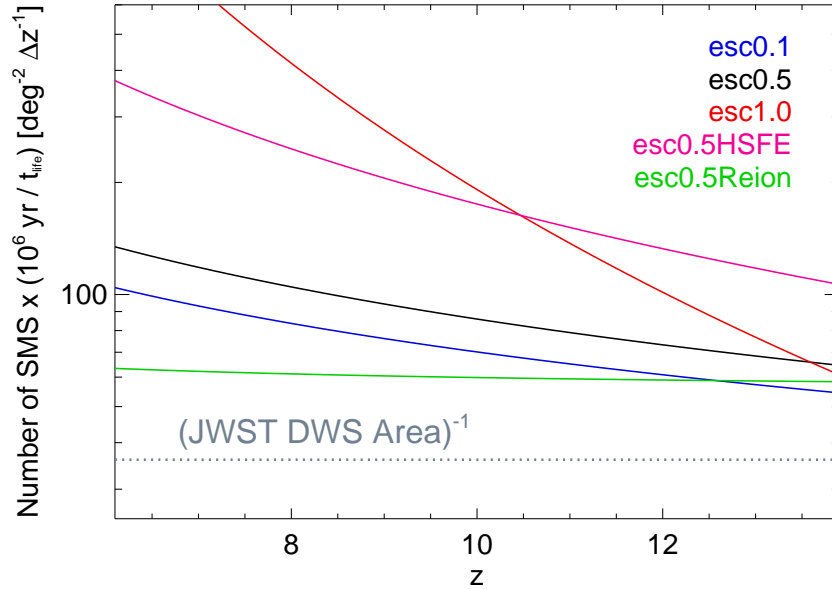


Figure 3.14: The number of supermassive stellar progenitors of direct collapse black holes, as observed on the sky per square degree per redshift interval (Δz), as a function of redshift z . The number of supermassive stars is given by the fits shown in Fig. 7 and in Table 3, for each of the five cases shown. The gray dotted line shows the number of supermassive stars that must be present for at least one per redshift interval ($\Delta z = 1$) to appear in the field of view of the Deep-Wide Survey planned for the JWST. For all cases the survey should be large enough for at least a few to of the order of 10 supermassive stars to lie within the field of view. Strong continuum and $H\alpha$ and $He II \lambda 1640$ emission lines may be detected from these objects.

We note that rapidly accreting SMS are expected to have distinct observational signatures which could be detected by the JWST, as discussed by Johnson et al. (2012a). In particular, these objects may emit strong continuum radiation below the Lyman limit, and they are likely to exhibit both strong $H\alpha$ and $He II \lambda 1640$ recombination line emission. An important difference between these objects and others with strong recombination line emission is that they may also be very weak $Ly\alpha$ emitters, due to the trapping of $Ly\alpha$ photons in the optically thick accretion flows feeding their growth. The detection of objects exhibiting these observational signatures would provide important constraints on both the nature and abundance of the stellar seeds of direct collapse black holes.

3.5 Summary

In this paper, we present the results from a N -body, DM only simulation of a $3.4 \text{ Mpc} h^{-1}$ co-moving box from cosmological initial conditions. On top of this simulation, we developed

a SAM which takes into account the self consistent global build up and local variation of the LW radiation field due to the Pop III and Pop II stellar sources. The merging histories of haloes are also tracked in order to account for metal pollution from previous episodes of star formation. This allowed us to identify the possible sites of DCBH and to investigate their environment. Though our simulation is not large enough to probe a wide range of environments, we show that even in such volumes, BH seeding by DCBHs could be a common phenomenon. Our study in this respect motivates the seeding of present-day SMBHs via the formation of DCBHs. The key findings of our work are summarised below.

1. DCBH formation sets in with the onset of Pop II star formation as the Pop II stars can easily produce $J_{\text{LW}} \geq J_{\text{crit}}^{\text{II}}$. On the other hand, LW radiation from Pop III stars is not able to exceed $J_{\text{crit}}^{\text{III}}$.
2. We find the first DCBH at $z \approx 12$, however the total number of such objects depends on the LW photon output of a given model.
3. In each of our cases, all the haloes that host DCBHs have close by LW sources within ~ 10 kpc.
4. We also find that the haloes that host DCBH at $z > 10$ are more clustered with external LW sources than the haloes that do not host DCBH. Also, the DCBHs that appear later at $z < 10$ are less clustered than the DCBHs that appear at $z > 10$ and may exist at the centres of galaxies of various morphological types at $z = 0$.
5. In our model including reionisation, we are able to match recent claims made by T11 about the population of obscured IMBHs, by assuming both Eddington ($f_{\text{edd}} = 0.1$, $\epsilon = 0.2$) and sub-Eddington ($f_{\text{edd}} = 0.4$, $\epsilon = 0.1$) accretion modes for the DCBHs.
6. We find that for all our cases, the JWST should be able to detect at least a few of the supermassive stellar precursors of these DCBHs over a wide range of redshifts ($z > 6$).

Our results are subject to limitations due to the modelling approach we chose. The halo threshold mass assumed in our work for Pop II star formation sets the clock for DCBH formation. In our current work, we have set the mass threshold for Pop II star formation to $10^8 M_{\odot}$ following the work of Maio et al. (2011), however setting it to a lower value would allow for the Pop II stars to form earlier in the box. This would lead to an earlier epoch of DCBH formation but it is difficult to predict their abundance at later times. Note that we also set the mass threshold for structure formation (Pop III, Pop II or DCBH) to

$V_c = 20 \text{ km s}^{-1}$ between $6 < z < 11$, which only further quenches the DCBH formation rate.

Note that our simulated volume is smaller than typical volumes probed by current observations and does not include sources as luminous as the ones detected in the surveys. Thus our predicted SFRD should be somewhat lower than the observed ones. Based on the observational constraints, as shown in Fig. 3.3 and 3.4, we estimate that our computed value of J_{bg} could be lower by a factor of $\simeq 2$ at a given redshift. A higher level of LW background would make it relatively easy to reach J_{crit} and would also imply the quenching of Pop III star formation in a larger number of minihaloes. Whether this would also lead to a higher number of DCBHs is non-trivial to predict.

In principle, SN explosions from neighbouring stellar populations can enrich a pristine halo early on in its lifetime (Maio et al., 2011). This could also reduce the number of DCBHs we find in our study, if the metal enrichment is high enough to alter the cooling properties of the gas (Omukai et al., 2008). However, it is very likely that the metals carried in the SN wind may not be mixed into the dense gas at the centre of the halo where DCBH formation occurs (e.g. Cen & Riquelme, 2008) within the timescale of DCBH formation which is $\approx 2 - 3 \text{ Myr}$.

The gas within the haloes identified as DC candidates would still need to collapse without fragmentation into a central massive object. The study by LN06 explores a mechanism where a Toomre-stable gaseous disc in a pristine low spin halo can effectively redistribute its angular momentum, thereby preventing fragmentation and eventually forming a DCBH. The aim of our next study is to self consistently explore the mechanism suggested by LN06, on top of our existing framework, which should in principle greatly reduce the number of DCBH host haloes since low spin haloes at such high redshifts are quite rare (eg. Davis & Natarajan, 2010).

The accreting discs of both Pop III remnant BHs and DCBHs could also emit LW photons (e.g. Pelupessy et al., 2007; Alvarez et al., 2009; Jeon et al., 2011), where the emission would depend on both the BH mass and accretion rate (Greif et al., 2008). However, a recent study (Johnson et al., 2011) has shown that due to the low accretion rate of these BHs, their contribution to the LW specific intensity can be quite low outside the halo at $\sim 1 \text{ kpc}$, i.e. the typical virial radius of BH host haloes at high redshifts. Due to the uncertainty in the emission characteristics of BH accretion disc, we focus on the stellar components to account for the LW radiation in our model. Also, the X-ray feedback from accretion discs could heat the gas in surrounding haloes, thereby preventing them from collapsing and making stars (e.g. Mirabel et al., 2011; Tanaka et al., 2012), hindering the formation of DCBHs in the neighbouring pristine massive haloes. We plan to explore the impact of accreting BHs on the formation of DCBHs in a future study.

Since the plausibility of direct collapse in a pristine halo depends on the number of LW photons reaching it, we find a clear degeneracy in the various cases that span the (f_{esc}, α) parameter space. The degeneracy in the number of LW photons produced in our cases could be broken by comparison of the BH mass function or the mass density of BHs that we find with those inferred for BHs from observations at $z > 6$. Another possibility is via the detection of SMSs in the planned surveys of the JWST which could also shed light on

the plausibility of this scenario as a SMS is believed to be the precursor of a DCBH (e.g. Begelman, 2010).

Our results shed new light on the long-standing argument that only very close star-halo pairs could give rise to DCBHs and that a characteristic length of ~ 10 kpc is the maximum distance within which a halo must see a LW source in order to have direct collapse of gas (D08). We find that although a source must exist within 10 kpc, it is not necessary that a single source produces all of the LW radiation which accounts for J_{crit} ; there is a contribution from the cosmological background LW radiation field, as well as from a number of local sources producing J_{crit} . However, in all the cases, it is only the Pop II star clusters that produce all (or most) of the J_{crit} . Pop III stars alone never produce enough LW photons to achieve J_{crit} .

It is interesting to note that even in the worst-case scenario for the formation of DCBHs i.e. the model including reionisation feedback (esc0.5Reion), we still find a few DCBHs, which hints towards the high plausibility of the DCBH scenario. While photoionisation strongly inhibits the formation of Pop III stars in smaller pristine haloes, it still allows for Pop II star formation in massive enough enriched haloes, which produce the necessary background.

Allowing the DCBHs to grow via different modes of Eddington accretion gives rise to a range of possibilities for the BH mass function, and can readily account for the presence of supermassive black holes by $z = 7$. The expected number of SMBH is a few per comoving Gpc^3 , in accordance with the inferred number of quasars at $z > 6$ (Fan et al., 2003, 2006; Mortlock et al., 2011). We over predict the number of such SMBHs but argue that our work is an upper limit for the existence of such objects. However, the study by T11 (see also Willott, 2011; Fiore et al., 2012) suggests the possibility of a large number of intermediate mass black holes at $z > 6$. They infer (via extrapolation) the presence of an obscured population of intermediate mass BHs by looking at the stacked X-ray luminosity signals of high redshift galaxies. We are able to match their claim at $z \sim 8$ in our reionisation model, assuming both Eddington and sub-Eddington accretion modes for the DCBHs. Independent of the claim made by T11, on the basis of our model we argue that a population of BHs must be present at $z > 6$ due to the sheer number of DCBH host haloes that we find.

A precise seeding mechanism of BHs at early redshifts in cosmological simulations is important in order to explain the AGN luminosity functions, growth of massive BHs and the evolution and properties of galaxies at lower redshifts. The environment of these BHs would play an important role in determining their evolution and the Eq. 3.27 is a first step towards constraining the environments and masses of seed BHs. Using a semi-analytical model, which takes into account the halo histories and the spatial variation of the LW flux, we were able to parameterise the fraction of newly formed haloes with $T_{\text{vir}} > 10^4$ K that are able to host DCBH as a function of redshift. The equation is an outcome of our model where we are able to resolve haloes with masses in the range $10^{6-7} M_{\odot}$ and could thus serve as a sub-grid model for the seeding of BHs in large scale cosmological simulations, which we will pursue in a future study.

Chapter 4

Unravelling obese black holes in the first galaxies ¹

We predict the existence and observational signatures of a new class of objects that assembled early, during the first billion years of cosmic time: Obese Black-hole Galaxies (OBGs). OBGs are objects in which the mass of the central black hole initially exceeds that of the stellar component of the host galaxy, and the luminosity from black-hole accretion dominates the starlight. Conventional wisdom dictates that the first galaxies light up with the formation of the first stars; we show here that, in fact, there could exist a population of astrophysical objects in which this is not the case. From a cosmological simulation, we demonstrate that there are sites where star formation is initially inhibited and direct-collapse black holes (DCBHs) form due to the photo-dissociating effect of Lyman-Werner radiation on molecular hydrogen. We show that the formation of OBGs is inevitable, because the probability of finding the required extra-galactic environment and the right physical conditions in a halo conducive to DCBH formation is quite high in the early universe. We estimate an OBG number density of 0.009 Mpc^{-3} at $z \sim 8$ and 0.03 Mpc^{-3} at $z \sim 6$. Extrapolating from our simulation volume, we infer that the most luminous quasars detected at $z \geq 6$ likely transited through an earlier OBG phase. Following the growth history of DCBHs and their host galaxies in an evolving dark matter halo shows that these primordial galaxies start off with an over-massive BH and acquire their stellar component from subsequent merging as well as in-situ star formation. In doing so, they inevitably go through an OBG phase dominated by the accretion luminosity at the Eddington rate or below, released from the growing BH. The OBG phase is characterised by an ultra-violet (UV) spectrum $f_\lambda \propto \lambda^\beta$ with slope of $\beta \sim -2.3$ and the absence of a Balmer Break. OBGs should also be spatially unresolved, and are expected to be brighter than the majority of known high-redshift galaxies. They could also display broad high-excitation emission lines, as expected from Type-I active galactic nuclei (AGN), although the strength of lines such as NV and CIV will obviously depend on the chemical enrichment of the host galaxy. OBGs could potentially be revealed via *Hubble Space Telescope* (HST) follow-up

¹This chapter is published as the study Agarwal et al. (2013)

imaging of samples of brighter Lyman-break galaxies provided by wide-area ground-based surveys such as UltraVISTA, and should be easily uncovered and studied with instruments aboard the *James Webb Space Telescope* (JWST). The discovery and characterization of OBGs would provide important insights into the formation of the first black-holes, and their influence on early galaxy formation.

4.1 Introduction

It is now well-established that most present-day galaxies harbour a quiescent super-massive black hole (SMBH), with a mass approximately one thousandth of the mass of stars in the bulge (Ferrarese & Merritt, 2000; Häring & Rix, 2004). Such a correlation is strongly suggestive of coupled growth of the SMBH and the stellar component, likely via regulation of the gas supply in galactic nuclei from the earliest times (e.g. Silk & Rees, 1998; Haehnelt & Kauffmann, 2000; Fabian et al., 2002; King, 2003; Thompson et al., 2005; Robertson et al., 2006; Hopkins et al., 2009; Natarajan & Treister, 2009; Treister et al., 2011, see however Hirschmann et al. 2010).

Since the same gas reservoir fuels star formation and feeds the black hole, a connection between these two astrophysical processes regulated by the evolving gravitational potential of the dark matter halo is arguably expected. However, understanding when and how this interplay commences has been both a theoretical and observational challenge for current theories of structure formation.

In this letter, we explore the formation and evolution of the first massive black-hole seeds and the first stars during the earliest epochs in order to explore the onset of coupling between the black hole and the stellar component. Our calculation incorporates two new physical processes that have only been recently recognised as critical to understanding the fate of collapsing gas in the early universe. The first is the computation of the Lyman-Werner (LW) radiation (11.2 – 13.6 eV) that impacts gas collapse in the first dark-matter haloes (as it is able to efficiently dissociate the H₂ molecules, thereby preventing cooling via molecular hydrogen; e.g. Haiman et al. (2000)). The second is the implementation of our growing understanding of the role of the angular momentum of the baryonic gas in the collapse process (Lodato & Natarajan, 2006; Davis & Natarajan, 2010). Including these two processes within the context of the standard paradigm of structure formation, predicts the possible existence of a new class of object in the high-redshift Universe in which black-hole growth commences before, and continues to lead the build up of the galaxy stellar population for a significant period of time. We define an OBG as a phase in a galaxy’s evolution where post DCBH formation, the BH at least initially dominates over the stellar mass and is accreting at a rate sufficiently high enough to outshine the stellar component.

OBGs may provide a natural stage of early black-hole/galaxy evolution en route to the most luminous quasars already observed to be in place at $z \simeq 6$ with estimated black-hole masses $M_{\text{BH}} \simeq 10^9 M_{\odot}$. Observationally, such objects should appear similar to moderate-luminosity AGN, but with very low-luminosity host galaxies, and low metallicities.

4.2 Methodology

Our model is a modified version of Agarwal et al. (2012), A12 here after, where they identify the sites of DCBH formation by calculating the total amount (spatial and global) of LW radiation seen by any given halo within a cosmological N-body dark-matter only simulation using a semi-analytic model for the star formation in these haloes. The key features of A12 are summarised below:

1. The DM only N-body simulation is run from $z = 30$ to $z = 6$ with a box size of $\sim 3.4 \text{ Mpc } h^{-1}$ and DM particle mass of $6500 \text{ M}_\odot h^{-1}$. This was chosen so that we can resolve a minimum halo mass $\sim 10^5 \text{ M}_\odot$ with 20 particles, similar to the minimum halo mass that can host a Pop III star at $z = 30$ (Tegmark et al., 1997).
2. Both Pop III and Pop II star formation are allowed, and halo histories are tracked in order to determine if a halo is metal free.
3. Many realisations of the model are run to study the effect of different LW escape fractions, Pop II star formation efficiencies, gas outflow rates due to supernova feedback, number of Pop III stars forming per halo and reionisation feedback. The results presented here are based on the run with a LW escape fraction of 1.0 and a Pop II star-formation efficiency of 0.005 with a burst mode of star formation. We create Pop II stars in a single burst that is placed randomly between the two time steps for which we use the burst mode template (Fig. 7e) from STARBURST99 (Leitherer et al., 1999). Using the burst mode leads to a peak in LW emission at 10^{-42} erg/s for a 1 Myr old, 10^6 M_\odot Pop II star cluster which drops to 10^{-38} erg/s at 700 Myr.
4. The LW specific intensity in units of $10^{-21} \text{ erg s}^{-1} \text{ cm}^{-2} \text{ Hz}^{-1} \text{ sr}^{-1}$, J_{LW} is computed self-consistently depending on the type, mass and age of the stellar population, and with two components: a global and a local contribution. A pristine halo is considered for Pop III star formation or treated as a DCBH candidate depending on the halo's virial temperature and the J_{LW} that it is exposed to.
5. The number density of DCBH sites can be up to 0.1 Mpc^{-3} at $z = 6$, much higher than previously anticipated (Dijkstra et al., 2008).

In the present study we refine the model of DCBH formation and also follow the subsequent growth of these seeds as identified in A12. We discuss new additions to the A12 model in the subsections below.

4.2.1 DCBH forming haloes

A DCBH forms in our model if a pristine massive halo is exposed to $J \geq J_{\text{crit}}^2$ (Wolcott-Green et al., 2011) and satisfies both the spin and size criterion required for the disc to withstand frag-

²Note that J_{crit} is the critical level of LW radiation required by a pristine atomic cooling halo to undergo direct collapse. The critical level of extragalactic LW radiation required by a pristine atomic cooling halo from Pop III stars, ~ 1000 and from Pop II stars $\sim 30 - 100$ (Wolcott-Green et al., 2011)

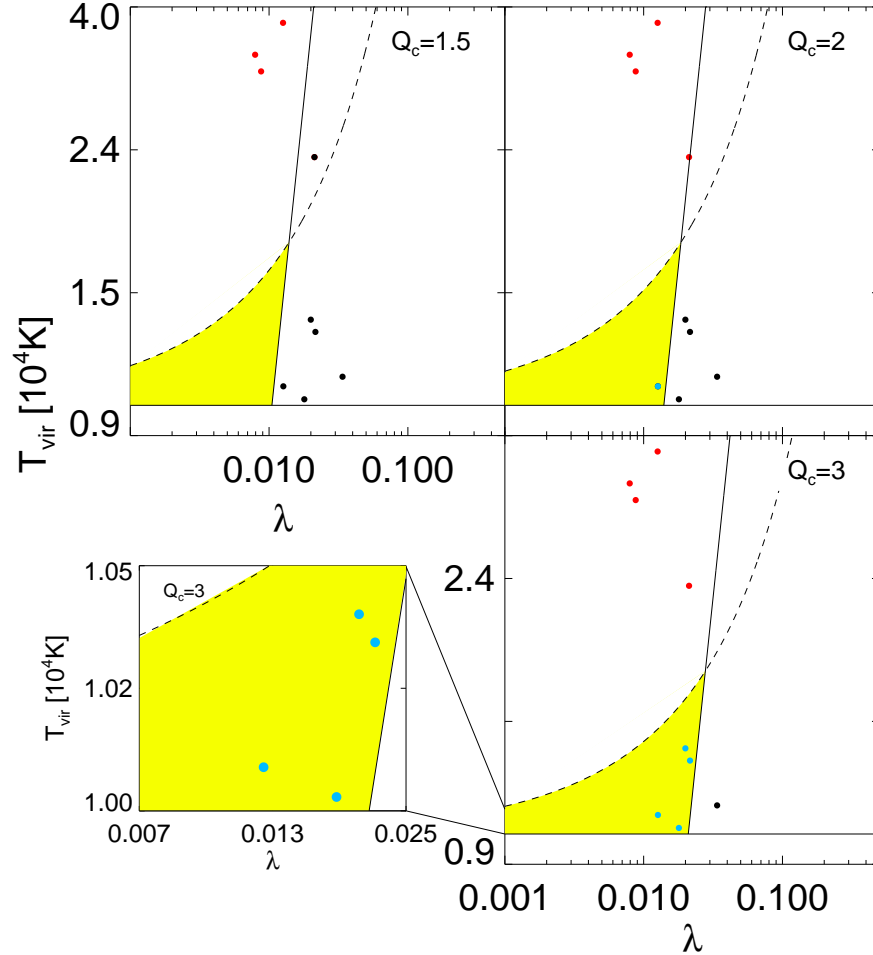


Figure 4.1: The temperature/spin distribution of pristine massive dark-matter haloes that are exposed to $J_{\text{LW}} \geq J_{\text{crit}}$. The virial temperature, T_{vir} , is plotted against the halo spin parameter, λ , for all DCBH candidates with Toomre stability parameter $Q_c = 1.5, 2, 3$. The nearly-vertical solid curve represents the value of λ_{max} and all haloes with spin less than this critical value lie to the left of this line (red points), whereas those with larger spin lie to the right (black points). The upper limit on the scale-length of the hosted disc given the allowed $T_{\text{vir}} - \lambda_{\text{max}}$ combination is marked as the dashed line. Any halo in the yellow region, i.e. below the dashed line and to the left of the solid vertical curve will host a DCBH (blue points) in our model. Note that the yellow region shrinks as Q_c decreases, thereby reducing the probability of finding a halo that can form a DCBH. Inset: A zoom-in on the $T_{\text{vir}} - \lambda$ distribution of the four DCBH candidates in our fiducial case with $Q_c = 3$.

mentation (Lodato & Natarajan, 2006, 2007, LN06 and LN07 hereafter). Note that the J_{crit} is always produced by stellar sources external to the pristine DCBH candidate halo as internal sources would pollute the gas inside the halo. We assume the collapsing gas in pristine haloes will settle into a disc whose stability against fragmentation determines whether it will be able to collapse to a BH or will fragment into star-forming clumps (LN06, LN07). Assuming that initially the baryons have the same specific angular momentum as the halo, the halo must have a spin, λ , lower than a characteristic value, λ_{max} , for a given Toomre stability parameter Q_c , for which the pristine gaseous disc is exactly marginally stable and above which no accretion can take place onto the central region (LN06). The critical spin is given as

$$\lambda_{\text{max}} = \frac{m_{\text{d}}^2 Q_c}{8j_{\text{d}}} \sqrt{\frac{T_{\text{gas}}}{T_{\text{vir}}}}, \quad (4.1)$$

where m_{d} is the disc mass expressed as a fixed fraction (0.05) of the total baryonic mass in the halo (Mo et al., 1998), j_{d} is the specific angular momentum of the disc that is also a fixed fraction (0.05) of the halo's overall angular momentum (LN06), T_{vir} is the virial temperature of the halo and T_{gas} is the temperature of the gas in the disc which depends on whether atomic or molecular hydrogen is the dominant cooling species. In our case, since the halo is exposed to $J \geq J_{\text{crit}}$, the dominant coolant is atomic hydrogen and T_{gas} is set to 8000 K. The second condition comes from the limit that the disc must be cooler than a characteristic temperature above which the gravitational torques required to redistribute the angular momentum become too large and can disrupt the disc. T_{max} is used as a proxy for size of the disc and is defined as

$$T_{\text{max}} = T_{\text{gas}} \left(\frac{4\alpha_c}{m_{\text{d}}} \frac{1}{1 + M_{\text{BH}}/m_{\text{d}}M} \right)^{2/3}, \quad (4.2)$$

where α_c is a dimensionless parameter (0.06) relating the critical viscosity to the gravitational torques in a halo with DM mass, M . This provides a mass estimate for the assembling DCBH (LN07)

$$M_{\text{BH}} = m_{\text{d}}M \left(1 - \sqrt{\frac{8\lambda j_{\text{d}}}{m_{\text{d}}^2 Q_c} \left(\frac{T_{\text{gas}}}{T_{\text{vir}}} \right)^{1/2}} \right), \quad (4.3)$$

for $\lambda < \lambda_{\text{max}}$ and $T_{\text{vir}} < T_{\text{max}}$.

We find that the inclusion of these two criteria for efficient angular momentum transport and accretion within the disc, in addition to our existing framework for the treatment of LW radiation feedback, fundamentally alters the progression of structure formation in these haloes, and impacts the observable characteristics of stars and the BHs within them.

We plot the $T_{\text{vir}} - \lambda$ distribution of pristine atomic cooling haloes that are exposed to $J_{\text{LW}} \geq J_{\text{crit}}$, for different values of Q_c in Fig. 1. The haloes with spin in the range $\lambda < \lambda_{\text{max}}$ are marked in red, with the almost-vertical solid curve representing λ_{max} , whereas the ones with $\lambda > \lambda_{\text{max}}$ are plotted in black. The size constraint in order for the disc to withstand

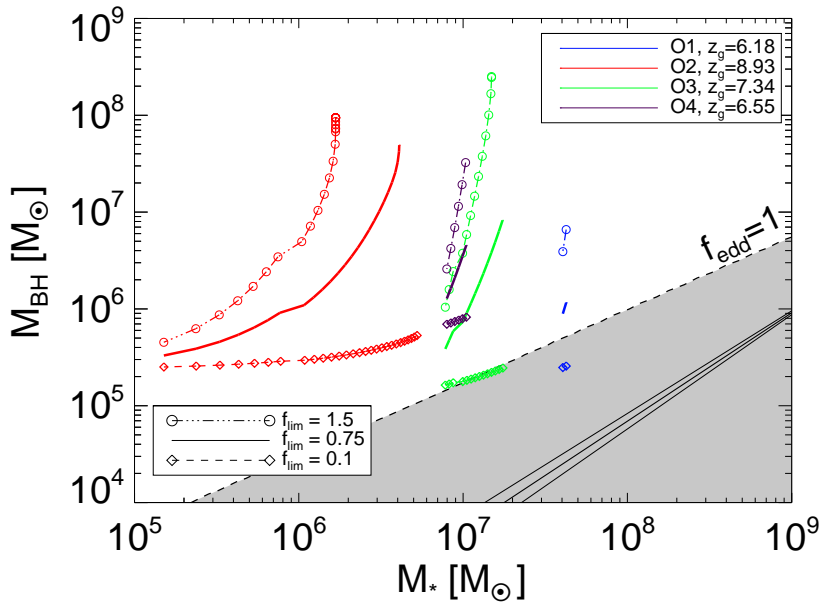


Figure 4.2: Predicted redshift evolution of M_{BH} and M_* for the four OBGs in our simulation down to $z = 6$. We show the tracks for different fractions of the Eddington accretion rate $f_{\text{lim}} = 1.5, 0.75$ (fiducial), 0.1 . The parameter z_g denotes the redshift when the galaxy becomes an OBG and first appears on this plot. The shaded portion represents the region where the BH’s accretion rate would have to be larger than the Eddington limit for the galaxy to qualify as an OBG. In solid-black lines, we show the local $M_{\text{BH}} - M_{\text{bulge}}$ relation and the $1-\sigma$ error in the fit (Häring & Rix, 2004).

fragmentation is denoted by the dashed curve. These limits together constrain DCBH formation to a small allowed domain in the $T_{\text{vir}} - \lambda$ plane marked by the yellow region.

Note that LN06, LN07 require the gas disc to be marginally stable i.e. $Q_c \sim O(1)$. Given that the actual high-redshift disc parameters are uncertain, we choose values of Q_c close to unity and use $Q_c = 3$ in our fiducial model, which sets an upper limit on the number of DCBHs with reasonable disc parameters and for which the disc sizes are not too large. This yields DCBHs (blue points) with a co-moving number density of 0.03 Mpc^{-3} in our fiducial case with $Q_c = 3$, and $f_{\text{lim}} = 0.75$ (see the following section for f_{lim}).

4.2.2 Star Formation

In our model, Pop III stars form in pristine haloes subject to the following physical prescriptions/effects, discussed in A12 in more detail.

- Pop III star formation is prohibited due to LW feedback in pristine haloes with $2000 \leq T_{\text{vir}} < 10^4 \text{ K}$ even when $J_{\text{LW}} < J_{\text{crit}}$ (Machacek et al., 2001; O’Shea & Norman, 2008).

A pristine mini-halo that is subject to even a small value of LW radiation needs to be above a characteristic mass to host a Pop III star due to the partial dissociation (and hence inefficient cooling) of H₂ molecules.

- Pop III stars form following a top-heavy Salpeter IMF with mass limits dependent on halo's virial temperature, i.e. a single star with mass cut-offs at [100, 500] M_⊙ in haloes with 2000 ≤ T_{vir} < 10⁴ K and 10 stars with mass cut-offs at [10, 100] M_⊙ in haloes with T_{vir} ≥ 10⁴ K.

We consider a halo polluted if it has hosted a star or merged with a halo hosting a star. We set a mass threshold of $M > 10^8 M_{\odot}$ for polluted haloes to form Pop II stars (Kitayama et al., 2004; Whalen et al., 2008; Muratov et al., 2012), following the reasoning that a halo needs to be massive enough to allow for the fall back or the retention of metals ejected from a previous Pop III star formation episode. In these polluted haloes, baryons are allowed to co-exist in the form of *hot* non-star-forming gas, *cold* star-forming gas, stars, or those locked into a DCBH that might have formed in or ended up in the halo through a merger.

We assume in our model that a DM halo is initially comprised of hot gas, $M_{\text{hot}} = f_b M_{\text{DM}}$, where f_b is the universal baryon fraction and M_{DM} is the halo's current DM mass³. We add non-star-forming gas to the halo by calculating the accretion rate, \dot{M}_{acc} , defined as

$$\dot{M}_{\text{acc}} \equiv \frac{f_b \Delta M_{\text{DM}} - M_{*,\text{p}} - M_{\text{out,p}} - M_{\text{BH}}}{\Delta t}, \quad (4.4)$$

In this model ΔM_{DM} is amount by which the DM halo grows between two snapshots separated by Δt years. $M_{*,\text{p}}$ and $M_{\text{out,p}}$ represents the total stellar mass and net mass lost (from both cold and hot gas reservoir) in previous SN outflows at the beginning of the time step, respectively. M_{BH} is the total mass of the DCBH in the halo.

The hot gas, M_{hot} , converts into cold gas, M_{cold} , by collapsing over the dynamical time⁴ of the halo, t_{dyn} . Pop II star formation can then occur via a Kennicutt-type relation Kennicutt (1998)

$$\dot{M}_{*,\text{II}} = \frac{\alpha}{0.1 t_{\text{dyn}}} M_{\text{cold}}, \quad (4.5)$$

where α is the star formation efficiency set to 0.005 (SFE) and the factor $0.1 t_{\text{dyn}}$ is motivated by the angular momentum conservation condition for the central galaxy in a DM halo (Kauffmann et al., 1999; Mo et al., 1998, and see A12 for a descriptions of the parameters used).

In Pop II star forming haloes, the outflow rate due to SN feedback is computed via the relation: $\dot{M}_{\text{out}} = \gamma \dot{M}_{*,\text{II}}$, where $\gamma = \left(\frac{V_c}{V_{\text{out}}}\right)^{-\beta}$ Cole et al. (2000).

We set $V_{\text{out}} = 110 \text{ km s}^{-1}$ and $\beta = -1.74$ resulting in typical values of $\gamma \approx 20$, following the results of the high resolution hydrodynamical simulations of the high redshift Universe (Dalla Vecchia and Khochfar 2013, in prep).

³Using a lower baryon fraction linearly affects the BH mass and evolution discussed in this work.

⁴ t_{dyn} is defined as the ratio of the halo's virial radius to the circular velocity defined for the infall mass and infall redshift

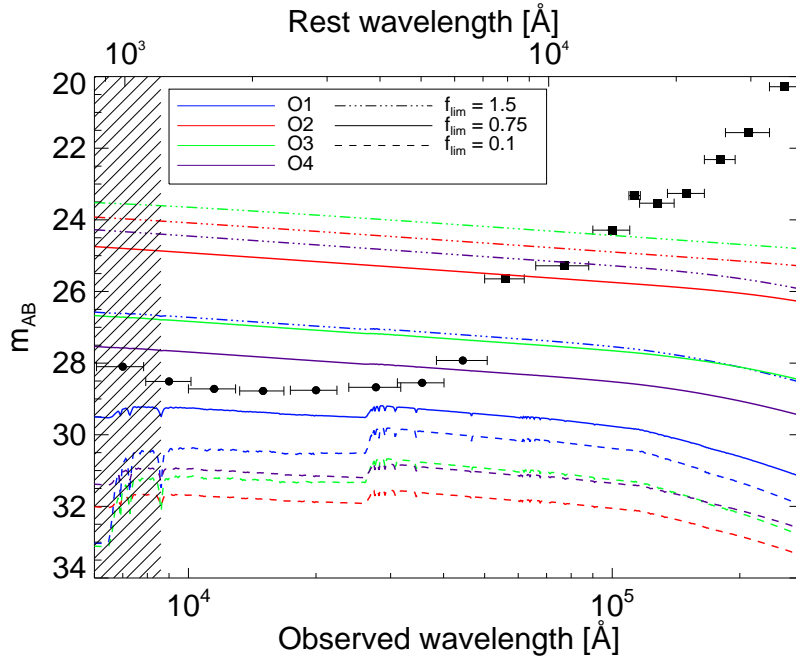


Figure 4.3: OBG candidates and their observability with JWST at $z \sim 6$. We plot the observed flux density in AB magnitudes for all the OBGs, while varying the maximal allowed accretion rate, f_{lim} . When the BH accretion dominates the spectrum there is virtually no Balmer break, and the UV slope is obviously fixed by the accreting black hole. The black points denote the flux limits and bandpass widths of NIRCcam (circles) and MIRI (squares) wide filters, assuming a 10,000 second exposure with JWST and a S/N ratio of 10. The shaded area marks the wavelength region shortward $\text{Ly}\alpha$, where intergalactic neutral hydrogen is expected to completely absorb the OBG signal.

We track the evolution of baryons with the following set of coupled differential equations for the individual baryonic components:

$$\dot{M}_{\text{cold}} = \frac{M_{\text{hot}}}{t_{\text{dyn}}} - \dot{M}_{*,\text{II}} - \dot{M}_{\text{out}} - \dot{M}_{\text{BH,cold}} , \quad (4.6)$$

$$\dot{M}_{\text{hot}} = \dot{M}_{\text{acc}} - \frac{M_{\text{hot}}}{t_{\text{dyn}}} - \dot{M}_{\text{BH,hot}} . \quad (4.7)$$

Equations 4.4, 4.5, 4.6 and 4.7 are solved numerically over 100 smaller time steps between two snapshots.

4.2.3 Growth of a DCBH

Haloes hosting DCBHs are initially not massive enough and are not polluted enough to lead to Pop II star formation (Schneider et al. 2002). It is reasonable to assume that prior

to the introduction of a stellar component, the gas reservoir is still massive enough to feed the central BH. At this stage the accreting DCBH might appear as a mini-quasar, but of essentially zero metallicity. Following this epoch, however, the BH grows by accreting gas available in the halo, unchallenged by any further star formation until Pop II stars start forming in the halo, or until the halo merges with another halo hosting stars. The stellar component and the BH from this point on begin to grow in tandem, marking the onset of the OBG phase. How the two components evolve in detail is sensitive to the accretion rate and subsequent merging history - a parameter space that we have explored extensively.

Once a DCBH forms in a halo, it is allowed to grow at a fixed fraction f_{lim} of the Eddington accretion rate, assuming that both the cold gas and hot gas can be accreted by the BH. The upper limit of the accretion rate is set by the parameter f_{lim} that we vary between individual runs. If the total gas available during our integration time steps for accretion is less than this fraction, the total mass available sets the accretion rate. We run our model for $f_{\text{lim}} = [1.5, 1.0, 0.75, 0.1]$ to explore the parameter space. From the model, at any given time step, Δt (in Myr), the accretion efficiency computed from the gas reservoir is

$$f_{\text{model}} = \ln(1 + M_{\text{g}}/M_{\text{BH}}) \times \frac{\epsilon}{(1 - \epsilon)} \frac{450 \text{ Myr}}{\Delta t}, \quad (4.8)$$

where M_{g} is the total gas available in the halo at timestep Δt and M_{BH} is the DCBH mass with the radiative efficiency, ϵ , set to 10 %. The accretion efficiency then used for the actual computation of the increase in the DCBH mass is

$$f_{\text{acc}} = \min[f_{\text{model}}, f_{\text{lim}}], \quad (4.9)$$

Finally, we write

$$M_{\text{BH,final}} = M_{\text{BH,ini}} \exp\left(f_{\text{acc}} \frac{1 - \epsilon}{\epsilon} \frac{\Delta t}{450 \text{ Myr}}\right), \quad (4.10)$$

Our fiducial case corresponds to a LW escape fraction of 1.0, Pop II star formation efficiency of 0.005, $Q_c = 3$ and $f_{\text{lim}} = 0.75$. Note that the number of DC sites are directly dependant on f_{esc} and α , where increasing the values of those parameters leads to a higher number of DC sites (A12). The number of DCBHs that form from those sites directly depends on Q_c , where a higher value of Q_c leads to a higher number of DCBHs. The BH accretion parameters only affect the mass accreted by the DCBH as seen in Fig. 4.2 (see section 4.3). In haloes which host a DCBH but are not massive enough to form Pop II stars, the gas is assumed to be hot and diffuse (i.e. has not condensed over the dynamical time of the halo). In haloes which host a DCBH and a Pop II stellar component, both the hot and cold phases of gas are assumed to contribute to the accretion process. The total mass accreted by the DCBH is split into hot and cold components depending on the ratio of the hot and the cold gas reservoirs. We do not assume any feedback from the accreting DCBH affecting star formation in the galaxy. We do this to avoid inserting a correlation between the BH and stars by assuming such a feedback loop since the precise nature of accretion and feedback in galactic nuclei is largely unknown at $z > 6$.

Table 4.1: Summary of cases considered in our work.

Name	Symbol	Value
Pop II star formation efficiency	α	0.005
LW escape fraction	f_{esc}	1.0
Radiative efficiency	ϵ	0.1
Limiting Eddington Accretion fraction	f_{lim}	0.1-1.5
Toomre Parameter	Q_c	1.5-3

To summarise, the total gas mass available for accretion, and hence the total mass accreted by the DCBH, depends on whether Pop II stars are forming in the halo or not. If there is no assembling Pop II stellar component, the DCBH is assumed to accrete from the hot gas reservoir, i.e the limiting accretion efficiency, $f_{\text{acc}}^{\text{hot}}$, is determined via eqs. 4.8 and 4.9 using the hot gas (M_{hot} in eq. 4.8) in the halo.

$$M_{\text{BH,final}} = M_{\text{BH,ini}} \exp \left(f_{\text{acc}}^{\text{hot}} \frac{1 - \epsilon}{\epsilon} \frac{\Delta t}{450 \text{ Myr}} \right), \quad (4.11)$$

If the halo hosts a Pop II stellar component, the limiting accretion efficiency, $f_{\text{acc}}^{\text{hot+cold}}$, is determined via eqs. 4.8 and 4.9 using the hot and cold gas ($M_{\text{hot}} + M_{\text{cold}}$ in eq. 4.8) in the halo.

$$M_{\text{BH,final}} = M_{\text{BH,ini}} \exp \left(f_{\text{acc}}^{\text{hot+cold}} \frac{1 - \epsilon}{\epsilon} \frac{\Delta t}{450 \text{ Myr}} \right), \quad (4.12)$$

The net BH mass accreted in a time step, $M_{\text{BH,acc}} = M_{\text{BH,final}} - M_{\text{BH,ini}}$, can then be written as a sum of the hot ($M_{\text{BH,acc}}^{\text{hot}}$) and cold ($M_{\text{BH,acc}}^{\text{cold}}$) components

$$M_{\text{BH,acc}} = M_{\text{BH,acc}}^{\text{hot}} + M_{\text{BH,acc}}^{\text{cold}}, \quad (4.13)$$

The individual masses are computed as,

$$M_{\text{BH,acc}}^{\text{cold}} = R M_{\text{cold}}, \quad (4.14)$$

$$M_{\text{BH,acc}}^{\text{hot}} = (1 - R) M_{\text{hot}}, \quad (4.15)$$

$$(4.16)$$

where $R = \frac{M_{\text{cold}}}{M_{\text{hot}}}$, if $M_{\text{cold}} < M_{\text{hot}}$, else $R = \frac{M_{\text{hot}}}{M_{\text{cold}}}$. $M_{\text{BH,acc}}^{\text{cold}}$ and $M_{\text{BH,acc}}^{\text{hot}}$ are then used in eq. 4.6 and 4.7 to compute the updated hot and cold gas fractions.

4.3 Results

For $Q_c = 3$, we find four OBGs, named O1–O4, in our simulation box. The stellar and black-hole growth tracks of these OBGs are shown in Fig. 2, colour coded as O1–blue, O2–red, O3–green, O4–purple, respectively. The fiducial case ($f_{\text{lim}} = 0.75$) is marked by

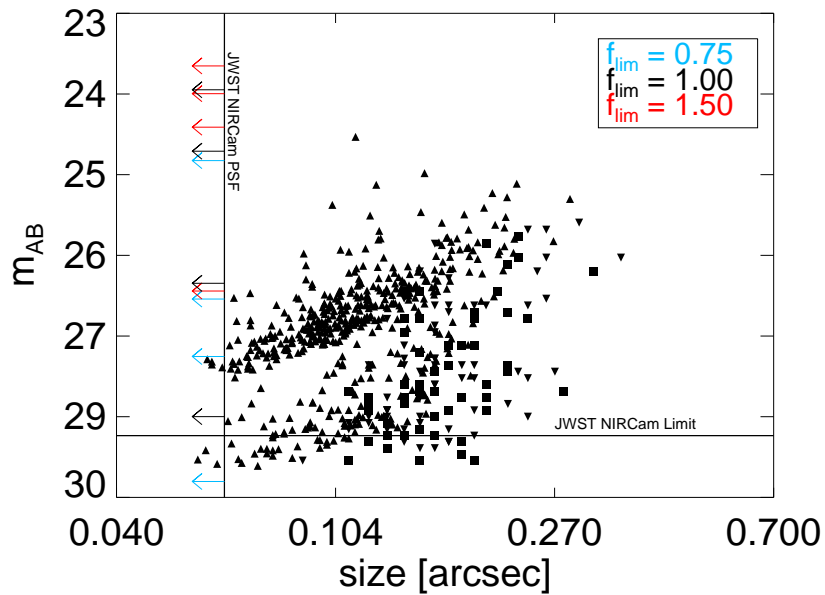


Figure 4.4: Size versus magnitude relation. The HUDF galaxies, not corrected for point spread function (PSF), at $z = 6, 7, 8$ are represented by upright triangles, downward triangles and squares respectively. Observational limits and the PSF of the NIRCcam are plotted as the straight lines. The OBGs O1–O4 in our sample, denoted by the arrows pointing left, would be unresolved objects that could be brighter than the galaxies. Note that we have excluded the $f_{lim} = 0.1$ case from this plot as the m_{AB} for the OBGs is quite high.

the solid curves and the open triangles and circles denote the time-steps at $f_{\text{lim}} = 0.1, 1.5$. The grey shaded region is where the BH would need to accrete at super-Eddington rates for the galaxy to appear as an OBG. Since these objects have $M_{\text{BH}} > M_*$, the nuclear emission can dominate the starlight even when accreting at significantly sub-Eddington rates in the non-shaded region.

Note that these OBGs preferably form in low mass atomic cooling haloes as seen in Fig. 1. Almost all the DC candidate haloes meet the spin cut, but only the lower mass haloes, close to $10^7 M_{\odot}$, meet the size cut to allow for the formation of the DCBH. We also report that DCBH host haloes are in fact satellites of larger haloes hosting Pop II stars, in which the DCBH haloes eventually end up. This is, expected as the critical value of the LW radiation is generally produced by the larger star forming halos forming a close-pair with the DC candidate halo. The abundances of these objects at $z \sim 6$ is similar to the ones reported by Volonteri & Begelman (2010), for their 'low-threshold' case of DC seed formation.

4.3.1 Observational predictions

After identifying the sites of DC (A12), inclusion of physical processes that leads to their formation (LN06), enables the calculation of the observational signatures of OBGs. Haloes that harbour growing DCBH seeds with no (or little) associated stellar component merge into haloes that have formed the first and second generation of stars. We compute the observed spectral energy distribution (SED) of these copiously accreting DCBH seeds and the population of stars within the OBGs. To model the stellar component of the SED, we use the stellar masses and ages from our merger tree and derive the spectrum using STARBURST99 (Leitherer et al., 1999). The accretion disc spectrum is modelled as a radiating blackbody with a temperature profile of the disc given by the alpha-disc model (Pringle, 1981). Since OBGs are expected to lie in haloes of low metallicity we do not include any dust absorption in our models. Note that an OBG is characterised by possessing an actively accreting BH and an underlying stellar population that is Pop III or Pop II or both, however an OBG might appear as what has often been referred to as mini-quasars in the very early stages of its evolution when no stellar component is found in the DCBH host galaxy.

The UV-optical SED of an OBG is inevitably dominated by the accretion onto the central black hole. The predicted SEDs of the OBGs over the wavelength range observable with the NIRCAM (Near Infra-red Camera) and MIRI (Mid-Infra red Instrument) instruments aboard NASA's proposed *James Webb Space Telescope* (JWST) are shown in Fig. 4.3. The stellar spectrum dominates the OBG spectrum only when the BH is limited to $< 0.1 f_{\text{edd}}$ at all times. However, such a low rate would be incompatible with the dramatic mass growth rates expected of the most massive, early black holes (e.g. Sijacki et al., 2009).

We note that the magnitude of our brightest OBGs could be $m_{\text{AB}} \approx 25$, comparable to the brightest putative Lyman-break galaxies uncovered at $z \simeq 7$ in ground-based surveys such as UltraVISTA (Bowler et al., 2012). However, it will be hard to distinguish OBGs from Lyman-break galaxies with ground-based imaging because, while the predicted UV

continuum black-hole emission is expected to be relatively blue (with a UV slope $\beta \sim -2.3$, where $f_\lambda \propto \lambda^\beta$), it is not significantly bluer than that displayed by the general galaxy population at these early times (e.g. Dunlop et al., 2012). OBGs are also of course expected to display a negligible Balmer break. However, while it is interesting that the stack of the brightest Lyman-break galaxies in UltraVISTA shows at most a very weak Balmer break, it will still require extremely high-quality mid-infrared photometry to conclusively rule out the possibility that the UV-optical SED of a putative Lyman-break galaxy is incompatible with that produced by a very young stellar population.

Identification of OBGs amidst the observed high-redshift galaxy population will therefore require high-resolution imaging with HST and ultimately JWST. With $M_{\text{BH}} > M_*$, an OBG accreting at a reasonable fraction of the Eddington limit should certainly appear unresolved and point-like in high-resolution rest-frame UV (observed near-infrared) imaging. As illustrated in Fig. 4, it is already known that the vast majority of *faint* high-redshift galaxies uncovered via deep HST imaging are resolved (see Oesch et al., 2010; Ono et al., 2012), but this does not rule out the existence of an OBG population with a surface density $< 1 \text{ arcmin}^{-2}$, and HST follow-up of the brighter and rarer high-redshift ($z \simeq 7$) objects uncovered by the near-infrared ground-based surveys is required to establish whether or not they are dominated by central black-hole emission.

4.4 Summary

In this study, we report the possible existence of OBGs, at $z > 6$ in which the DCBH precedes the epoch of stellar assembly and outshines the stellar component in for a considerable fraction of the galaxy's lifetime. Our $3.41 \text{ Mpc } h^{-1}$ box produces about 4 of these OBGs. Although this is not a cosmological average owing to the small box size, the main aim of this study is to discuss the physical conditions that could lead to the existence of OBGs, which are effects that operate on a scale of less than a few tens of physical kpc, mostly insensitive to our chosen box-size.

Besides the observational features discussed, like all active galactic nuclei, OBGs are expected to display broad-line emission from highly excited species in the vicinity of the black hole. However, as OBGs have very low metallicity, it is unclear whether lines such as NV and CIV are expected to be detectable even given high-quality near-infrared spectroscopy, and Lyman- α is often severely quenched by neutral Hydrogen as we enter the epoch of reionisation.

Thus, the best observational route to establishing whether OBGs exist, and if so constraining their number density (and ultimately their evolving luminosity function), appears to be via deep imaging of putative high-redshift Lyman-break galaxies, with sufficient angular resolution to prove they are unresolved, coupled with sufficiently accurate photometry to prove any point-like objects cannot be dwarf star contaminants (see, for example Dunlop, 2012).

The discovery of an OBG could in principle settle the long standing debate on whether DCBHs can form and be the seeds of the first SMBHs (A12, Dijkstra et al., 2008; Volonteri et al.,

2008; Volonteri & Natarajan, 2009; Johnson et al., 2012b; Bellovary et al., 2011). Uncovering this population holds great promise for understanding the onset of black hole and host galaxy growth.

Chapter 5

Direct collapse black hole candidates in hydrodynamical simulations

5.1 Introduction

It is clear that to understand DCBH formation, one must first probe its plausibility, i.e. the conditions required for a halo to qualify as a direct-collapse (DC) candidate and then probe the collapse process. During collapse the gas cloud must withstand fragmentation into Pop III stars and lose its angular momentum to result in a high density gas core which could ultimately result in a DCBH if it can accrete at $\sim 0.1 - 1 M_{\odot}/\text{yr}$ for 10^{5-6} Myr. Several hydrodynamical simulations have been employed to study the processes by which gas could lose angular momentum and lead to the formation of a dense cloud in a pre-collapsible stage, for e.g. turbulence has been found to be one of the main agents via which gas can accumulate at the centre of metal-free atomic cooling haloes (Wise et al., 2008; Latif et al., 2013). However, the formation of a galactic-type disc has also been reported (Regan & Haehnelt, 2009). In their study, Dijkstra et al. (2008) (D08 hereafter) used Monte Carlo merger trees to predict the existence of such sites in the high-redshift Universe. They employed two-point correlation functions and halo mass functions and predicted a few DC sites per co-moving Gpc^3 volume. A recent study by Agarwal et al. (2012) (as described in Chapter 3) used their suite of semi-analytical models, on top of a cosmological N-body simulation, to predict the abundance of DC sites at $z \sim 6$. Their model included tracking halo histories using merger trees and the spatial variation of LW radiation from both Pop III and Pop II stars to predict as many as few DC sites per co-moving Mpc^3 .

The aim of the current study is to use a cosmological hydrodynamic simulation from the suite of simulations that are a part of the *First Billion Years Simulation* (FiBY) project (Khochfar et al, in prep., Dalla Vecchia et al. in prep, Johnson et al 2013), and identify DCBH halo candidates. This is one of the first studies to employ cosmological hydrodynamical simulations to study the haloes that are ideal sites for DC, check if the gas in these haloes could undergo DCBH formation and furthermore.

The FiBY simulation includes the most relevant physical processes required to identify sites of possible DCBH formation such as star formation, feedback from supernovae, metal enrichment and a spatially varying LW radiation field. This study is organised as follows, we first briefly describe the FiBY simulation and the modelling of LW radiation and self-shielding in Sec. 5.2, followed by the results of our study in Sec. 5.3 where we discuss the nature of the DC sites, their merger histories and the nature of the galaxies in their local neighbourhood. Finally the summary and discussion is presented in Sec. 5.4.

5.2 Methodology

5.2.1 FiBY Simulation

The simulation used for this project is one out of the suite of the First Billion Years (FiBY) project (Khochfar et al. 2013 in prep.), the details of which are to be described elsewhere (Dalla Vecchia et al. 2013 in prep.). However, we will highlight the key features of the simulation we used in this section.

A modified version of the smoothed-particle hydrodynamics (SPH) code GADGET (Springel et al., 2001; Springel, 2005) which was previously developed in the Overwhelmingly Large Simulations (OWLS) project (Schaye et al., 2010), was used for the project. The simulation was run with an equal number of gas and dark matter (DM) particles, 684^3 each, in a box with side length of 4 cMpc. The mass of a DM particle is $m_{\text{DM}} = 6161 M_{\odot}$, and gas particle, is $m_{\text{gas}} = 1253 M_{\odot}$ which allows us to resolve a $\sim 10^5 M_{\odot}$ halo with ~ 10 particles and a minimum Jeans mass of $O(10^5) M_{\odot}$ with 100 gas particles (Bate & Burkert, 1997).

Star formation and SNe feedback

Star formation is based on a pressure law, designed to match the Kennicutt-Schmidt relation (Kennicutt, 1998), as discussed in Schaye & Dalla Vecchia (2008). The threshold density for star formation is set to $n = 10 \text{ cm}^{-3}$ which is sufficient to account for LW feedback in pristine haloes (see Johnson et al., 2013, J13 hereafter). Pop III stars follow a Salpeter IMF (Salpeter, 1955) with upper and lower mass limits at $21 M_{\odot}$ and $500 M_{\odot}$ and are allowed to form in regions with metallicity $Z < 10^{-4} Z_{\odot}$, with $Z_{\odot} = 0.02$. Pop II stars follow a Chabrier IMF (Chabrier, 2003) and are allowed to form in regions with metallicity $\geq 10^{-4} Z_{\odot}$. For a critical discussion of the choices of the IMF and critical metallicity for star formation, we request the reader to refer to J13 and Maio et al. (2011).

One of the main sources that pollute the primordial gas with metals are the Pop III stars that end their lives as SNe. We model the feedback from both Pop III and Pop II SNe in the form of a prompt injection of thermal energy into the ISM that surrounds the star particle (Dalla Vecchia & Schaye, 2012). Pop II SNe feedback is included by stochastically distributing 10^{51} erg of thermal energy for each SNe, to neighbouring SPH particles which are simultaneously assigned a gas temperature of $10^{7.5}$ K. Feedback from Pop III SNe are also implemented similarly except that we differentiate between the Pop III SNe and inject

10^{51} erg per SN for stellar masses $8 M_{\odot} \lesssim M_{*} \lesssim 100 M_{\odot}$ (type II SN) and 3×10^{52} erg per SN for initial stellar masses $140 M_{\odot} \lesssim M_{*} \lesssim 260 M_{\odot}$ (Heger et al., 2003).

Metal enrichment of the gas surrounding the star particles is modelled by assuming that Pop II and Pop III star particles are continuously releasing hydrogen, helium, and metals into the surrounding gas. The metals released follow abundances computed in accordance with the tabulated yields for types Ia and II SNe, and from asymptotic giant branch (AGB) stars. These elements are then allowed to mix with the neighbouring SPH particles in the surrounding IGM, in proportions that are weighted by the SPH kernel. The approach employed here is similar to that of Tornatore et al. (2007); Wiersma et al. (2009). The same technique is used for metal enrichment from Pop III stars except that the metal yields are computed for type II SNe and PISNe following (Heger et al., 2003; Heger & Woosley, 2010).

Modelling of LW radiation in FiBY

We model the LW radiation specific intensity, J_{LW} (in units of 10^{-21} erg s^{-1} cm^{-2} Hz^{-1} sr^{-1}), in the form of a mean background as well as a spatially varying radiation intensity depending on the local distribution of stellar sources. The mean free path of LW photons in the early Universe can be ~ 10 physical Mpc (e.g. Haiman et al. 1997), which is more than twice the length of our simulated box. Therefore in order to compute the background we use the approach by Greif & Bromm (2006) which estimates a spatially uniform LW background as function of stellar mass density and redshift. We modify their approach to express the background as a function of the star formation rate computed per co-moving volume, $\dot{\rho}_{*}$, at any given redshift

$$J_{\text{LW,bg,III}} \simeq 1.5 \left(\frac{1+z}{16} \right)^3 \left(\frac{\dot{\rho}_{*,\text{III}}}{10^{-3} M_{\odot} \text{ yr}^{-1} \text{ Mpc}^{-3}} \right), \quad (5.1)$$

$$J_{\text{LW,bg,II}} \simeq 0.3 \left(\frac{1+z}{16} \right)^3 \left(\frac{\dot{\rho}_{*,\text{II}}}{10^{-3} M_{\odot} \text{ yr}^{-1} \text{ Mpc}^{-3}} \right). \quad (5.2)$$

For each of the stellar populations, the background at each simulation time step is estimated by relating it to the SFRs of Pop III and Pop II stars individually (see J13) and using $\eta_{\text{LW,III}} = 2 \times 10^4$ for Pop III stars and $\eta_{\text{LW,II}} = 4000$ for Pop II stellar sources, consistent with Greif & Bromm (2006) for the given choice of IMFs in their study and our simulation. We assume here that the escape fraction of LW photons from their host haloes is equal to unity. However it is likely that this is an over-estimate, given that some fraction of LW photons are absorbed before escaping into the IGM (see e.g. Kitayama et al. 2004; also Ricotti et al. 2001). Although we assume that the ISM and IGM are optically thin to LW photons, we compute the self shielding and dissociating rates of H_2 and H^- molecules depending upon the local gas density (See Sec. 5.2.1). Note that we only use stellar populations with ages < 5 Myr for computing the background and the spatial variation, as the majority of LW photons are emitted within this time interval owing to

either the lifetimes of the most massive stars or the spectral energy distribution of the sources (Schaerer, 2002; Leitherer et al., 1999).

As shown in Chapter 3, the local variation of LW radiation can be up to 4–5 orders of magnitude higher than the global mean (see also Ahn et al., 2009, D08). We account for this variation at any given spatial point in our box by summing up the contribution of the all local sources that are less than 5 Myr old by using the following formulation

$$J_{\text{LW,local}}^{\text{III}} = \sum_{i=1}^{N_{*,\text{III}}} 15 \left(\frac{r_i}{1 \text{ kpc}} \right)^{-2} \left(\frac{m_{*,i}}{10^3 M_{\odot}} \right), \quad (5.3)$$

and

$$J_{\text{LW,local}}^{\text{II}} = \sum_{i=1}^{N_{*,\text{II}}} 3 \left(\frac{r_i}{1 \text{ kpc}} \right)^{-2} \left(\frac{m_{*,i}}{10^3 M_{\odot}} \right), \quad (5.4)$$

where for every i^{th} individual star particle of mass $m_{*,i}$, r_i is its distance from the point in physical coordinates and $N_{*,\text{III}}$ and $N_{*,\text{II}}$ are the total number of Pop III and Pop II star particles respectively. This formula is a result of the η_{LW} parameter described previously and the 5 Myr age limit on the stellar sources where we assume that the LW photons are produced at a constant rate. Note that we differentiate between the LW stellar yields and also account for the photons at energies ≥ 0.75 eV while calculating the total H^- photodetachment rate, as explained in Sec. 5.2.1.

Self shielding and dissociation rates: H_2 , H^-

The effects of self shielding can greatly impact the overall dissociation rates of molecular hydrogen (e.g. Draine & Bertoldi, 1996; Glover & Brand, 2001). We follow the approach of Wolcott-Green et al. (2011) (WG11 hereafter) and employ a technique that depends only on the locally stored quantities of each SPH particle to avoid computational bottlenecks. The self shielding of H_2 molecules is computed as function of the local column density, N_{H_2} , defined by the local Jeans length (see J13) as

$$N_{\text{H}_2} = 2 \times 10^{15} \text{ cm}^{-2} \left(\frac{f_{\text{H}_2}}{10^{-6}} \right) \left(\frac{n_{\text{H}}}{10 \text{ cm}^{-3}} \right)^{\frac{1}{2}} \left(\frac{T}{10^3 \text{ K}} \right)^{\frac{1}{2}}, \quad (5.5)$$

where f_{H_2} is the H_2 fraction, n_{H} is the number density of hydrogen nuclei, and T is the gas temperature.

For a given gas particle with temperature T , and column density N_{H_2} , the self shielding factor can be defined as (see J13)

$$f_{\text{ss}}(N_{\text{H}_2}, T) = \frac{0.965}{(1 + x/b_5)^{1.1}} + \frac{0.035}{(1 + x)^{0.5}} \times \exp \left[-8.5 \times 10^{-4} (1 + x)^{0.5} \right], \quad (5.6)$$

where $x \equiv N_{\text{H}_2}/5 \times 10^{14} \text{ cm}^{-2}$ and $b_5 \equiv b/10^5 \text{ cm s}^{-1}$. Also, b represents the Doppler broadening parameter, which in case of molecular hydrogen can be formulated as

$$b \equiv (k_{\text{B}}T/m_{\text{H}})^{\frac{1}{2}}, \quad (5.7)$$

which leads to

$$b_5 = 2.9 \left(\frac{T}{10^3 \text{ K}} \right)^{\frac{1}{2}}. \quad (5.8)$$

The above formulation allows us to parameterise self shielding, i.e. the factor by which the level of LW radiation seen by a gas particle is attenuated.

The reaction rates for H_2 and H^- are computed on the basis of Shang et al. (2010) and we account for the global and local LW radiation flux by expressing the dissociation rates of H_2 , k_{H_2} , as

$$k_{\text{H}_2,\text{diss},\text{total}} = k_{\text{H}_2,\text{diss},\text{bg}} + k_{\text{H}_2,\text{diss},\text{local}} \quad (5.9)$$

and the ionisation rate of H^- , k_{H^-} as

$$k_{\text{H}^-, \text{ion}, \text{total}} = k_{\text{H}^-, \text{ion}, \text{bg}} + k_{\text{H}^-, \text{ion}, \text{local}}, \quad (5.10)$$

where the rates are defined in J13.

5.3 Results

We will now discuss the selection criteria used to identify haloes as DC sites in the FiBY simulation analysed for this study. Once the occurrence of the sites is explained, we will look into the evolutionary history of these haloes. Finally, in order to understand their environment, we will discuss the nature of galaxies that produce the bulk of the LW radiation seen by these haloes.

5.3.1 Identifying the DC sites

DCBHs form in atomic-cooling haloes that host galaxies with pristine gas, and therefore have seen no prior episodes of star formation (Oh & Haiman, 2002). This implies that in its past, the halo must have been continuously exposed to a level of LW radiation flux, enough to suppress Pop III star formation. We select metal-free, atomic-cooling subhaloes with the highest levels of LW flux, $J_{\text{LW}} \geq J_{\text{crit}}$, which have never hosted a star in their past as potential DC candidates. To summarise our selection criteria, we look at the gas within the subhalo with the following properties

- Virial temperature, $T_{\text{vir}} \gtrsim 10^4 \text{ K}$, the atomic-cooling limit for the halo.
- Metallicity, $Z = 0 Z_{\odot}$, i.e. pristine metal free gas.

Table 5.1: Details of the DC candidate haloes identified in the sample.

	Halo Mass [M_{\odot}]	Gas Mass [M_{\odot}]	redshift	$J_{\text{sim}}^{\text{II}}$
DC0	2.37×10^7	4.54×10^6	10.49	145.90
DC1	2.65×10^7	3.93×10^6	10.49	31.56
DC2	3.13×10^7	4.03×10^6	9.65	33.81
DC3	3.25×10^7	5.42×10^6	9.65	38.75
DC4	4.11×10^7	6.63×10^6	9.25	69.97
DC5	3.27×10^7	6.75×10^6	8.86	47.09

- Stellar mass, $M_* = 0$ and star formation rate, $\dot{\rho}_* = 0$, throughout the history of the halo.
- $J_{\text{LW}} \geq J_{\text{crit}}$, the LW specific intensity as seen by the halo exceeds the critical value.

Since the simulation outputs store the value of LW radiation for the gas particles after being treated for H_2 self-shielding, we also compute the value of LW radiation as seen by the particle pre-self-shielding. We use the prescription outlined in Sec. 5.2.1 (described in J13) to calculate the factor, f_{ss} for each particle such that

$$J_{\text{sim}} = f_{\text{ss}} J_{\text{incident}} , \quad (5.11)$$

where J_{sim} is the value of LW radiation stored in the simulation output for each particle. We then take the mean of J_{incident} over all halo particles to obtain the value of J_{LW} .

We identify DCBH sites the first time they appear and follow the merging history of their hosting halo ensuring we avoid double counting of possible DCBH sites. We find 6 haloes that meet our criteria for DCBH formation and we will refer to them to DC0–DC5. The values of gas and DM masses, redshift and the value of the LW specific intensity for the identified sample is listed in Table 5.1. For the sample of six haloes, we find that only $J_{\text{crit}}^{\text{II}}$ ($= 30$) (Shang et al., 2010) is exceeded in these haloes, whereas the $J_{\text{crit}}^{\text{III}}$ ($= 1000$) level (Wolcott-Green et al., 2011) is never reached.

We study the evolution of the LW specific intensity in the DC haloes, right until the point that they are identified as DC candidates. We look into the merger history of each DC candidate and for its most-massive subhalo progenitors, we check the minimum and maximum value of the net LW flux seen by the gas particles in the subhalo. This net LW flux is a sum of the global and the local flux and will determine whether or not the halo can host a Pop III star (O’Shea & Norman, 2008). We plot the corresponding LW flux–history of DC3 and DC5 in Fig. 5.1–5.2 where the regions bound by the maximum and minimum values of $J_{\text{LW}}^{\text{III}}$ and $J_{\text{LW}}^{\text{II}}$ are depicted in in blue and in dark–yellow respectively, with the total denoted in dark–red. The dark–blue line denotes the value of LW specific intensity required by the halo (given its mass) at each redshift, to host a Pop III star (see Eq. 2

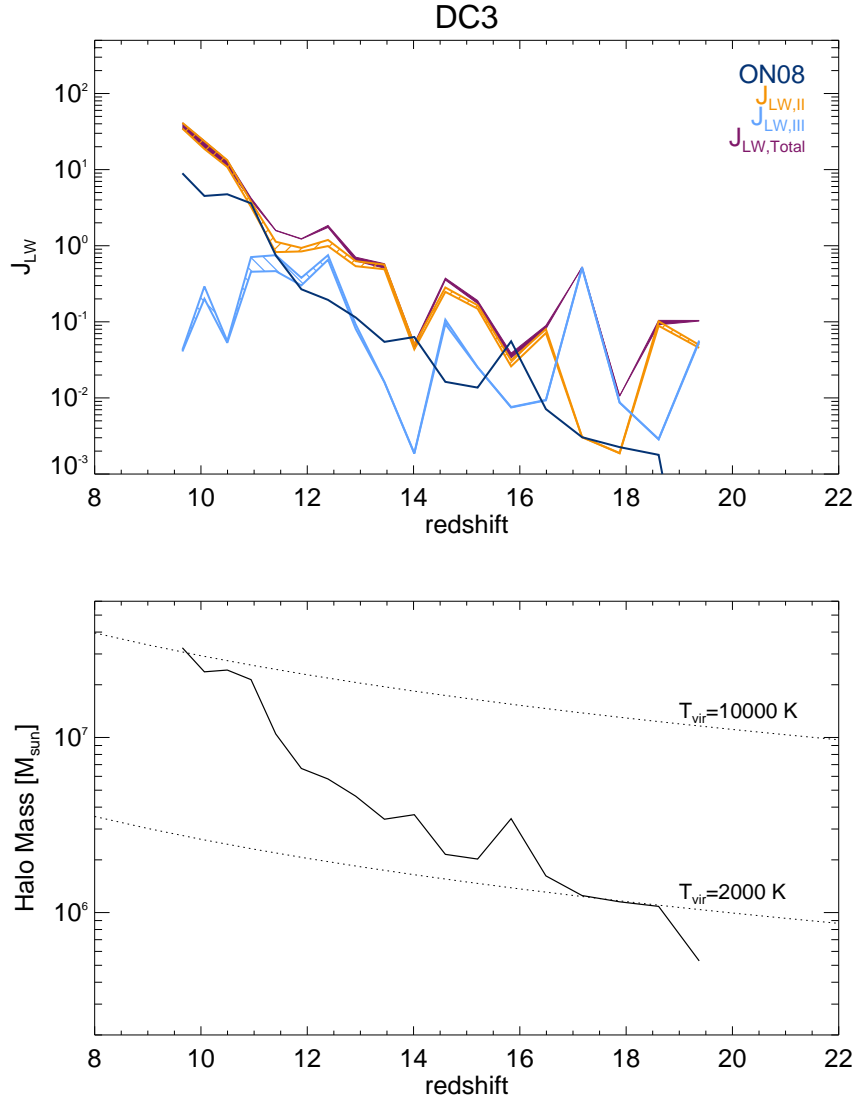


Figure 5.1: *Top Panel:* The J_{LW} radiation as seen by DC3 in its past. We track the DC halo all the way to its *birth* using our merger trees and plot the maximum and minimum value of the local LW radiation seen by the particles in the halo at each epoch. The $J_{LW,III}$ is shown in blue, $J_{LW,II}$ is shown in dark-yellow, the total is shown in dark-red and the dark-blue line denotes the level of LW specific intensity required by the halo at the given redshift to host a Pop III star (Eq. 2 in ON08). *Bottom Panel:* The mass of the halo plotted against redshift. The dotted lines correspond to the limits of $T_{vir} = 2000$ & 10^4 K at each redshift.

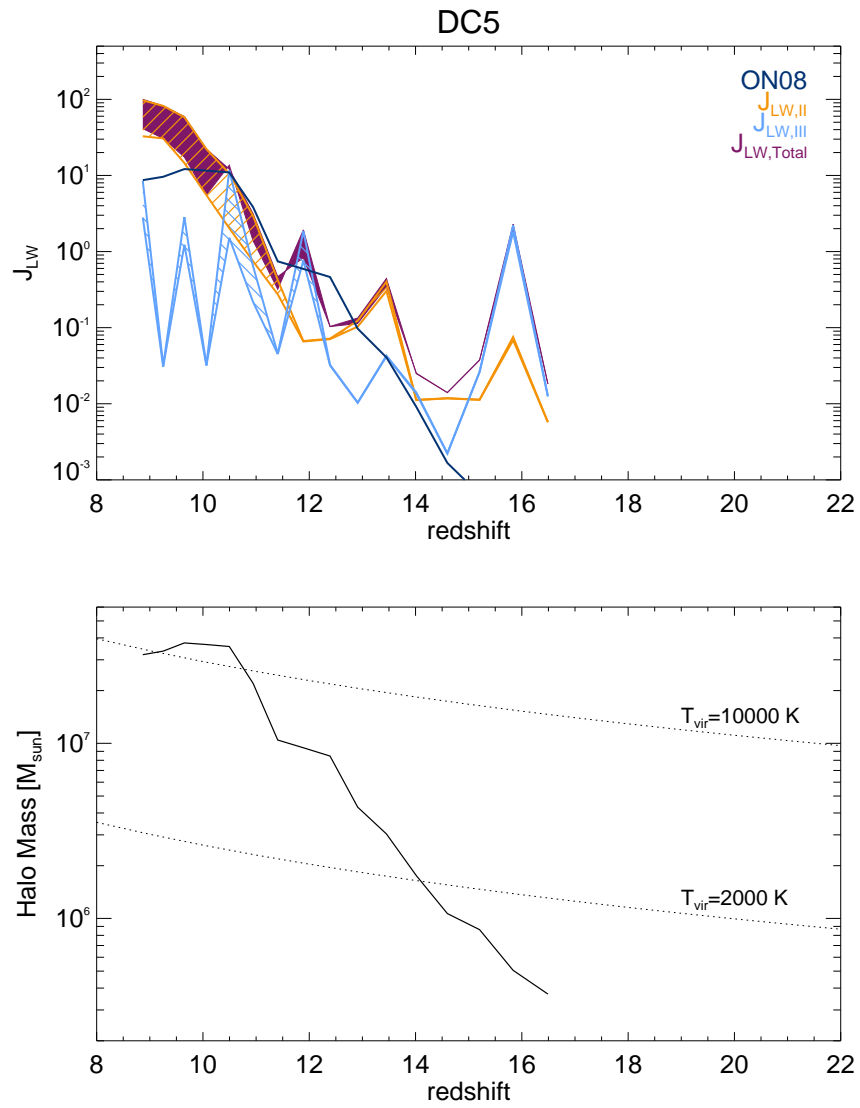


Figure 5.2: Same as in Fig. 5.1 except for DC5.

in ON08). In other words, if the red shaded region is above the black line, the halo can not host a Pop III star. The evolution of the halo mass against redshift is also plotted in the bottom panel. Note that at early times, Pop III stars are able to dominate the overall LW flux seen by the halo but the trend quickly reverses as soon as Pop II stars are able to form efficiently, thereby inhibiting Pop III star formation in close-by pristine mini-haloes. The lowest redshift in the plots signifies the epoch at which the halo is identified as a DC candidate.

Note that at times, the total LW specific intensity (red shaded region) is below the ON08 estimate, implying that the halo could potentially host Pop III stars which in fact is not the case in the simulation. This can be attributed to the fact that the ON08 results were based on idealistic simulations of two haloes and although they were able to successfully extend the analysis of Machacek et al. (2001), their fit represented by Eq. 2 is not representative of a statistical ensemble where a possible scatter would be evident.

5.3.2 The environment of DCBHs

Given that a critical level of LW radiation is imperative for DCBH formation, one would expect them to form in satellite haloes¹ that later fall into a larger galaxy which was giving out a major part of the LW radiation (Chapter 3, Chapter 4, D08). In Fig.5.3, we plot the merger history of the DCBH haloes. The left-branch depicts the main-progenitors, to the right of which we plot the merger history of the DCBH candidate halo (marked by X). In the top panels of Fig.5.4–5.6, we show the local variation of $J_{\text{LW}}^{\text{II}}$ from the neighbouring galaxies (marked by the star symbol) that produce $J_{\text{crit}}^{\text{II}}$ in the XY, YZ and XZ plane(s), centred around the DC candidate halo (marked as the black dot). The corresponding metallicity of the gas and stars in the same region (averaged over 10 physical kpc over the remaining axis in each plane) centred around the DC candidate (marked as the open circle) is shown in the bottom most panel. We will now discuss the figures in detail.

- *Merger Trees*: The first-progenitor branch of the galaxy with which the DC candidate eventually merges is shown towards the left of the plot. The merger history of the main progenitor halo with which the DC candidate subhalo (marked by an X) merges, is shown to the right. The entire merger tree is colour coded by the halo mass. The enclosing circles imply that a given halo is the most massive within its FoF group.
- *LW slices*: The local value of $J_{\text{LW}}^{\text{II}}$ colour coded to its value on a 50×50 physical kpc² grid, centred around the DC candidate (shown as the black filled circle) at the redshift at which it is identified (see Table 5.1). The galaxies, all of which are external to the DC candidate subhalo, are denoted by star symbols and the dashed lines mark the $J_{\text{crit}}^{\text{II}} = 30$ contour, which in some cases is resultant of more than one galaxy.

¹In this study, a satellite refers to a subhalo that is not the most massive one in its *friends-of-friends*, FoF, halo.

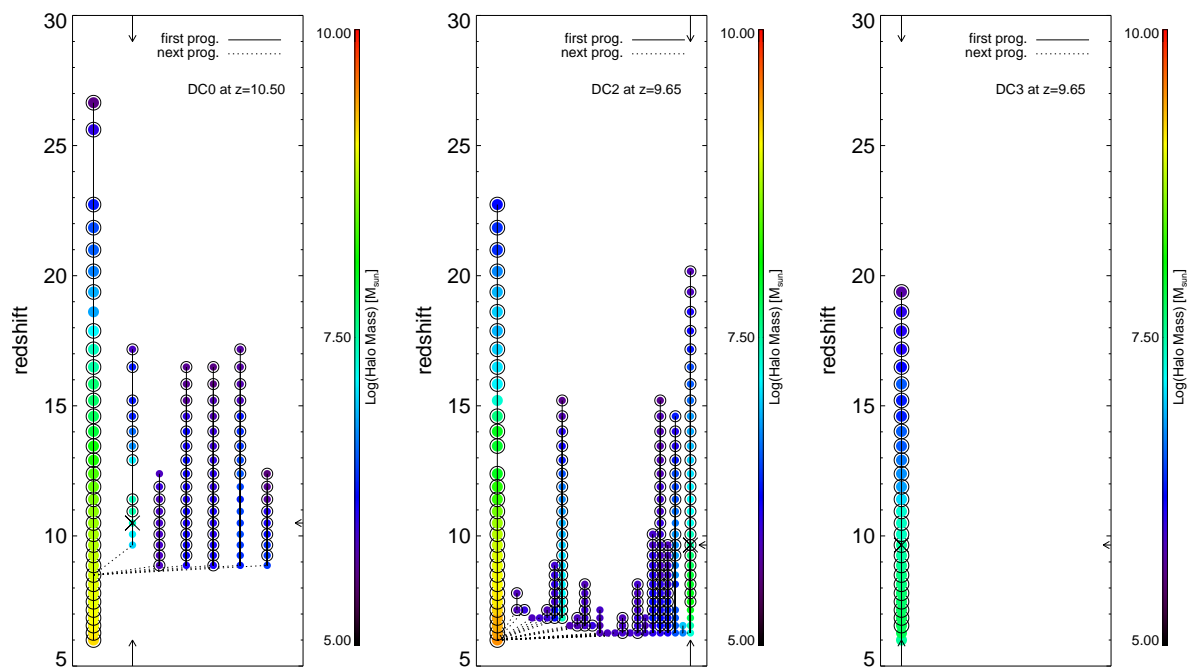


Figure 5.3: The merger tree for the DCBH candidate haloes, DC0, DC2 and DC3 marked by the cross (use arrows to guide the eye). The left-branch represents the main progenitor branch of the halo with which the DC candidate merges. On the right of this branch, we plot the merger history of the main progenitor halo with which the DC candidate merges. Enclosed circles imply that the halo is the most massive halo within its FoF group. The haloes are colour-coded by their DM mass.

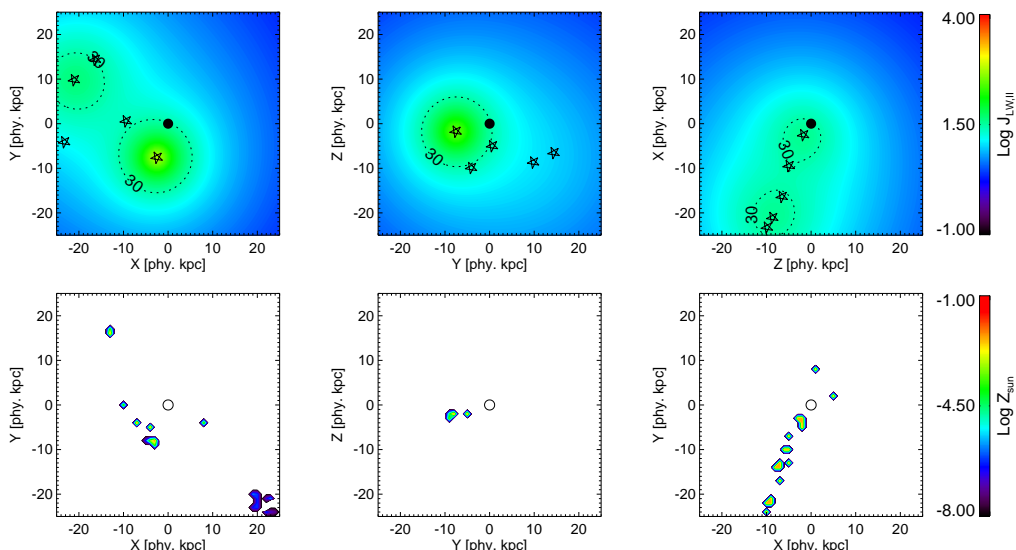


Figure 5.4: *Top*: $J_{\text{LW,local}}^{\text{II}}$ slices along the XY, YZ and ZX plane centred around DC0 (black dot) spanning 50 physical kpc along each axis. The neighbouring galaxies producing the $J_{\text{LW,local}}^{\text{II}}$ are marked by a star symbol. The dotted contour line marks the region enclosing $J_{\text{crit}}^{\text{II}} = 30$. *Bottom*: Metallicity slices along the XY, YZ and ZX plane centred around DC0 (empty circle) spanning 50 physical kpc along each axis and averaged over 10 physical kpc over the remaining axis. Note that despite the close proximity of galaxies, the DC candidate exists in a metal free region.

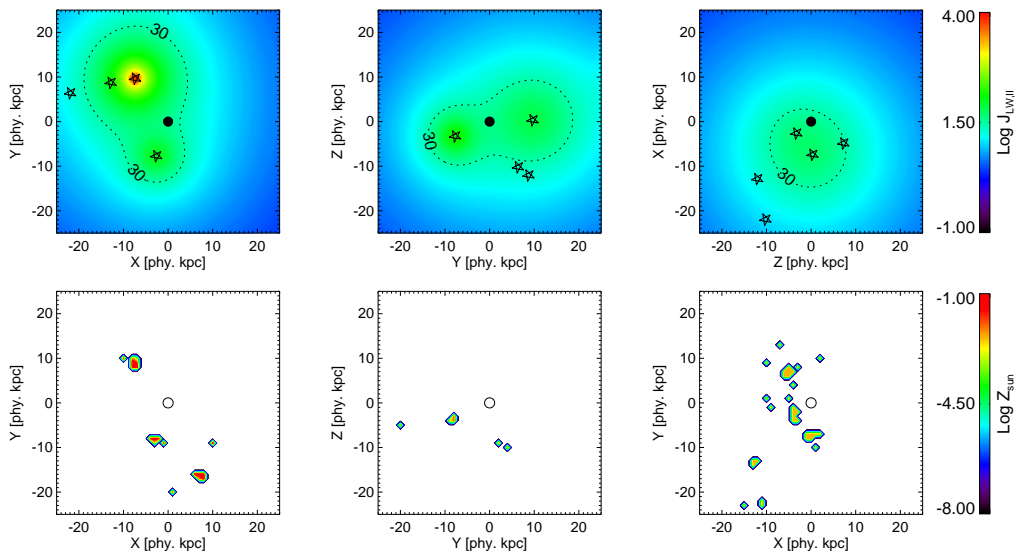


Figure 5.5: Same as in Fig. 5.4 but for DC2.

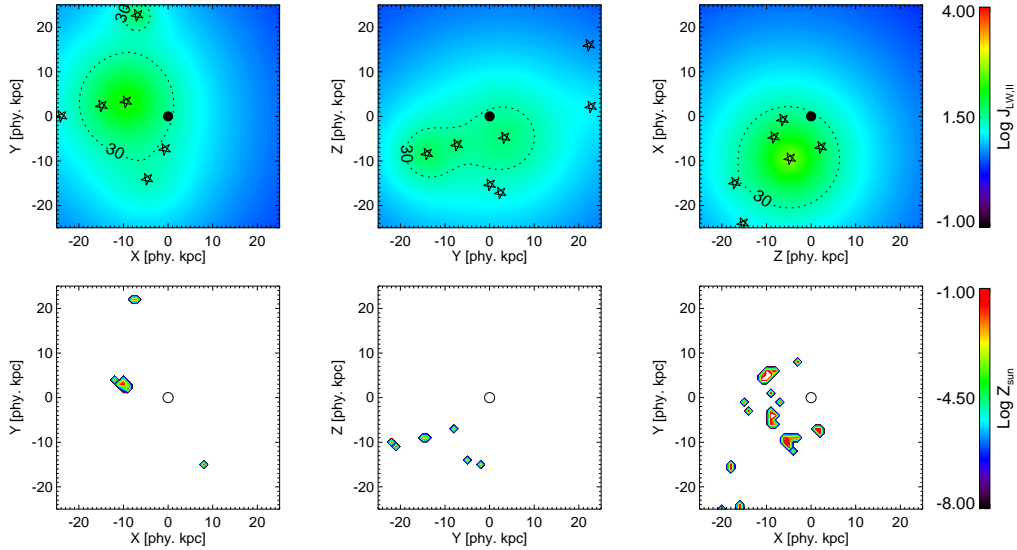


Figure 5.6: Same as in Fig. 5.4 but for DC3.

- *Metallicity slices:* The corresponding metallicity of gas and stars clearly depicts that the DC candidate resides in a zero metallicity region. The colour coding of the metallicity is done with respect to the solar value, $Z_{\odot} = 0.02$.

On the basis of the above stated points, three distinct scenarios in which a halo can host a DCBH site emerge,

Case 1

- *Formation in a site close to one dominant galaxy and subsequent merging with it* (DC0, DC1, DC4, DC5).

In this case (see left panel Fig. 5.3), the DC halo virialises near a massive galaxy that formed early in the simulation. The galaxy has already had a prior episode of star formation or was polluted by a neighbouring galaxy that led to an onset of Pop II star formation. The LW flux from the galaxy is high enough to quench star formation in its vicinity. Note that this quenching of star formation in the vicinity of the large galaxy proves extremely beneficial to the existence of a DC candidate halo later on. The quenching of star formation makes certain that no Pop III stars form in pristine minihaloes and explode as SNe later on to pollute the DC candidate halo.

Case 2

- *Formation in a clustered environment with subsequent merging with one of the nearby sources* (DC2).

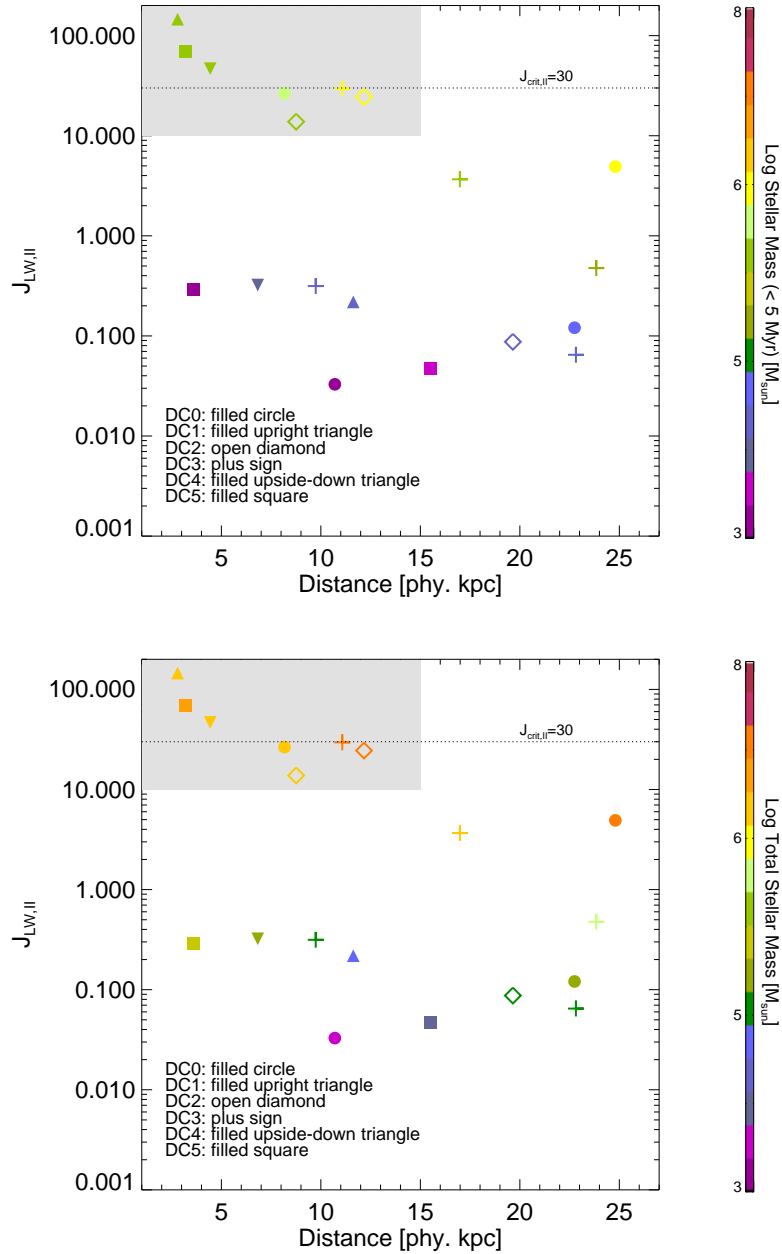


Figure 5.7: The LW specific intensity produced by each of the neighbouring galaxies at a given distance as seen in the LW contour plots of Fig. 5.4-5.6. Each set of symbols corresponds to a DC candidate, where the symbols represent a galaxy found in the field. We colour code the galaxies by their stellar mass that is < 5 Myr old (top panel) and the total stellar mass (bottom panel).

The critical level of LW radiation is a combined effect of various galaxies close to the DC halo. Note that some of the galaxies could also be the satellites of a larger galaxy. In this case both the DC halo and the larger galaxy's host haloes virialise quite early on (with $T_{\text{vir}} \sim 2000$ K), almost at the same epoch (see middle panel Fig. 5.3), but the larger galaxy's halo is considerably larger which allows it to first host a Pop III star first, followed by Pop II star formation. However, it appears that the larger galaxy in this case is not able to produce the critical LW flux by itself and is aided by other galaxies (top panel Fig. 5.5).

Case 3

- *Formation in clustered environment without subsequent merging* (see DC3).

One would expect all the DC haloes to be satellites of a galaxy, in which case, it is likely that the galaxy would give out critical LW flux. On the contrary, DC3 forms in a main progenitor branch, without any associated galaxy (see right panel Fig. 5.3). The LW radiation slices (top panel Fig. 5.6) reveal that there are other galaxies in the neighbourhood that are giving rise to the critical LW flux. These galaxies operate in a similar fashion as described in Case 1 above by quenching star formation and later on producing the critical LW flux.

5.3.3 Galaxies producing J_{crit}

Having established that the DC sites reside in special regions of low (or zero) metallicity and the critical LW specific intensity, we look into the neighbouring galaxies that produce the $J_{\text{crit}}^{\text{II}}$. In Fig.5.7, we plot the LW specific intensity versus the physical distance of each of the galaxies producing it, as seen in Fig. 5.4–5.6. Each symbol style represents a DC case, where the symbols correspond to the galaxies found in the 50×50 kpc² region of the DC site. In order to understand the nature of the stellar population in each galaxy that gives rise to $J_{\text{LW,local}}^{\text{II}}$, we colour code the symbols by the amount of stellar mass formed within 5 Myr in the top panel and the total stellar mass of the same galaxies in the bottom panel.

The galaxies that produce $J_{\text{LW}}^{\text{II}} \geq 10$ have formed at least $\sim 5 \times 10^5 M_{\odot}$ in stars within the past 5 Myr, i.e. a SFR of $\sim 0.5 M_{\odot}/\text{yr}$, and are also predominantly composed of Pop II stars. For all the DC sites, at least one galaxy with a stellar mass larger than $10^6 M_{\odot}$ is found at a distance of $d \leq 15$ kpc. The grey region bounds these two limits of $J_{\text{LW}}^{\text{II}} = 10$ and $d = 15$ kpc. The massive galaxies that lie in the grey region are the ones that contribute either solely (most noticeably: DC1, DC4, DC5, i.e. filled up right triangle, filled upside down triangle and filled square) or cumulatively (most noticeably: DC2, i.e. open diamonds) to $J_{\text{crit}}^{\text{II}}$, represented by the dotted line in each of the panels.

5.4 Summary and Discussion

In this study, we have employed one of the FiBY project’s simulations to pin–point the location and environment of metal–free, atomic cooling haloes within a cosmological hydrodynamical simulation. We report a high LW flux that is considerably higher than the global mean in the 6 candidates that could harbour a DCBH. Our attempt was to quantify if any such sites could exist in a cosmological simulation that forms Pop III and Pop II stars self–consistently and includes metal dispersion via SNe and stellar winds. In order to identify such DC sites, we have used the J_{crit} as one of the many conditions outlined in Sec. 5.3.1. However, the actual value of J_{crit} is subject to the underlying assumptions made on the stellar spectra that give rise to it.

The critical value of the LW specific intensity that favours the formation of DCBHs has been derived in the literature by studying haloes in isolation where an ideal atomic–cooling halo is selected from a cosmological setup and is irradiated, with an increasing level of LW flux, until the critical point at which H_2 cooling becomes insufficient is reached (Bromm & Loeb, 2003; Shang et al., 2010; Wolcott-Green et al., 2011). Note that this is an assumption on the physical conditions, as the halo under question would be subject to LW feedback from neighbouring galaxies right since its birth. Therefore the previous calculations of J_{crit} might have been overestimated. The exposure of the halo to LW flux ever since its birth was self–consistently accounted for in the FiBY simulation analysed in this study. However, note that, the reaction rates that relate to the photodissociation of H_2 (that are directly dependant on the stellar–spectra) were not renormalised to account for the simulated spectral energy distributions of the stellar populations used in the project. Thus, the photo–dissociation of H_2 might have been overestimated in the FiBY simulation analysed in this study.

The sample of 6 haloes identified in this study hints towards the haloes being possible sites of DCBH. Whether or not they form a DCBH would depend on the state of the subsequent gas collapse, which could be probed by extracting these haloes and simulating them in a zoom hydrodynamical simulation that has a high enough resolution. The fact that we have a handful of DC sites in our 4 Mpc side–box suggest that DCBHs do not need high σ –regions to form, and in fact, can even form in stand alone haloes that happen to be in the vicinity of a few modestly star forming galaxies that cumulatively produce the critical level of LW radiation (see DC3, Fig.5.3).

The subsequent accretion process and the final mass that these DCBHs attain would be highly dependant on the mergers that the DC haloes go through. DC0, DC1, DC4, DC5 follow the scenario where a DC halo merges with a larger galaxy at some point during its evolution. Note that upon formation, the DCBH could engulf a major fraction of the gas in its host galaxy (see for e.g. Schleicher et al., 2013), thereby running out of gas for subsequent accretion. Mergers with larger gas rich galaxies could turn on the accretion process again, aiding these DCBHs to attain supermassive scales (A13). Note that DC4 and DC5 end up in the same galaxy at $z = 6$, hinting towards the possible event of a DCBH merger in the early Universe. This sort of event, if common, could also further help in explaining the growth of massive seed BHs to supermassive scales, where upon

undergoing a merger, the seeds could double their mass and continue to grow by gas accretion. However, note that mergers are subject to gravitational recoil and dynamical friction effects, which could hinder the growth of these DCBHs, thereby prohibiting them from attaining supermassive scales by $z \sim 6$.

Chapter 6

Outlook

So far we have tried to understand the plausibility of DCBHs and their impact on the growth of the first galaxies. The work presented in Chapter 3 & 4 hint towards a high plausibility of the DCBH scenario, where the abundance of the population of galaxies harbouring a DCBH could be $\sim 0.01 \text{ Mpc}^{-3}$ at $z = 6$. We also discussed the possible ways in which these DCBHs could be observationally confirmed, i.e. by observing the SMS that lead to their formation or the OBGs that harbour them, but one will have to wait till the launch of *JWST* to test our predictions. One could constrain the abundances of DCBHs we find using the cosmic X-ray background, which is believed to be mostly a result of accreting BHs. The X-ray output from the DCBHs can be predicted on the basis of our work and can then be compared to the value that is observed out to redshifts of $z \sim 6$. Of course, the work would be subject to the underlying accretion models and the assumptions made on the origin of the cosmic X-ray background.

Studying DCBH systems could also help in understanding the onset of BH feedback in a galaxy. As we saw in Chapter. 4, the nature of OBGs, that harbour a DCBH and a stellar component, is very different to the galaxies that we see in the local Universe. Note that the OBGs have a stellar mass comparable to the BH mass right at the onset of the BH–stellar co–evolutionary phase. This hints towards the possibility that the BH feedback could be quite efficient in quenching star formation for extended periods of time.

In Chapter. 5 we discussed the existence of DC sites in a cosmological hydrodynamical simulation, where the haloes that are DCBH candidates are exposed to a level of LW flux that prohibits Pop III star formation during their entire history. Re–simulating these haloes with their LW histories, in an isolated hydrodynamical set up that self–consistently treats the chemical evolution of the gas to very high densities $\sim 10^{20} \text{ cm}^{-3}$, would shed new light on the collapse process itself. Such a study would also lead to a more consistent estimate of the critical LW flux required by a halo to undergo direct collapse, as its history of continuous exposure to LW radiation would also be accounted for.

The current computational framework does not allow one to resolve the minihaloes that are critical to the formation of DCBHs (resolvable in simulations with box–length $\lesssim 15 \text{ Mpc}$) and the high mass haloes (resolvable in simulations with box–length $O(100) \text{ Mpc}$) that play host to the brightest quasars we see across cosmic time. It would be interesting to

construct a self-consistent BH seeding model where the seeding of stellar BHs and massive BHs depends on a halo's local environment. Such seeding models could be incorporated in large scale simulations that attempt to explain the observed quasar abundances at $z \sim 6$ all the way down to $z \sim 0$. However connecting a small volume, similar to the ones employed in the thesis, to larger volumes is a challenging task.

We have attempted to study the abundance of haloes that could possibly harbour DCBHs in the first billion years of our Universe's evolution. However, one would have to self-consistently simulate the process of gas collapse in these DCBH halo candidates to connect the abundances of DCBH sites to the efficiency of DCBH formation. Our analysis suggests a population of galaxies with intermediate mass black holes must exist at $z > 6$, but are unobservable due to inefficient BH accretion or observational limitations. The observations of OBG signatures in the current *HST* surveys would point towards the high plausibility of the scenario, however, one would have to wait till the launch of *JWST* to conclusively test the theories surrounding the formation of the first quasars and galaxies.

Appendix A

Mass function and distance analysis¹

A.1 Details of Methodology: Chapter 2

A.1.1 Mass Function at $z = 6$

We plot the mass function of the haloes in our work at $z = 6$ in Fig. A.1. The red and blue lines depict the subfind and FoF halo mass function in our work respectively. It is clear from the plot that we probe the low mass end of the mass function at $z = 6$.

A.1.2 Selection of LW sources

The stellar populations (both Pop III and Pop II) are the primary source of LW radiation at early epochs. However, only certain sources can contribute to a LW radiation background at any given snapshot. Two important processes govern the fate of these LW photons; first, they might get cosmologically redshifted out of the LW band while simultaneously, the photons from the bluer end of the spectrum enter the LW range and second, these photons can get absorbed by the neutral hydrogen present in the early Universe. Haiman et al. (2000) looked at the absorption of these photons by the neutral hydrogen present in the Universe. They concluded that the Δz_{LW} over which a LW photon can exist is quite small since it gets readily absorbed by atomic hydrogen present in the un-reionised Universe. The LW band range lies very close and even overlaps with transitions that occur in atomic hydrogen, hence the mean free path for a LW photon is smaller than the distance it can travel before it gets cosmologically redshifted out of the band (Haiman et al., 2000, Fig. 16). Using the relation

$$\frac{1 + z_{\text{max}}}{1 + z_{\text{obs}}} = \frac{\nu_i}{\nu_{\text{obs}}}, \quad (\text{A.1})$$

one can easily compute the maximum redshift ($z_{\text{max}} > z_{\text{obs}}$) at which a photon emitted at frequency ν_i can contribute to the LW band, at a given observation redshift (z_{obs}) for a given observation frequency (ν_{obs}). The upper limit on the lookback redshift (z_{lb}) or

¹Appendix to Chapter 2

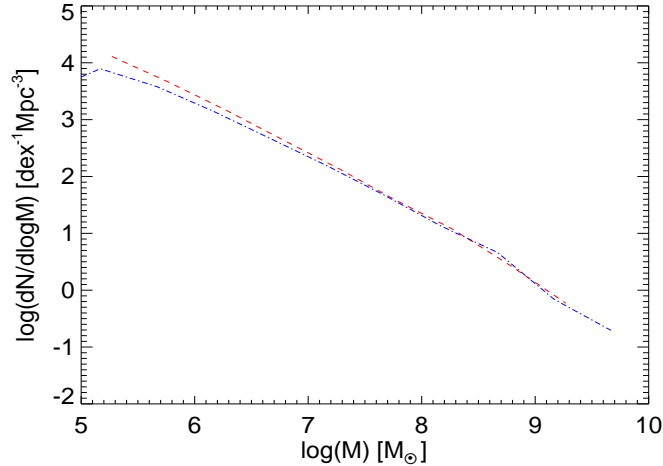


Figure A.1: The mass function of haloes at $z = 6$. The red dashed line depicts the mass function of subhaloes and blue dashed-dotted line represents the FoF mass function in our work.

lookback time (t_{lb}) can be obtained by setting $\nu_1 = 12.1$ eV (owing to the Lyman- β line) and $\nu_{\text{obs}} = 11.2$ eV for any given redshift. Hence while calculating the mean LW background for a given redshift, we only count the stars whose photons originate after t_{lb} . To do this, we define two important parameters for each star/stellar population in our study; the time of formation, which refers to the age of the Universe when the star was formed denoted by t_{form} and the age of the Universe when the star died denoted by

$$t_{\text{contrib}} = t_{\text{form}} + t_{\text{life}} . \quad (\text{A.2})$$

The lifetime t_{life} of the star depends on the mass of the star and is computed using the fits mentioned in Table 3.1 for Pop III stars (typical t_{life} of a $100 M_{\odot}$ star ≈ 2.79 Myr) and Padovani & Matteucci (1993) for Pop II star cluster (typical t_{life} for a Pop II cluster weighted by IMF used ≈ 10 Gyr). Hence, the selection criteria for sources contributing to the J_{bg} becomes

$$t_{\text{contrib}} \geq t_{\text{lb}} . \quad (\text{A.3})$$

In addition to Eq.A.3, the selection criteria for stars that can contribute locally to the LW radiation level also needs to be considered. In order to do this, we use a similar approach to KA09, and analyse the past light cone of a halo and compare it the world lines of the sources. At a given timestep t_i , we check if LW photons from a source can contribute to the J_{local} in a halo by comparing the physical distance between the source and the halo's position, with the time required for the radiation to travel between the birth of the source and t_i , and the death of the source and t_i . In case of emission from Pop II stellar clusters, we also calculate their age in order to determine *when* the photons were actually emitted (Fig. 3.2).

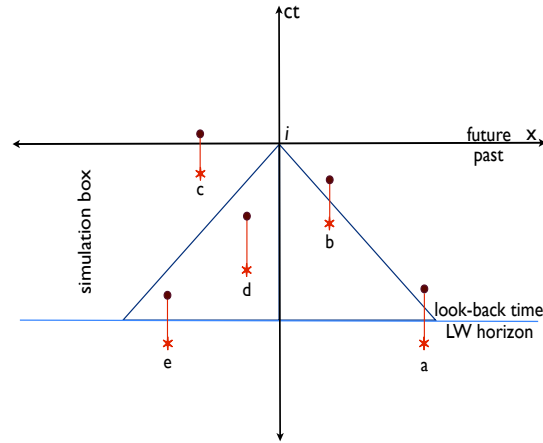


Figure A.2: Lightcone diagram for the selection criteria of LW sources in our work. Red stars indicate the t_{form} and maroon filled circles represent the t_{contrib} for a stellar source. The halo for which the LW intensity is to be calculated is placed at i whose past lightcone is marked in dark blue. Although all the sources a, b, c, d, e satisfy the Eq. A.3 and will contribute to J_{bg} , only the LW photons from stellar sources a and b can make it to the halo following Eq. A.4 and A.5 and will contribute to J_{local} .

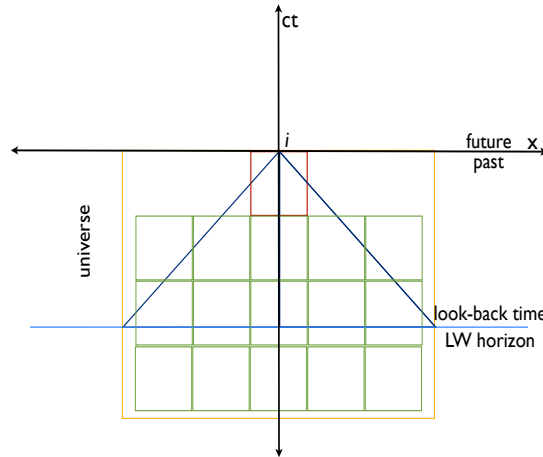


Figure A.3: A halo is (periodically) placed at the centre of one of the sides of the simulation box (red) at epoch i . The halo's past lightcone is denoted by the dark blue lines. The light blue line marks the lookback time computed using A.1. The actual background J_{LW} would come from the entire Universe (orange box) which can in turn be imagined as a conglomerate of smaller simulation boxes (green). The background J_{LW} is computed using the red box but it is assumed that the same mean J_{LW} would exist throughout the Universe (orange box).

We describe our prescription for selecting stars that are considered to contribute spatially to the LW intensity in a halo at time t_i by writing the conditions

$$d_{\text{s-h}} \leq D_{\text{lt,if}} , \quad (\text{A.4})$$

$$d_{\text{s-h}} \geq D_{\text{lt,ic}} , \quad (\text{A.5})$$

where $d_{\text{s-h}}$ is the physical source-halo distance, t_i is the age of the Universe at snapshot i , $D_{\text{lt,if}}$ and $D_{\text{lt,ic}}$ represent the physical distance light can travel between t_i and t_{form} and between t_i and t_{contrib} respectively (see Fig. A.2 for more details). Hence if a source/star satisfies Eqs. A.3, A.4 and A.5 then it contributes locally to the LW radiation level and the selection criteria for the sources that can contribute to J_{bg} is given by Eq.A.3.

It is important to note that every halo early on in the Universe is expected to be exposed to a minimum level of J_{LW} given by Eq. 3.12 and 3.13 which is an approximation to the mean-background level of radiation that is believed to be present *everywhere* in the Universe. Hence, in Eqs. 3.12 and 3.13 we assume that the SFR density in a \sim few Mpc-side box (and hence the comoving density of stars) would be the same everywhere in the Universe (see Fig. A.3).

Bibliography

- Agarwal B., Davis A. J., Khochfar S., Natarajan P., Dunlop J. S., 2013, MNRAS, 432, 3438
- Agarwal B., Khochfar S., Johnson J. L., Neistein E., Dalla Vecchia C., Livio M., 2012, MNRAS, 425, 2854
- Ahn K., Shapiro P. R., Iliev I. T., Mellema G., Pen U.-L., 2009, ApJ, 695, 1430
- Alvarez M. A., Wise J. H., Abel T., 2009, ApJL, 701, L133
- Barkana R., Loeb A., 2001, Physics Reports, 349, 125
- Bate M. R., Burkert A., 1997, MNRAS, 288, 1060
- Becker R. H. et al., 2001, arXiv, astro-ph
- Becklin E. E., Neugebauer G., 1968, Astrophysical Journal, 151, 145
- Begelman M. C., 1978, MNRAS, 184, 53
- Begelman M. C., 2010, MNRAS, 402, 673
- Begelman M. C., Rossi E. M., Armitage P. J., 2008, MNRAS, 387, 1649
- Begelman M. C., Volonteri M., Rees M. J., 2006, MNRAS, 0, 060606025740011
- Bellovary J., Volonteri M., Governato F., Shen S., Quinn T., Wadsley J., 2011, ApJ, 742, 13
- Bouwens R. J., Illingworth G. D., Franx M., Ford H., 2008, ApJ, 686, 230
- Bowler R. A. A. et al., 2012, MNRAS, 426, 2772
- Bromm V., Larson R. B., 2004, ARA&A, 42, 79
- Bromm V., Loeb A., 2003, ApJ, 596, 34
- Bromm V., Yoshida N., 2011, ARA&A, 49, 373

- Bromm V., Yoshida N., Hernquist L., McKee C. F., 2009, *Nature*, 459, 49
- Cen R., Riquelme M. A., 2008, *ApJ*, 674, 644
- Chabrier G., 2003, *The Publications of the Astronomical Society of the Pacific*, 115, 763
- Ciardì B., Ferrara A., Abel T., 2000, *ApJ*, 533, 594
- Ciardì B., Ferrara A., Marri S., Raimondo G., 2001, *MNRAS*, 324, 381
- Clark P. C., Glover S. C. O., Klessen R. S., 2008, *ApJ*, 672, 757
- Clark P. C., Glover S. C. O., Klessen R. S., Bromm V., 2011, *ApJ*, 727, 110
- Cole S., Lacey C. G., Baugh C. M., Frenk C. S., 2000, *MNRAS*, 319, 168
- Croton D. J. et al., 2006, *MNRAS*, 365, 11
- Davis A. J., Natarajan P., 2010, *MNRAS*, 407, 691
- Dalla Vecchia C., Schaye J., 2012, *MNRAS*, 426, 140
- de Bernardis P. et al., 2000, *Nature*, 404, 955
- Devecchi B., Volonteri M., Rossi E. M., Colpi M., Zwart S. P., 2012, *MNRAS*, 421, 1465
- Dicke R. H., Peebles P. J. E., Roll P. G., Wilkinson D. T., 1965, *Astrophysical Journal*, 142, 414
- Dijkstra M., Haiman Z., Mesinger A., Wyithe J. S. B., 2008, *MNRAS*, 391, 1961
- Dijkstra M., Haiman Z., Rees M. J., Weinberg D. H., 2004, *ApJ*, 601, 666
- Dopcke G., Glover S. C. O., Clark P. C., Klessen R. S., 2013, *ApJ*, 766, 103
- Dotan C., Shaviv N. J., 2012, eprint arXiv, 1203.4372, 10 pages, 7 figures
- Draine B. T., Bertoldi F., 1996, *Astrophysical Journal* v.468, 468, 269
- Dunlop J. S., 2012, arXiv: 1205.1543, astro-ph.CO
- Dunlop J. S. et al., 2012, arXiv: 1212.0860, astro-ph.CO
- Eisenstein D. J., Loeb A., 1995, *ApJ*, 443, 11
- Fabian A. C., Wilman R. J., Crawford C. S., 2002, *MNRAS*, 329, L18
- Fan X. et al., 2006, *The Astronomical Journal*, 132, 117
- Fan X. et al., 2003, *The Astronomical Journal*, 125, 1649

- Ferrarese L., Merritt D., 2000, *ApJ*, 539, L9
- Fiore F., Puccetti S., Mathur S., 2012, *Advances in Astronomy*, 2012, 9
- Fixsen D. J., 2009, *ApJ*, 707, 916
- Fixsen D. J., Cheng E. S., Gales J. M., Mather J. C., Shafer R. A., Wright E. L., 1996, *Astrophysical Journal* v.473, 473, 576
- Frebel A., Johnson J. L., Bromm V., 2007, *MNRAS*, 380, L40
- Gardner J. P. et al., 2006, *Space Science Reviews*, 123, 485
- Gebhardt K. et al., 2000, *ApJ*, 539, L13
- Gebhardt K. et al., 2003, *ApJ*, 583, 92
- Genzel R., Hollenbach D., Townes C. H., 1994, *Reports on Progress in Physics*, 57, 417
- Glover S. C. O., 2011, arXiv, astro-ph.CO
- Glover S. C. O., Brand P. W. J. L., 2001, *MNRAS*, 321, 385
- Greif T. H., Bromm V., 2006, *MNRAS*, 373, 128
- Greif T. H., Bromm V., Clark P. C., Glover S. C. O., Smith R. J., Klessen R. S., Yoshida N., Springel V., 2012, *MNRAS*, 424, 399
- Greif T. H., Glover S. C. O., Bromm V., Klessen R. S., 2010, *ApJ*, 716, 510
- Greif T. H., Johnson J. L., Klessen R. S., Bromm V., 2008, *MNRAS*, 387, 1021
- Greif T. H., Springel V., White S. D. M., Glover S. C. O., Clark P. C., Smith R. J., Klessen R. S., Bromm V., 2011, *ApJ*, 737, 75
- Gültekin K. et al., 2009a, *ApJ*, 695, 1577
- Gültekin K. et al., 2009b, *ApJ*, 698, 198
- Haehnelt M. G., Kauffmann G., 2000, *MNRAS*, 318, L35
- Haiman Z., Abel T., Rees M. J., 2000, *ApJ*, 534, 11
- Haiman Z., Rees M. J., Loeb A., 1997, *ApJ*, 476, 458
- Häring N., Rix H.-W., 2004, *ApJ*, 604, L89
- Heger A., Fryer C. L., Woosley S. E., Langer N., Hartmann D. H., 2003, *ApJ*, 591, 288
- Heger A., Woosley S. E., 2002, *ApJ*, 567, 532

- Heger A., Woosley S. E., 2010, ApJ, 724, 341
- Hinshaw G. et al., 2012, eprint arXiv, 1212, 5226
- Hirschmann M., Khochfar S., Burkert A., Naab T., Genel S., Somerville R. S., 2010, MNRAS, 407, 1016
- Hopkins A. M., 2004, ApJ, 615, 209
- Hopkins P. F., Murray N., Thompson T. A., 2009, MNRAS, 398, 303
- Hosokawa T., Omukai K., Yorke H. W., 2012, eprint arXiv, 1203, 2613, 11 pages, 10 figures
- Hosokawa T., Omukai K., Yoshida N., Yorke H. W., 2011, Science, 334, 1250, (c) 2011: Science
- Hummel J., Pawlik A., Milosavljevic M., Bromm V., 2011, arXiv, astro-ph.CO
- Inayoshi K., Omukai K., 2011, MNRAS, 416, 2748
- Janka H.-T., Langanke K., Marek A., Martínez-Pinedo G., Müller B., 2007, Physics Reports, 442, 38
- Jeon M., Pawlik A. H., Greif T. H., Glover S. C. O., Bromm V., Milosavljevic M., Klessen R. S., 2011, eprint arXiv, 1111, 6305
- Johnson J. L., 2010, MNRAS, 404, 1425
- Johnson J. L., Bromm V., 2007, MNRAS, 374, 1557
- Johnson J. L., Dalla V. C., Khochfar S., 2013, MNRAS, 428, 1857
- Johnson J. L., Greif T. H., Bromm V., 2008, MNRAS, 388, 26
- Johnson J. L., Khochfar S., Greif T. H., Durier F., 2011, MNRAS, 410, 919, 2010 The Authors. Journal compilation 2010 RAS
- Johnson J. L., Whalen D. J., Fryer C. L., Li H., 2012a, ApJ, 750, 66
- Johnson J. L., Whalen D. J., Holz D. E., 2012b, arXiv: 1211.0548, astro-ph.CO
- Kauffmann G., Colberg J. M., Diaferio A., White S. D. M., 1999, MNRAS, 303, 188
- Kennicutt R. C., 1998, ApJ, 498, 541
- Khochfar S., Silk J., 2011, Monthly Notices of the Royal Astronomical Society: Letters, 410, L42
- King A., 2003, ApJ, 596, L27

- Kitayama T., Yoshida N., Susa H., Umemura M., 2004, *ApJ*, 613, 631
- Komatsu E. et al., 2011, *ApJS*, 192, 18
- Koushiappas S. M., Bullock J. S., Dekel A., 2004, *MNRAS*, 354, 292
- Kuhlen M., Krumholz M., Madau P., Smith B., Wise J., 2011, arXiv, astro-ph.CO
- Laporte N. et al., 2012, arXiv, astro-ph.CO
- Latif M. A., Schleicher D. R. G., Schmidt W., Niemeyer J., 2013, arXiv: 1304.0962, astro-ph.CO
- Leitherer C. et al., 1999, *ApJ*, 123, 3
- Lepp S., Stancil P. C., Dalgarno A., 2002, *Journal of Physics B: Atomic*, 35, 57
- Li C., Jing Y. P., Mao S., Han J., Peng Q., Yang X., Mo H. J., van den Bosch F., 2012, eprint arXiv, 1206, 3566
- Li Y., 2011, arXiv, astro-ph.CO, 8 pages, 4 figures. Submitted to *ApJ*
- Liddle A., 2003, *An Introduction to Modern Cosmology*
- Lodato G., Natarajan P., 2006, *MNRAS*, 371, 1813
- Lodato G., Natarajan P., 2007, *MNRAS: Letters*, 377, L64
- Machacek M. E., Bryan G. L., Abel T., 2001, *ApJ*, 548, 509
- Maio U., Ciardi B., Dolag K., Tornatore L., Khochfar S., 2010, *MNRAS*, 407, 1003
- Maio U., Khochfar S., Johnson J. L., Ciardi B., 2011, *MNRAS*, no
- Mannucci F., 2007, *At the Edge of the Universe: Latest Results from the Deepest Astronomical Surveys ASP Conference Series*, 380, 87
- Mather J. C. et al., 1994, *ApJ*, 420, 439
- Mesinger A., Dijkstra M., 2008, *MNRAS*, 390, 1071
- Milosavljević M., Bromm V., Couch S. M., Oh S. P., 2009, *ApJ*, 698, 766
- Mirabel I. F., Dijkstra M., Laurent P., Loeb A., Pritchard J. R., 2011, *Astronomy & Astrophysics*, 528, 149
- Mo H., van den Bosch F. C., White S., 2010, *Galaxy Formation and Evolution*, cambridge University Press
- Mo H. J., Mao S., White S. D. M., 1998, *MNRAS*, 295, 319

- Mori M., Ferrara A., Madau P., 2002, *ApJ*, 571, 40
- Mortlock D. J. et al., 2011, *Nature*, 474, 616, (c) 2011: *Nature*
- Muratov A. L., Gnedin O. Y., Gnedin N. Y., Zemp M., 2012, arXiv: 1212.0909
- Natarajan P., 2011, *Bulletin of the Astronomical Society of India*, 39, 145
- Natarajan P., Treister E., 2009, *MNRAS*, 393, 838
- Oesch P. A. et al., 2010, *ApJL*, 709, L21
- Oh S. P., Haiman Z., 2002, *ApJ*, 569, 558
- Okamoto T., Gao L., Theuns T., 2008, *MNRAS*, 390, 920
- Omukai K., 2001, *ApJ*, 546, 635
- Omukai K., Nishi R., 1998, *ApJ*, 508, 141
- Omukai K., Schneider R., Haiman Z., 2008, *ApJ*, 686, 801
- Ono Y. et al., 2012, arXiv: 1212.3869, 1212, 3869
- O'Shea B. W., Norman M. L., 2008, *ApJ*, 673, 14
- Paardekooper J.-P., Pelupessy F. I., Altay G., Kruip C. J. H., 2011, *Astronomy & Astrophysics*, 530, 87
- Padovani P., Matteucci F., 1993, *ApJ*, 416, 26
- Palla F., Salpeter E. E., Stahler S. W., 1983, *Astrophysical Journal*, 271, 632
- Park K., Ricotti M., 2011, *ApJ*, 739, 2
- Pelupessy F. I., Matteo T. D., Ciardi B., 2007, *ApJ*, 665, 107
- Penzias A. A., Wilson R. W., 1965, *Astrophysical Journal*, 142, 419
- Perlmutter S. et al., 1999, *ApJ*, 517, 565
- Petri A., Ferrara A., Salvaterra R., 2012, *MNRAS*, 422, 1690
- Planck-Collaboration P. et al., 2013, arXiv, astro-ph.CO
- Planck-Collaboration(2013) P. et al., 2013, arXiv, astro-ph.CO, 67 pages. Submitted to *Astronomy & Astrophysics*
- Pringle J. E., 1981, *Ann. Rev. Astron. Astrophys.*, 19, 137
- Rees M. J., 1978, *The Observatory*, 98, 210, a&AA ID. AAA022.141.054

- Regan J. A., Haehnelt M. G., 2009, MNRAS, 396, 343
- Ricotti M., 2008, FIRST STARS III: First Stars II Conference. AIP Conference Proceedings, 990, 364
- Ricotti M., Gnedin N. Y., Shull J. M., 2001, ApJ, 560, 580
- Ripamonti E., Abel T., 2004, MNRAS, 348, 1019
- Robertson B., Hernquist L., Cox T. J., Matteo T. D., Hopkins P. F., Martini P., Springel V., 2006, ApJ, 641, 90
- Rubin V. C., Burstein D., Ford W. K., Thonnard N., 1985, Astrophysical Journal, 289, 81
- Rybicki G. B., Lightman A. P., 1986, Radiative Processes in Astrophysics, iISBN: 0-471-82759-2
- Safraneck-Shrader C., Agarwal M., Federrath C., Dubey A., Milosavljevic M., Bromm V., 2012, arXiv, astro-ph.CO, 22 pages, 12 figures
- Salpeter E. E., 1955, ApJ, 121, 161
- Schaerer D., 2002, A&A, 382, 28
- Schaye J., Dalla Vecchia C., 2008, MNRAS, 383, 1210
- Schaye J. et al., 2010, MNRAS, 402, 1536
- Schleicher D. R. G., Palla F., Ferrara A., Galli D., Latif M., 2013, eprint arXiv, 1305, 5923
- Schneider R., Ferrara A., Natarajan P., Omukai K., 2002, ApJ, 571, 30
- Schneider R., Omukai K., Bianchi S., Valiante R., 2011, MNRAS, 1743
- Searle L., Zinn R., 1978, Astrophysical Journal, 225, 357, a&AA ID. AAA022.154.018
- Shang C., Bryan G. L., Haiman Z., 2010, MNRAS, 402, 1249
- Shapiro S. L., 2005, ApJ, 620, 59
- Sijacki D., Springel V., Haehnelt M. G., 2009, MNRAS, 400, 100
- Silk J., Rees M. J., 1998, A&A, 331, L1
- Smit R., Bouwens R. J., Franx M., Illingworth G. D., Labbé I., Oesch P. A., van Dokkum P. G., 2012, eprint arXiv, 1204, 3626
- Smith B. D., Turk M. J., Sigurdsson S., O'Shea B. W., Norman M. L., 2009, ApJ, 691, 441

- Spaans M., Silk J., 2006, *ApJ*, 652, 902
- Spergel D. N. et al., 2003, *The Astrophysical Journal Supplement Series*, 148, 175
- Springel V., 2005, *MNRAS*, 364, 1105
- Springel V. et al., 2005, *Nature*, 435, 629
- Springel V., Yoshida N., White S. D. M., 2001, *New Astronomy*, 6, 79
- Stacy A., Greif T. H., Bromm V., 2012, *MNRAS*, 422, 290
- Tanaka T., Haiman Z., 2009, *ApJ*, 696, 1798
- Tanaka T., Perna R., Haiman Z., 2012, eprint arXiv, 1205, 6467, 15 pages, 6 figures, submitted to *MNRAS*
- Tegmark M., Silk J., Rees M. J., Blanchard A., Abel T., Palla F., 1997, *ApJ*, 474, 1
- Thompson T. A., Quataert E., Murray N., 2005, *ApJ*, 630, 167
- Tornatore L., Borgani S., Dolag K., Matteucci F., 2007, *MNRAS*, 382, 1050
- Treister E., Schawinski K., Volonteri M., Natarajan P., Gawiser E., 2011, *Nature*, 474, 356
- Trenti M., Stiavelli M., 2009, *ApJ*, 694, 879
- Turk M. J., Clark P., Glover S. C. O., Greif T. H., Abel T., Klessen R., Bromm V., 2011, *ApJ*, 726, 55
- Volonteri M., 2010, *The Astronomy and Astrophysics Review*, 18, 279
- Volonteri M., Begelman M. C., 2010, *MNRAS*, 409, 1022
- Volonteri M., Lodato G., Natarajan P., 2008, *MNRAS*, 383, 1079
- Volonteri M., Natarajan P., 2009, *MNRAS*, 400, 1911
- Volonteri M., Rees M. J., 2005, *ApJ*, 633, 624
- Whalen D., O'Shea B. W., Smidt J., Norman M. L., 2008, *ApJ*, 679, 925
- Wiersma R. P. C., Schaye J., Theuns T., Dalla Vecchia C., Tornatore L., 2009, *MNRAS*, 399, 574
- Willott C. J., 2011, *ApJL*, 742, L8
- Willott C. J., McLure R. J., Jarvis M. J., 2003, *ApJ*, 587, L15
- Wise J. H., 2012, arXiv, astro-ph.CO

Wise J. H., Abel T., 2007, *ApJ*, 671, 1559

Wise J. H., Abel T., 2008, *ApJ*, 685, 40

Wise J. H., Cen R., 2009, *ApJ*, 693, 984

Wise J. H., Turk M. J., Abel T., 2008, *ApJ*, 682, 745

Wolcott-Green J., Haiman Z., Bryan G. L., 2011, *MNRAS*, 1673

Wright E. L. et al., 1994, *ApJ*, 420, 450

Wyithe S., Loeb A., 2011, eprint arXiv, 1111.5424, 10 pages, 4 figures. Submitted to *MNRAS*

Yajima H., Choi J.-H., Nagamine K., 2011, *MNRAS*, 412, 411

Yoshida N., 2006, *New Astronomy Reviews*, 50, 19

Yoshida N., Abel T., Hernquist L., Sugiyama N., 2003, *ApJ*, 592, 645

Yoshida N., Omukai K., Hernquist L., 2008, *Science*, 321, 669

Yoshida N., Omukai K., Hernquist L., Abel T., 2006, *ApJ*, 652, 6

Zwart P., McMillan S., Stephen, 1999, eprint arXiv, 12022

Acknowledgements

I am fortunate to find myself at a stage where I can thank all the people who have been an integral part of the journey that has ultimately led to the shaping of this thesis. I would like to start off by thanking my supervisor, Dr. Sadegh Khochfar, who gave me the opportunity to come to Munich and be a part of the TMoX group. His guidance and direction through these years has instilled an inquisitive spirit in me to learn and achieve even more than I think I am capable of.

I owe a lot to my collaborator and mentor Priya, whose excitement at the prospects of our work made the projects all the more exciting. I will forever be thankful to her for the warm welcomes and professional guidance that she has happily provided me with over the years.

My thesis committee: Prof. Andreas Burkert and Dr. Mark Dijkstra, were always there with an interesting insight to the problems I was facing and trying to solve. Their outlook towards my work and constructive criticism helped me in the final shaping of each of the projects that I undertook. The TMoX group: Jarrett, Claudio, Jan-Pieter, Andrew, Leila, Fabrice, Volker, Eyal and Umberto, played the role of the approachable postdocs and confidants to whom I could turn to in the no-so-rare moments of Ph.D. related catastrophes. I could not have wished for a better group, and will forever be the lucky sole-Ph.D. student.

My office mates: Manuel and Alessandro, will fondly be remembered, who although younger than me in Ph.D. years, provided me with the unlimited free candy, treats and coffees. The people at MPE, who made life so much easier, I do know how I would have survived the system without you: Christa and Birgit. Michelle thanks for the tips on submission and latex. Ilona's smiles, samosas and cakes kept me going on those Sundays and all other weekdays, when food was a luxury and smiles were rare. Vlad, your frisbee and conversation antics always kept me on my feet, thanks for the induced caffeine effects. I would like to thank Chervin, the friend on the other side of the wall, who helped me in keeping it real. Guido, thanks for the good times and teaching me how to cook Italian pasta without ketchup. My adopted parents: Jonny and Alessia, thanks for keeping me in check and making sure I at least tried to be healthy: physically, mentally and psychologically. Although my presence in your lives might have led you in to pulling out your hair, you certainly helped me keep mine.

Finally, my real family: dad, mom and sis, you tolerated my radio silence for days. Without your encouragement during the early years, this would not have been possible.

Lebenslauf

Bhaskar Agarwal

Max Planck for Extraterrestrial Physics
Giessenbachstr., 85748 Garching, Germany
agarwalb@mpe.mpg.de
Date of Birth: 5 March 1986
Nationality: Indian

Education

- **Ph.D.** **Aug. 2010 - Present**
Max Planck for Extraterrestrial Physics, Germany (expected)
Theoretical Modelling of Cosmic Structures Group (TMoX)
Advisor: Dr. Sadegh Khochfar
Dissertation: 'Formation of massive seed black holes by direct collapse in the early Universe.'
- **M.Sc. Astronomy** **Sept. 2007 - Sept. 2008**
University of Sussex, U.K.
Advisor: Dr. Kathy Romer
Dissertation: 'A critical analysis of joint fitting techniques on the clusters identified via the Sunyaev-Zel'dovich effect.'
- **B.Sc. Physics, 2007** **Jul. 2004 - Jul. 2007**
University of Pune, India
Advisor: Dr. Raka V. Dabhade
Dissertation: 'Building a Dipole Antenna to detect Solar Flares at 20Mhz.'

Publications

- PUBLISHED *Ubiquitous seeding of supermassive black holes by direct collapse.*
Bhaskar Agarwal, Sadegh Khochfar, Jarrett L. Johnson, Eyal Neis-
tein, Claudio Dalla Vecchia and Mario Livio. (arXiv:1205.6464).
- Unravelling obese black holes in first galaxies.*
Bhaskar Agarwal, Andrew J. Davis, Sadegh Khochfar, Priya Natara-
jan. (arxiv:1302.6996).
- IN- *The First Billion Years Simulation: Metal free atomic cooling haloes as*
PREPARATION *precursors to massive black hole seeds.*
Bhaskar Agarwal, Jarrett Johnson, Sadegh Khochfar, Claudio Dalla
Vecchia.
- The First Billion Years Simulation: Reionisation feedback from direct*
collapse black holes.
Jan-pieter Paardekooper, **Bhaskar Agarwal**, Jarrett Johnson, Sadegh
Khochfar, Claudio Dalla Vecchia.
- Using the cosmic X-ray background to constrain the direct collapse black*
hole seed abundances.
Bhaskar Agarwal, Sadegh Khochfar.
- CONFERENCE *The Growth of the Stellar Seeds of Supermassive Black Holes.*
PROCEEDINGS Jarrett L. Johnson, **Bhaskar Agarwal**, Daniel J. Whalen, Claudio
Dalla Vecchia, Christopher L. Fryer, Sadegh Khochfar, Hui Li, Mario
Livio (proceedings of "First Stars IV", held in Kyoto, Japan, May 21-25,
2012)

Professional Experience

- MEMBER OF LOCAL ORGANISING COMMITTEE **16 June 2013- 21 June 2013**
Cosmic Dawn at Ringberg, Ringberg 2013
Organised by the TMOX group at Max Planck for Extraterrestrial Physics.
- MEMBER OF LOCAL ORGANISING COMMITTEE **26 June 2011- 1 July 2011**
First Galaxies Workshop, Ringberg 2011

Organised by the TMOX group at Max Planck for Extraterrestrial Physics.

- RESEARCH ASSISTANT Jan. 2009 - Mar. 2010
Indian Space Research Organisation (ISRO) and Fergusson College, India
ISRO assisted project on ‘Observing Meteor Showers in Pune’

- TEMPORARY LECTURER, B.Sc. Physics Jan. 2009 - Feb. 2010
Fergusson College, University of Pune, India
Astronomy and Astrophysics I-II
Classical Mechanics I-II

- GUEST LECTURER Jan. 2009
Fergusson College, University of Pune, India
Public lectures on Cosmology for the International Year of Astronomy 2009 (IYA).

Conferences and Workshops

TALKS

Poster: Massive seed black holes by direct collapse in the First Billion Years Simulation.

Massive Black Holes: Birth, Growth and Impact, KITP, August 5-19 2013, University of California, Santa Barbara, U.S.A.

Why should one care about direct collapse black holes?

Gas Dynamics and Star Formation in the Extreme Environment of Galactic Nuclei Rinberg Castle, 18-22 March 2013.

Seminar, Maryland University, College Park, U.S.A, 11 December 2012.

Science Coffee, Space Telescope Science Institute, Baltimore, U.S.A, 10 December 2012.

Special Seminar, University of Columbia, New York, U.S.A, 6 December 2012.

Wednesday Seminar, Yale University, New Haven, U.S.A, 5 December 2012.

Institute for Theory and Computation Seminar, Harvard University, Cambridge, U.S.A, 30 November 2012.

Origin of supermassive black holes and onset of black hole–bulge relation.

39th COSPAR scientific assembly, *Probing the high redshift universe*, Mysore, India, 16 July 2012.

Galaxy Evolution Discussion Group Seminar (GEDG), Oxford University, U.K., 15 March 2012.

Direct Collapse Black Holes: A realistic scenario for SMBH seeds?

First Galaxies Workshop 2011, Ringberg, Germany 26 June – 1 July 2011.

OPINAS seminar, Max Planck Institute for Extraterrestrial Physics, Garching, Germany, 29 November 2011.

WORKSHOPS

Early Galaxy Formation in LCDM Cosmology. The 30th Jerusalem Winter School in Theoretical Physics, Jerusalem, Israel, 31 December 2012–10 January 2013.

IMPRS Summer School 2010- *First Stars and Cosmic Reionisation.* Max Planck Institute for Astronomy, Heidelberg, Germany, 6–10 September 2010.

Astrophysics Research School. University of Central Lancashire, U.K., 15 – 19 December 2007.

OTHER The Royal Astronomical Society Meeting on *The Sunyaev-Zel'dovich Effect*. London, U.K., 14 December 2007.

Solar Flare Monitoring Station at Fergusson College, Pune. As the co-author at the International Conference on the Challenges for Solar Cycle- 24 (ICCSC-24), Physical Research Lab (PRL), Ahmedabad, India, January 2007.

Raman Memorial Conference. Physics Department, University of Pune, 24-25th February 2006.

Technical Expertise

- Proficient in IDL and experienced with C/C++ and Matlab.
- Proficient in analysing merger tree outputs and running the required code.
- Experienced in working with the Gadget2 output in both binary and HDF format.
- Experienced in designing websites and managing weekly blogs.